KfK 2812
Dezember 1979

Test of the EG&G Two-Phase Mass Flow Rate Instrumentation at Kernforschungszentrum Karlsruhe

Analysis Report Vol. 1: Test Results from LOFT Production DTT and a LOFT Type Gamma Densitometer

J. Reimann, H. John, R. Löffel
Institut für Reaktorbauelemente
Laboratorium für Isotopentechnik

C. W. Solbrig, L. L. Chen, L. D. Goodrich
EG&G Idaho Inc., INEL

Kernforschungszentrum Karlsruhe

KERNFORSCHUNGSZENTRUM KARLSRUHE
Institut für Reaktorbauelemente
Laboratorium für Isotopentechnik
Projekt Nukleare Sicherheit

KfK 2812

Test of the EG&G Two-Phase Mass Flow Rate Instrumentation at Kernforschungszentrum Karlsruhe

Analysis Report Vol.1: Test Results from LOFT Production DTT and a LOFT Type Gamma Densitometer

J. Reimann*
H. John*
R. Löffel**

C. W. Solbrig
L.L. Chen
L. D. Goodrich

Kernforschungszentrum Karlsruhe
*Institut für Reaktorbauelemente
**Laboratorium für Isotopentechnik

EG&G Idaho Inc.
Idaho National Engineering Laboratory

Kernforschungszentrum Karlsruhe GmbH
ISSN 0303-4003

ACKNOWLEDGEMENT

The authors wish to acknowledge the loop operators L. Pawlak and E. Wanner, the investigators who obtained the data D.J. Barnum, R.L. Crumley, A. Demski, R. R. Good, V.W. Hansen, H.J. Helbert, and R.D. Meininger and G.B. Shull and R.L. Hoskinson who contributed in compiling and reviewing the experimental data.

Last but not least, the support given to this project by the US NRC and the German BMFT and J.P. Hosemann from the KfK Project Nuclear Safety for his coordination is gratefully acknowledged.

Abstract

For many experiments which investigate the Loss-of-Coolant Accident (LOCA) in nuclear reactors, proper measurement of the two-phase mass flow rate is of great importance. This report presents the data analyses of experiments designed to understand the behavior of a free field drag disc turbine transducer (DTT) and a three beam gamma densitometer in steady-state horizontal steam-water and air-water flow. The pressure was varied between 2 and 75 bars, the experiments were made at a mass flow rate and void fraction range where various quite separated flow regimes occurred. Two different test sections with 103 mm ID (5" pipe) and 66 mm ID (3" pipe) were used.

Information on flow regime and phase distribution in the cross section was obtained with local impedance probes, measurements of the axial distribution of phase velocities in the test section piping were made with the radiotracer technique. These techniques were of great help for the physical interpretation of the single instrument readings. The dependence of the instrument readings on flow regime and void fraction is shown.

The best overall accuracy of mass flow rate determined by combining two of the three available instruments is obtained by the combination of gamma densitometer and drag disc. Evaluation of the mass flow rates from the three instrument readings, using different turbine models, does not improve the overall accuracy.

From the experiments, single calibration factors are determined which depend only on the gamma densitometer reading. This procedure considerably improves the accuracy of the mass flow rate evaluation for the combination of gamma densitometer and drag disc, and gives much better results, compared to the other models, for the slip and phase velocities when three signals are used.

A time averaged separated two-phase model for the DTT is postulated which shows that the DTT measures the local parameters. To obtain the pipe averaged mass flux, a density correction is proposed.

For some experiments the radiotracer technique combined with the gamma densitometer for measuring the mass flow rate was tested. This combination has the highest accuracy, independent of flow regime.

Zusammenfassung

Test der EG & G-Zweiphasenmassenstrom-Instrumentierung im Kernforschungszentrum Karlsruhe

Analysebericht Nr. 1: Ergebnisse der Tests des LOFT-DTT-und eines LOFT-Gamma-Densitometers

In vielen Experimenten zum Kühlmittelverlustunfall von Kernreaktoren ist die genaue Messung des zweiphasigen Massenstromes von großer Bedeutung. Dieser Bericht enthält die Datenanalyse von Experimenten zur Untersuchung des Verhaltens eines lokal messenden Drag Disc-Turbine-Transducers (DTT) und eines Dreistrahl-Gamma-Densitometers in stationärer, horizontaler Dampf-Wasser sowie Luft-Wasser-Strömung. Der Druck wurde variiert zwischen 2 und 75 bar, die Experimente wurden in einem Massenstrom- und Dampfvolumenanteils-Bereich durchgeführt, bei denen verschiedene, recht stark separierte Strömungsformen vorhanden waren. Zwei verschiedene Teststrecken mit Innendurchmessern von 103 mm (5" Teststrecke) sowie 66 mm (3" Teststrecke) wurden verwendet.

Lokale Impedanz-Sonden dienten zur Bestimmung der Strömungsform sowie zur Messung der Phasenverteilung im Strömungsquerschnitt, die Verteilung der Phasengeschwindigkeiten längs der Rohrachse wurde mit Radiotracer-Verfahren gemessen. Diese Meßtechniken waren sehr hilfreich für die physikalische Interpretation der einzelnen Meßsignale. Die Abhängigkeit dieser Signale von Strömungsform und Dampfvolumenanteil wird diskutiert.

Wird der Massenstrom durch zwei der drei Instrumente ermittelt, so ergibt sich im Mittel die höchste Genauigkeit durch die Kombination Gamma-Densitometer - Drag Disc. Die Verwendung verschiedener Turbinenmodelle zur Bestimmung des Massenstroms aus allen drei Signalen ergibt insgesamt keine Verbesserung der Genauigkeit.

Aus den Experimenten werden Kalibrierungsfaktoren gewonnen, die nur vom Gamma Densitometer Signal abhängen. Diese Vorgehensweise verbessert beträchtlich die Genauigkeit der Massenstrombestimmung für die Kombination Gamma-Densitometer - Drag Disc und ergibt sehr viel bessere Ergebnisse, verglichen mit den anderen Modellen, für den Schlupf und die Phasengeschwindigkeiten, wenn alle drei Signale verwendet werden.

Es wird ein zeitlich gemitteltes Strömungsmodell für den DTT aufgestellt, das zeigt, daß der DTT lokale Parameter mißt. Um den über dem Rohrquerschnitt

gemittelten Massenstrom zu erhalten, wird eine Dichtekorrektur vorgeschlagen.

In einem Teil der Versuche wurde ebenfalls das Radiotracer-Verfahren, kombiniert mit dem Gamma Densitometer, für die Messung des Massenstromes getestet. Diese Kombination ergibt die höchste Genauigkeit, unabhängig von der Strömungsform.

CONTENTS

List of Figures

List of Tables

1. Introduction

This report presents the data analyses of experiments designed to understand the behavior of a LOFT DTT and gamma densitometer in horizontal air-water and steam-water flow. In some of the experiments, the KfK-radiotracer technique was also tested in addition to the LOFT instrumentation. These data are also analysed. The experiments were carried out in the Karlsruhe Two-Phase Test Facility during a period from October to November of 1977. A detailed description of the test facility, the instrumentation, and the data acquisition is given in the data report /1/. This report also contains the calibration of the instruments in single phase flow, the readings of the single instruments in two-phase flow converted in metric engineering units, and the computed variables such as mass flow rates, various velocities and void fractions.

With additional information on the phase velocity distribution in the test section, the primary data are examined with the goal to physically interpret the data. As a result, empirical correlations and models for the mass flow rate (and slip and phase velocities) are derived and compared with existing models.

2. Short Description of Test Section, Instrumentation, and Test Matrix

The LOFT mass flux instrumentation test program consisted of two-phase calibrations in two different test sections, one a five-inch diameter pipe, and the other a three-inch pipe (Fig. 2.1). The instruments intended for calibration were the LOFT production Drag Disc Turbine Transducer (DTT) and a three beam gamma densitometer. Both test sections provide free field calibrations. That is, the DTT is smaller than the inside diameter of both test sections. The gamma densitometer is a three beam unit representative of the configuration used in LOFT, but modified to fit on a smaller pipe.

The reference mass flow rates were measured with orifices in single phase flow before mixing. The quality in the test section and the superficial velocities were computed using an enthalpy balance between the conditions (pressure, temperature) at the single phase flow measuring stations and the position of the instrumentation in the test section taking into account the heat losses between these positions. A detailed description of the facility is given in /2/.

Downstream of the mixing chamber outlet a pipe was positioned (length 1.36 m) which contained the junction to the bypass. In the tests reported in this volume this pipe had a diameter of 50 mm ID. To diverge from the 50 mm pipe to the 5" (103.2 mm ID) or 3" (66.6 mm ID) pipe test section, eccentrical adapters were used so that the bottom of the pipes were at the same elevation to prevent damming. The test sections had lengths of 5.2 m (5" pipe), and 5.93 m (3" pipe), respectively. Table 2.1 shows the positions of the gamma densitometer and the DTT in the test section in terms of the length to diameter ratio (L/d) and some other geometrical ratios which are important for the further discussions.

	Test Section Inlet A_{TS}/A_{50}	LOFT Densit. L/d	Scanning Densit. L/d	DTT L/d	Turbine d_T/d	Drag Disc d_{DD}/d
5" Test Section	4.24	32	-	33	0.36	0.01
3" Test Section	1.77	50	57	72	0.57	0.015

Table 2.1 Test Section Geometry and Measurement Locations

The drag disc diameter to pipe diameter ratio (d_{DD}/d) was very small for both test sections which means that the drag disc was measuring quite locally both in the 5" and 3" test section. The turbine diameter to pipe diameter ratio d_T/d was not so far below 1, especially for the 3" pipe, indicating that the turbine in the 5" pipe can be regarded as a "free field" instrument but in the 3" pipe rather between "free field" and "full flow". The area changes at the test section inlets A_{TS}/A_{50} which were different for the two configuration influenced the phase and velocity distributions at the test section inlets. To understand the flow at the locations of the single instruments it is essential to determine if the phase and velocity distributions at the measuring positions are still influenced by this special geometry or if a so called well developed two-phase flow exists.

Figure 2.1 also contains the additional instrumentation:
- the KfK radionuclide injection valves and the corresponding detectors for measuring the axial distribution of the phase velocities.
- the EG&G traversing reference gamma densitometer (scanning densitometer) for the measurement of a very accurate cross section averaged value of the density (void fraction, respectively).
- the KfK impedance probes: a vertically traversing probe in the 5" pipe for detection of flow regime and measurements of a vertical void fraction profile, two fixed built in probes in the 3" pipe for detecting flow regime.

Besides the difference in geometry, the 5" and 3" pipe tests were different concerning the test matrix:
- the 5" pipe test matrix included the following nominal test points:
  superficial gas velocity V_{sg} = 1; 5; 10 m/s
  superficial liquid velocity V_{sl} = 0.05; 0.1; 0.25; 0.5 m/s
  pressure p=2 bar (air-water), 4; 40; 75 bar (steam-water)
  Maximum mass flux (mass flow rate per unit area): $\dot{G}_{max} \approx 600$ kg/m^{2}s.
- The 3" pipe tests were made at $1 \lesssim V_{sg} \lesssim 10$ m/s with $0.5 \lesssim V_{sl} \lesssim 1.7$ m/s at pressures of 40 and 75 bar. The maximum mass flux was $\approx$ 1500 kg/m^{2}s. Most of the experiments were made at $\approx$ 1000 kg/m^{2}s.

Table 2.2 shows the two-phase test matrix in a map with the superficial velocities as coordinates. Some symbols are labeled with a vertical slash indicating that the radionuclide technique was also tested. There were performed 55 two-phase test points with the 5" pipe test section and 59 points with the 3" pipe test section. Additionally 23 single phase calibration points were made with the 5" pipe (12 points with cold water, 11 points with steam at 40 and 75 bar) and 7 points with the 3" pipe (steam, 40 bar).

As discussed later in detail, the flow pattern which occured in the two-phase flow experiments were characterized in general by a distinct stratification of the phases in the test section which complicates the

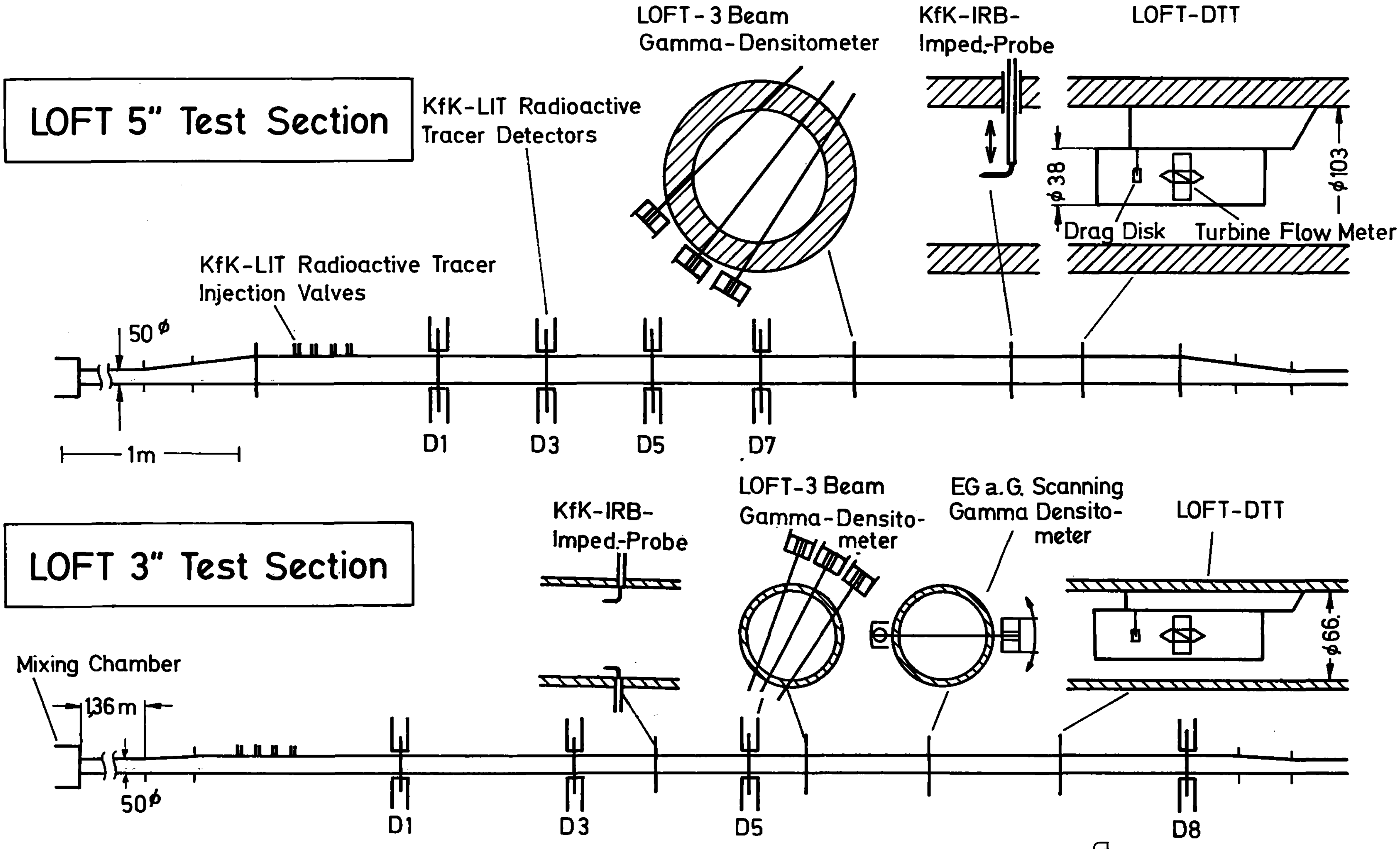

FIGURE 2.1 SCHEMATICAL SET UP OF TEST SECTION GEOMETRY AND MASS FLOW RATE INSTRUMENTATION

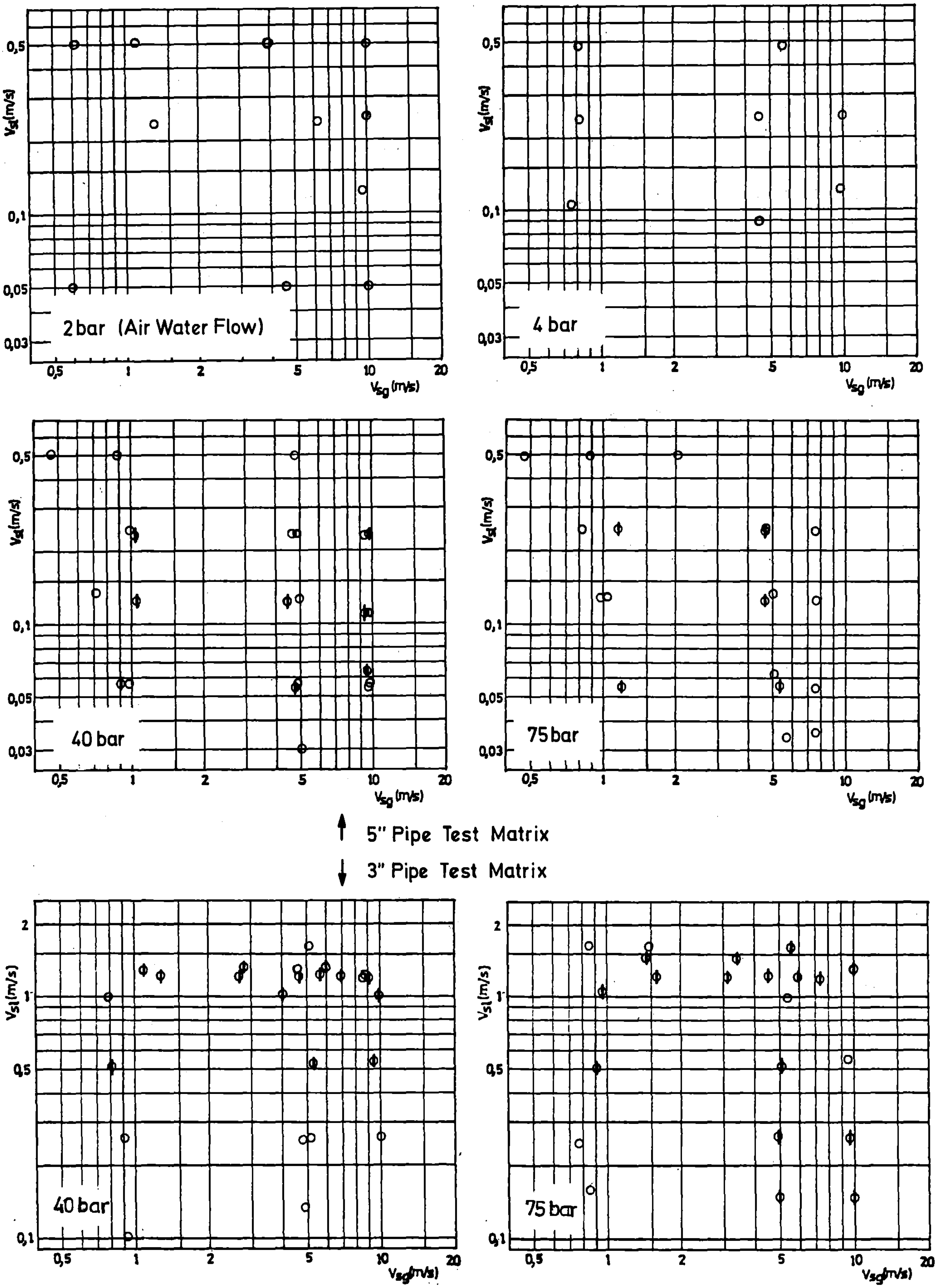

TABLE 2.2 TWO-PHASE TEST MATRIX FOR 5" AND 3" PIPE TESTS

analyses of signals from instruments measuring more or less locally in the cross section. These flow pattern are mostly different for the two test sections due to the different test matrix.

With these differences in test geometry and test matrix it is often convenient to discuss the 5" pipe and 3" pipe tests seperately. Of course, if possible, conclusions are drawn which can be generalized.

3. Results

The appendix contains a summary of the primary data for all test series. With these data the mass fluxes were evaluated using the following equations

$$\dot{G}_{\gamma-T} = \rho_\gamma V_T \quad (3.1)$$
$$\dot{G}_{\gamma-DD} = (\rho_\gamma (\rho V^2)_{DD})^{0,5} \quad (3.2)$$
$$\dot{G}_{T-DD} = (\rho V^2)_{DD}/V_T \quad (3.3)$$
$$G_{Rad-\gamma} = \alpha_\gamma \rho_g V_{Rg} + (1-\alpha_\gamma)\rho_1 V_{R1} \quad (3.4)$$

with V_T = turbine meter velocity

$(\rho V^2)_{DD}$ = drag disc momentum flux (kg/ms^2)

ρ_γ, α_γ = 3 beam densitometer density, void fraction, using a length weighting procedure

V_{Rg}, V_{Rl} = radiotracer phase velocities; measured between the detector positions $\overline{\text{D5-D7}}$ in the 5" pipe tests (Fig. 2.1) and interpolated from $\overline{\text{D3-D5}}$ and $\overline{\text{D5-D8}}$ on the densitometer position for the 3" pipe tests, respectively.

The Figures 3.1-3.4 show these mass fluxes as a function of the reference mass flux. Those test points having obviously incorrect instrument readings due to out of range measurements or other problems were excluded. A symbol with a vertical slash again indicates the test points where the radiotracer technique was included. There are the following tendencies:

- the mass fluxes evaluated with the combination of gamma densitometer and turbine meter $\dot{G}_{\gamma-T}$ are mostly higher than the reference values sometimes by a factor of 2. The scattering is quite large.

- the mass fluxes evaluated with the combination of gamma densitometer and drag disc $G_{\gamma-DD}$ have, for the 5" pipe a much higher accuracy associated with a smaller scattering. The 3" pipe tests results fall into two groups: one group with values slightly above the reference values, the other with values considerably below.
- the mass fluxes evaluated with the combination of turbine meter and drag disc G_{T-DD} generally too low for the 5" pipe tests and for a part of the 3" pipe tests. Again there are some values which are too high. The scattering of these results is large.
- the mass fluxes evaluated with the combination of radiotracer velocities and gamma densitometer $G_{Rad-\gamma}$ have a high accuracy. There is a small scattering around the correct value in the 5" pipe tests and a small scattering around a slightly too high value in the 3" pipe tests.

Regarding the pressure dependency, one observes that the scattering of data is much higher for the low pressure tests (air-water flow at ≈ 2 bar and steam-water flow at ≈ 4 bar) than that for the high pressure tests (steam-water flow at ≈ 40 bar and ≈ 75 bar).

Table 3.1 contains a summary of these results: $\bar{x}$ is the mean value, σ the standard deviation, N is the number of experiments without the obviously incorrect values, N_{total} is the total number of experiments with the corresponding instrumentation in operation. The line a) includes all experiments, the line b) the experiments where the radiotracer technique was also tested. Again the tendencies discussed are seen. The mass fluxes with the radiotracer and densitometer data were evaluated for all test points except the 7 points where the gamma densitometer obviously did not work satisfactorily. With this exception all data have about the same accuracy, including those data which belong to test points where both the turbine and drag disc were out of measuring range.

Assuming that the reference values are correct, the deviations of the results are caused by:

i: a physically wrong reading of the single instruments (instruments out of range, shift of transducers etc). The points where this obviously occurred were already omitted.

ii: the fact that the instruments are measuring more or less locally in the test section and that the instruments are located at different positions in the test section

iii: the equations used (3.1) - (3.3), because the equations are only correct for slip S = 1

These items are discussed in the following sections.

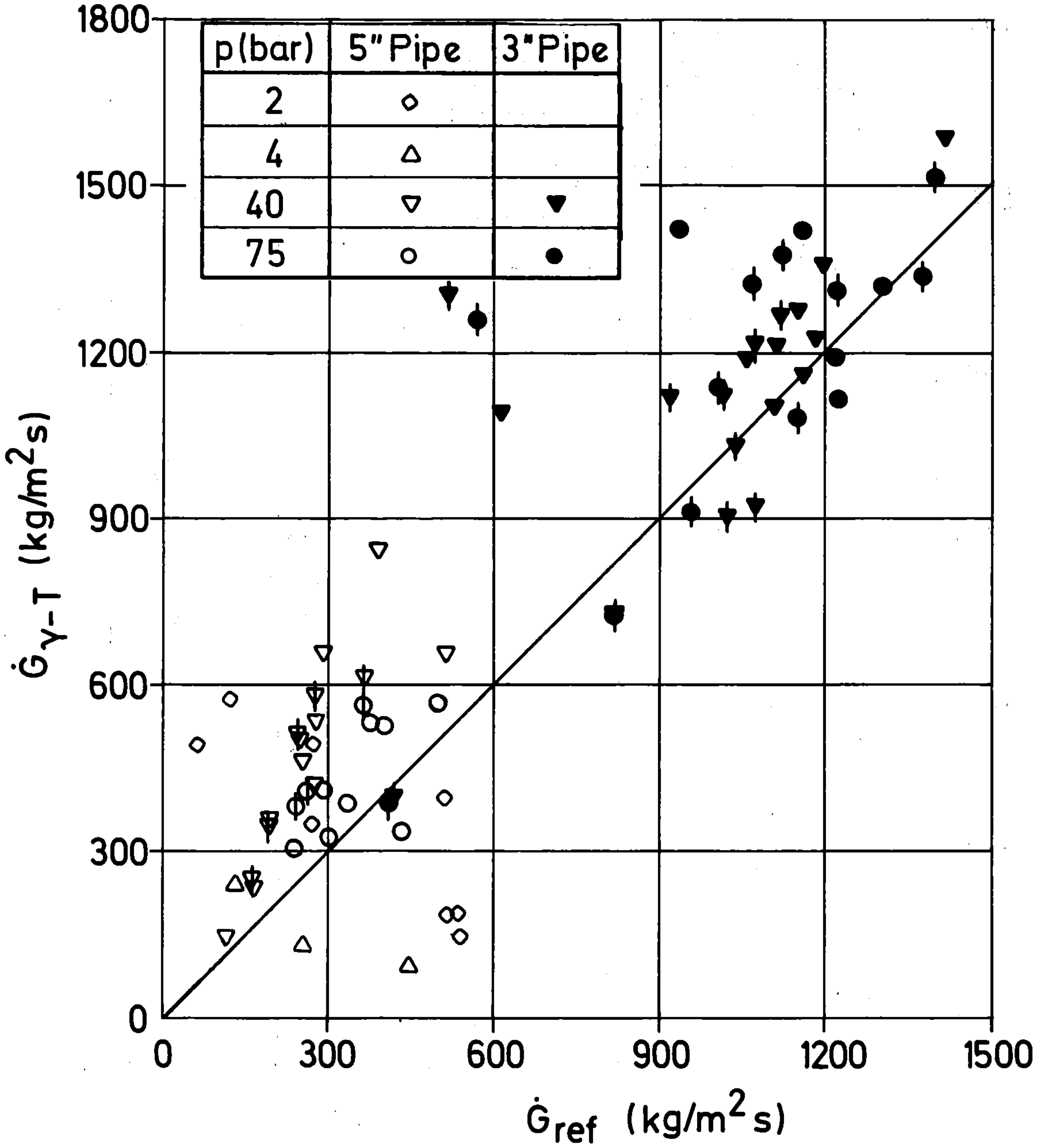

KfK

FIGURE 3.1 COMPARISON OF THE MASS FLUXES FROM THE COMBINATION GAMMA DENSITOMETER-TURBINE METER WITH THE REFERENCE MASS FLUXES

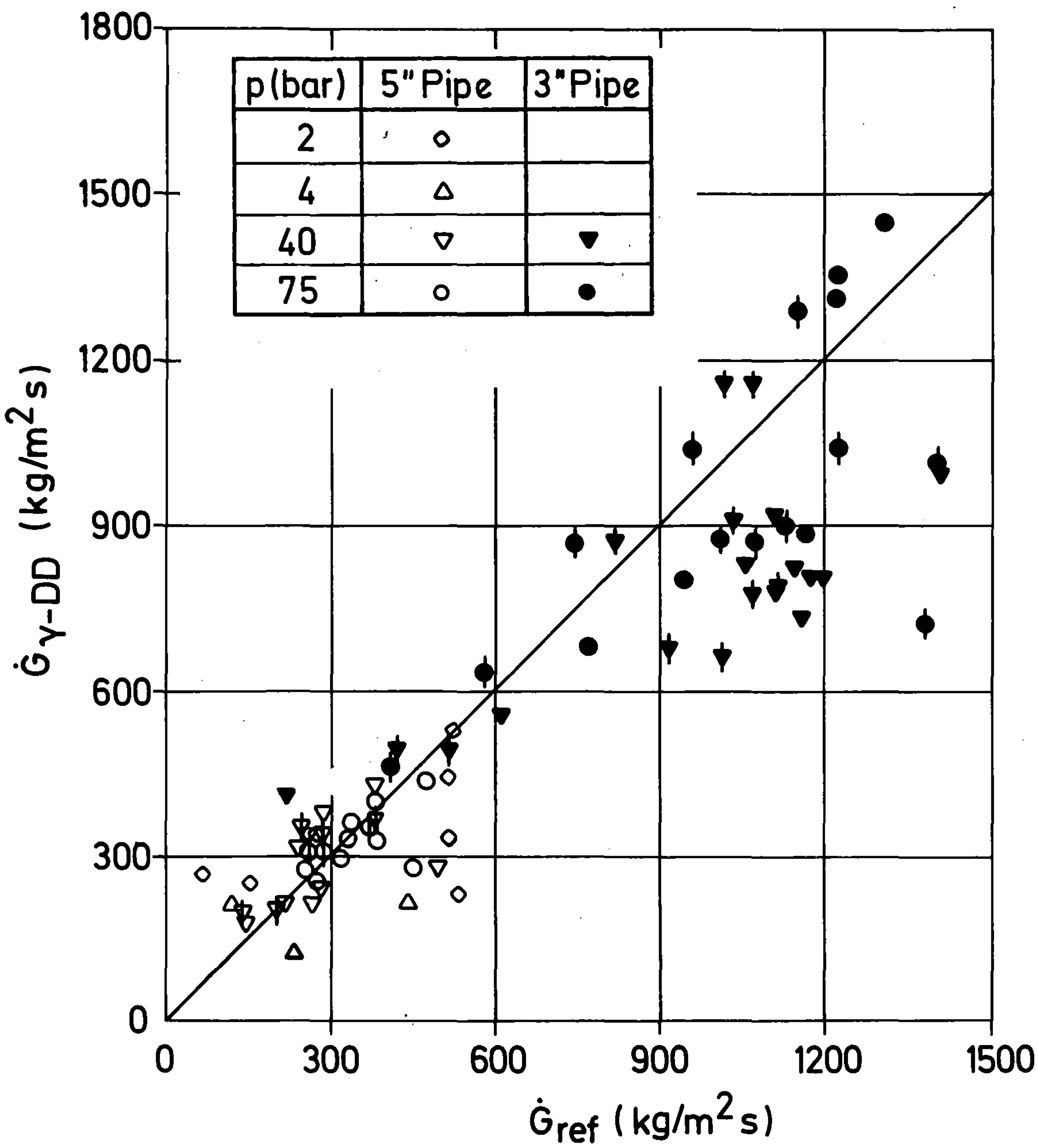

FIGURE 3.2 · COMPARISON OF THE MASS FLUXES FROM THE COMBINATION GAMMA DENSITOMETER-DRAG-DISC WITH THE REFERENCE MASS FLUXES

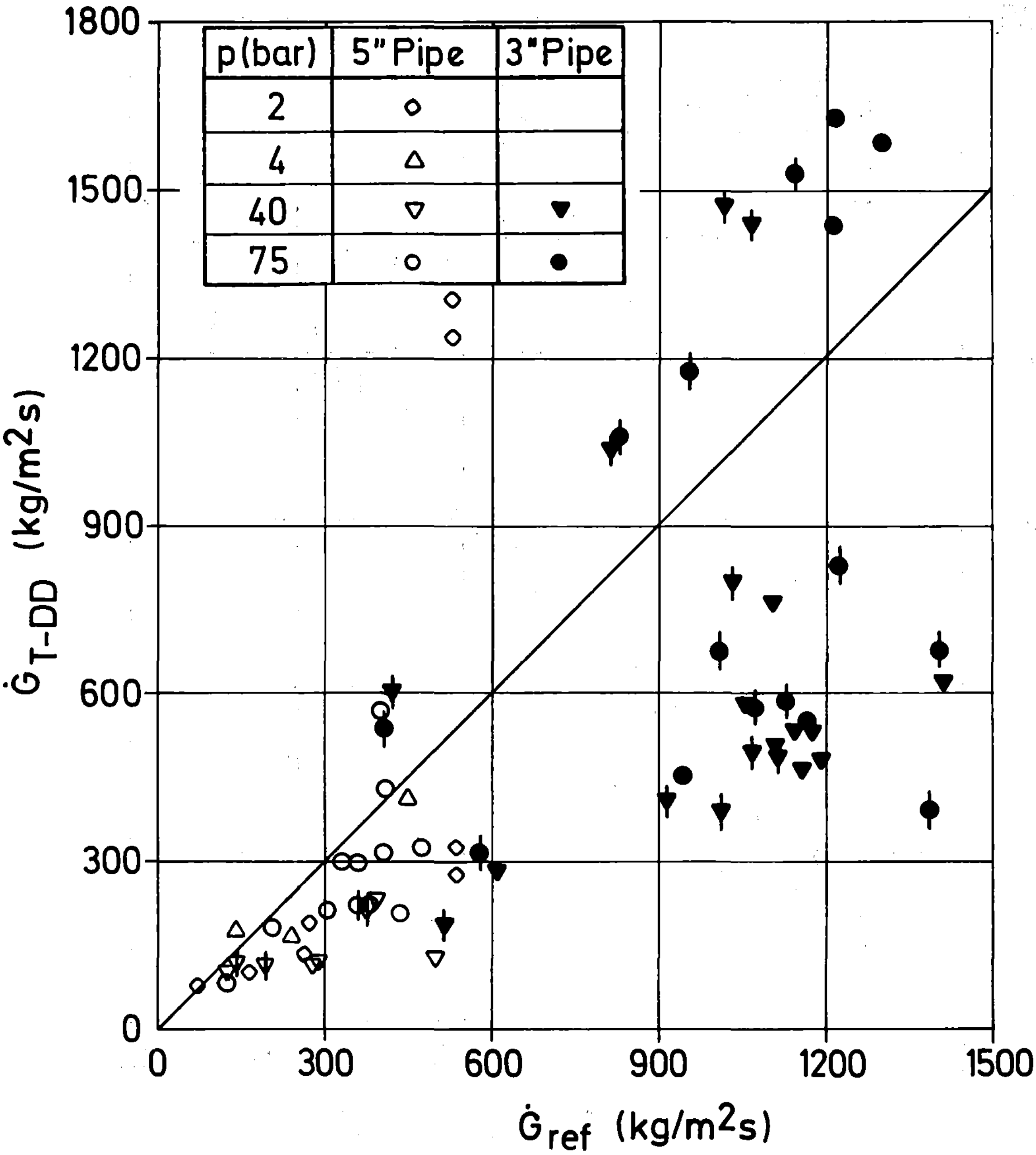

FIGURE 3.3 COMPARISON OF THE MASS FLUXES FROM THE COMBINATION TURBINE METER - DRAG DISC WITH THE REFERENCE MASS FLUXES

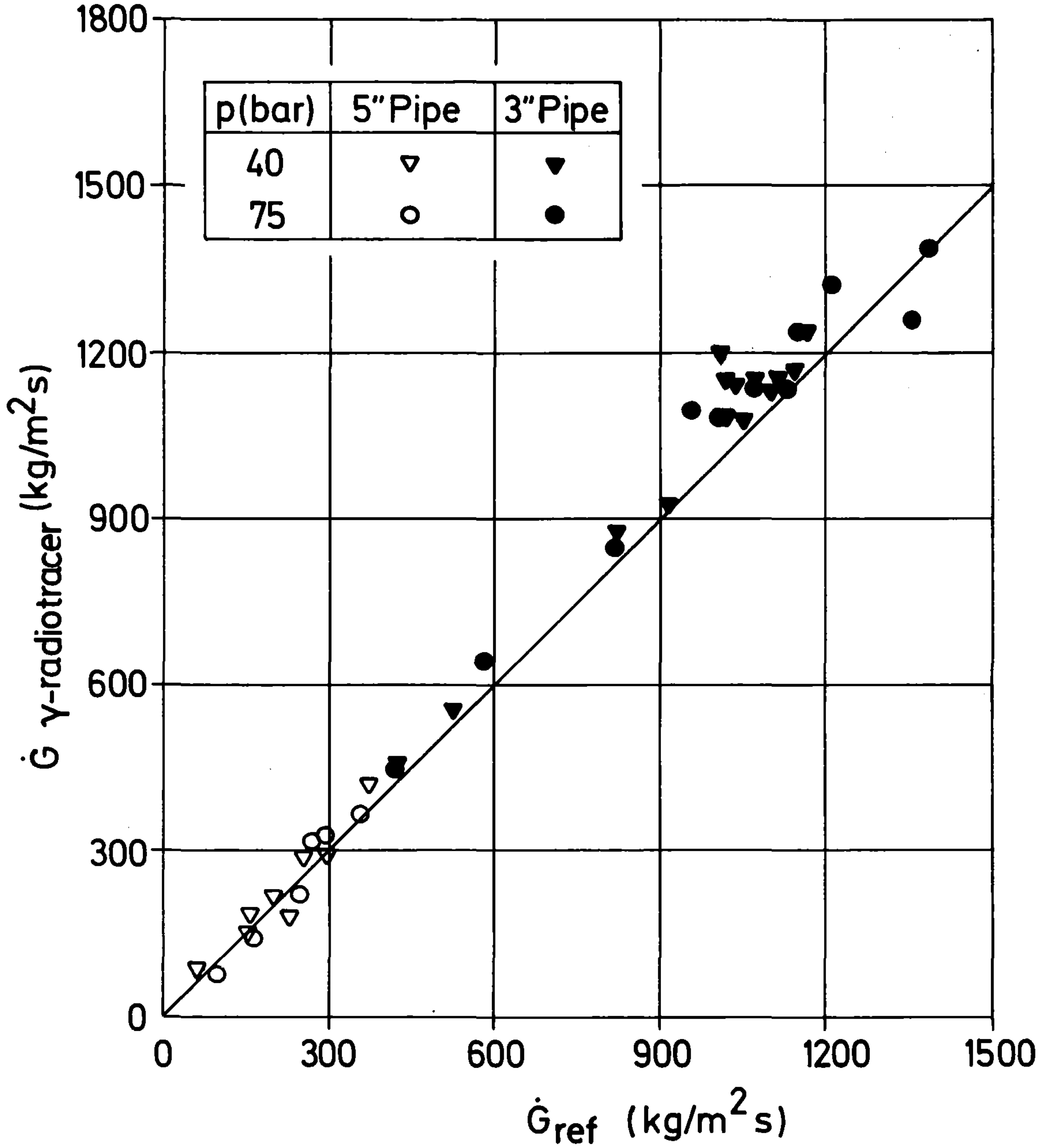

FIGURE 3.4 COMPARISON OF THE MASS FLUXES FROM RADIOTRACER AND GAMMA DENSITOMETER MEASUREMENTS WITH THE REFERENCE MASS FLUXES

			$\frac{G_{\gamma-T}}{G_{Ref}}$					$\frac{G_{\gamma-DD}}{G_{Ref}}$					$\frac{G_{T-DD}}{G_{Ref}}$					$\frac{G_{Rad-\gamma}}{G_{Ref}}$		
	p(bar)		2	4	40	75	40+75	2	4	40	75	40+75	2	4	40	75	40+75	40	75	40+75
5" Pipe Tests	$\bar{x}$	a	2,25	0,96	1,85	1,30	1,60	1,22	0,90	1,08	1,00	1,05	0,74	0,80	0,65	0,76	0,70	1,05	1,02	1,04
		b			1,93	1,56	1,79			1,17	1,07	1,13			0,71	0,74	0,72	1,03	1,08	1,05
	σ	a	2,51	0,98	0,30	0,23	0,39	0,80	0,63	0,23	0,08	0,18	0,25	0,22	0,19	0,13	0,18	0,11	0,08	0,09
		b			0,19	0,03	0,24			0,16	0,12	0,15			0,14	0,17	0,14	0,12	0,06	0,10
	N/N_{total}	a	$\frac{6}{11}$	$\frac{3}{8}$	$\frac{15}{23}$	$\frac{12}{19}$	$\frac{27}{42}$	$\frac{8}{11}$	$\frac{3}{8}$	$\frac{15}{23}$	$\frac{11}{19}$	$\frac{26}{42}$	$\frac{6}{11}$	$\frac{8}{8}$	$\frac{15}{23}$	$\frac{11}{19}$	$\frac{26}{42}$	$\frac{8}{8}$	$\frac{6}{6}$	$\frac{14}{14}$
		b			$\frac{5}{23}$	$\frac{3}{19}$	$\frac{8}{42}$			$\frac{5}{23}$	$\frac{3}{19}$	$\frac{8}{42}$			$\frac{5}{23}$	$\frac{3}{19}$	$\frac{8}{42}$	$\frac{5}{8}$	$\frac{3}{6}$	$\frac{8}{14}$
3" Pipe Tests	$\bar{x}$	a			1,18	1,14	1,16			0,83	0,92	0,87			0,67	0,87	0,76	1,07	1,07	1,07
		b			1,19	1,15	1,17			0,86	0,88	0,87			0,72	0,81	0,76	1,07	1,07	1,07
	σ	a			0,39	0,32	0,35			0,18	0,18	0,18			0,39	0,38	0,40	0,05	0,06	0,05
		b			0,44	0,34	0,39			0,19	0,18	0,18			0,42	0,38	0,40	0,05	0,06	0,05
	N/N_{total}	a			$\frac{19}{19}$	$\frac{16}{16}$	$\frac{35}{35}$			$\frac{19}{25}$	$\frac{16}{23}$	$\frac{35}{48}$			$\frac{19}{19}$	$\frac{16}{16}$	$\frac{35}{35}$	$\frac{15}{18}$	$\frac{12}{16}$	$\frac{27}{34}$
		b			$\frac{15}{19}$	$\frac{12}{16}$	$\frac{27}{35}$			$\frac{15}{25}$	$\frac{12}{23}$	$\frac{27}{48}$			$\frac{15}{19}$	$\frac{12}{16}$	$\frac{27}{35}$	$\frac{15}{18}$	$\frac{12}{16}$	$\frac{27}{34}$

$$\bar{x} = \frac{1}{n}\sum_{i=1}^{n} x_i \qquad \sigma = \left(\left(\Sigma x^2 - (\Sigma x)^2/n\right)/(n-1)\right)^{0.5}$$

TABLE 3.1 MEAN VALUES OF VARIOUS MASS FLOW RATE RATIOS

4. Analysis of the Two-Phase Flow in the Test Section

4.1 Flow Regimes and Phase Distribution in the 5" Pipe

For the interpretation of the signals of the single instruments the knowledge of the local two-phase flow parameters such as phase distribution in the cross section and slip is of great importance.

With the traversable impedance probe both the determination of flow regime and the measurement of a vertical void fraction profile are obtained (details of this technique in /3/, /4/). Additionally, the signals of the single beams of the gamma densitometer supplied information on the flow regime, and, with some assumptions, on the phase distribution. In this investigation, flow regime determination was based on impedance probe data due to the local measurements at many positions and the capability to detect small droplets (low density range) which is important in characterizing flow regimes. The gamma beam signals served as an additional check.

The Figures 4.1-4.4 show for some test points the time dependency of the impedance probe signals at different positions and the signals of the single gamma beams. The upper level of an impedance probe signal is indicating the gas phase, the lower level the liquid phase. An increasing gamma beam signal corresponds to an increasing water level. The impedance probe signal with the vertical position underlined is taken simultaneously with the gamma beam signals.

At low values of the superficial velocities $V_{sg} \lesssim 1$ m/s, $V_{sl} \gtrsim 0.125$ m/s) the phases were strongly separated. There were low frequency waves (typical frequency ≈ 0.2 Hz) with small amplitudes and a small bubble entrainment near the interface. Figure 4.1 shows an example of this flow pattern characterized as <u>stratified-wave flow.</u>

With increasing V_{sg} and V_{sl} the low frequency waves disappear. At steam-water flow at p$\approx$ 40 and $\approx$ 75 bar (high gas density) the interface became wavy (high frequency waves with small amplitudes); the bubble entrainment increased, some droplet entrainment occurred in the vicinity above the interface (Figure 4.2). This flow pattern is called <u>wave flow.</u> At low pressure (air-water flow at $p \approx 2$ bar and steam water flow at $p \approx 4$ bar) distinct waves existed with frequencies of $\lessapprox 1$ Hz and higher amplitudes (Figure 4.3) which caused a higher entrainment in both phases.

The flow pattern at $5<V_{sg}<10$ m/s is characterized as wave-droplet flow due to the increased number of droplets. At high pressure this entrainment is still restricted to a limited region above the interface. At low pressure the interface seemed to be rougher which causes a higher droplet production. At $V_{sg} \approx 10$ m/s sometimes droplets were detected even near the top of the pipe. The deposition of these droplets causes a thin eccentrical liquid film, and the transition to the annular droplet flow region is reached. Figure 4.4 shows an example of a test point at a high superficial gas velocity.

Figure 4.5 contains a comparison of the flow chart based on the experiments at 40 and 75 bar with the flow chart of Govier and Aziz /5/. There are differences in the range of high values of V_{sl} where from /5/ slug flow is predicted. The fact that in these experiments no slug flow occurred may have several reasons:

(i) Most of the flow charts are based mainly on air-water data from pipes with small diameters ($d < 50$ mm). Therefore it is not predicted correctly that (a) the slug flow region in steam-water flow becomes smaller with increasing pressure (as observed e.g. by /4/), (b) the flow boundaries depend on the pipe diameter: an increasing pipe diameter favors phase separation which shifts the boundary to slug flow to higher values of V_{sl} (described theoretically by Taitel and Dukler /6/).

(ii) There may be a considerable influence from the eccentrical expansion pieces which cause a phase separation at the test section inlet.

As shown with the impedance probe signals the waves were more strongly developed at low pressure than at high pressure. This tendency is also described by the model of Taitel and Dukler /6/ and this is the reason why the slug flow region is reached earlier at low pressures.

Because the signal analysis is concentrated on the high pressure data, these effects have not been investigated further.

Table 4.1 shows a summary of the 5" pipe tests where impedance probe data were available. The impedance probe signals from the air-water experiments were only used for the detection of flow regime, for the other experiments also the vertical void profile was measured. The column with the label $(y/d)_{\alpha=0}$ designates the height below which no gas was detected; $(y/d)_{\alpha=1}$ the height above which droplets no longer were detected; $(y/d)_{IF}$ the heigth of the interface level evaluated by the following way:

$$(y/d)_{IF} = \int_0^1 \alpha d(y/d)$$

This interface level corresponds to the height of the water level if both phases are totally separated. In the columns $IF_{Imp.pr}$ and $IF_{\gamma\text{-dens}}$ the interface levels, using the definition given in chapter 5.1, from the impedance probe and gamma densitometer are compared. The agreement of the last two columns is very good at low values of V_{sg}. With increasing V_{sg} the droplet entrainment increases. The deposition of droplets at the pipe wall is only measured by the gamma beams, and results in a lower void fraction than indicated by impedance probe data. Figure 4.6 shows the vertical void fraction profiles. At the same values of V_{sg} and V_{sl} the profiles at $p \approx 40$ and 75 bar agree very well; at $p \approx 4$ bar the profiles deviate due to the stronger wave formation.

4.2 Flow Regimes in the 3" Pipe

In these experiments two fixed impedance probes were used with a distance of ≈ 5 mm above the bottom and below the top of the pipe, respectively. Because two measuring positions do not give the same amount of information as a traversable probe, the time dependent signals of the gamma densitometer and the DTT were also used.

Table 4.2 shows the results. The values in the columns labeled with f show low frequency events; which occured at the upper probe location typical for slug flow. In these experiments some examples of elongated bubble flow also occurred, in form of long, well defined bubbles in the upper portion of the pipe.

Figure 4.7 shows the boundaries of the flow regimes. A distinction between wave and wave droplet flow is not made. In the parameter range where experiments were carried out with both test sections, the flow regime boundaries of the two test sections agree quite well. Therefore one single flow chart is proposed for all experiments. In the velocity range of V_{sl}>1 m/s and $0.7 \lesssim V_{sg} \lesssim 6$ m/s the flow pattern is dependent on pressure (similar tendencies as in /4/): at 40 bar slug flow is often detected, at 75 bar a wavy droplet flow (except test Nr. 6060) instead.

4.3 Axial Distribution of the Phase Velocities

As mentioned before, the eccentric expansion pieces caused a separation of the two-phase mixture at the test section inlet depending on the superficial velocities in the inlet pipe. At high superficial liquid velocities and low superficial gas velocities it is assumed that the phases were flowing quite separated through the inlet pipe. Passing the expansion section, the liquid phase was not much disturbed and came into the test section with a velocity not much smaller than that in the 50 mm pipe. The gaseous phase was decelerated much more by the cross section increase, and caused a slip S < 1 at the beginning of the test section. In the test section, the liquid phase was gradually decelerated (e.g. by wall friction) and the slip increased.

At high void fractions, an annular droplet flow is supposed to occur in the inlet pipe. In this case the liquid is decelerated much faster in the test section inlet and the slip reaches an almost constant value after a shorter flow length.

Figure 4.8 shows some examples of the axial phase velocity distributions measured with the radiotracer technique. At the low superficial velocities of the 3" pipe tests the slip at position $\overline{D1-D3}$ is still less than 1 and becomes greater than 1 at position $\overline{D3-D5}$. The phase velocities are extrapolated up to the position of the DTT. In most cases the phase velocities and with this the density (void fraction) are slightly different between the position of the densitometer and the DTT which gives rise to an error if the signals are combined. In addition, the figure contains the phase velocities evaluated with the gamma densitometer void fraction and the reference velocities and the velocity measured by the turbine.

4.4 Slip at the Position of the Gamma Densitometer

A very important quantity for further discussion is the slip S. Figure 4.9 shows slip values, drawn in the flow chart, calculated with the densitometer void fraction and the reference superficial velocities by

$$S = (V_{sg}/V_{sl})(1-\alpha_\gamma)/\alpha_\gamma$$

The values below $V_{sl} \tilde{=}$ 0.5 m/s belong to the 5" pipe tests (except the points indicated with a subscript); all values above V_{sl} > 0.5 m/s belong to the 3" pipe tests. The following tendencies are observed: slug flow regime slip is about 1.8, in wave droplet regime slip increases with decreasing V_{sl}; the highest slip values are are reached in the transition zone from wave to annular droplet flow. In this region slip is considerably dependent on pressure and density ratio, respectively: slip decreases with increasing pressure.

At $V_{sg} \lessapprox$ 1 m/s and high values of V_{sl}, the 5" pipe test points show values of S < 1. In this low range of V_{sg} the measuring accuracy of V_{sg} could be low. The fact that here the air-water and steam-water data at all pressures agree quite well is a check for the good measuring accuracy of the reference data also in this range. The 3" pipe test points at $V_{sl} \approx$ 0.5 m/s show higher slip values than these in the 5" pipe tests due to the smaller area change at the test section inlet and the higher L/D ratio.

In the test of the LOFT Modular DTT /11/ an 80 mm diameter inlet was used in connection with the 3" pipe test section. This caused quite opposite inflow effects compared with the 50 mm inlet pipe. Nevertheless a comparison of slip at the densitometer position in a map with superficial velocities as coordinates (similar to Figure 4.9) did not show a significant dependence on the inflow conditions. From this it may be concluded that the two-phase flow at the densitometer position is already quite well developed.

Figure 4.10 shows the slip as a function of the interface level $(y/d)_{IF}$ and the void fraction, respectively. The 5" pipe tests show a much higher scattering than the 3" pipe tests due to the larger variation of pressure and flow regime.

Omitting the 5" pipe tests at $V_{sg} \lesssim 1$ m/s (DTT below its measuring range, see Chapter 5), these discussions on the flow conditions in the test section may be summed up as follows:

The 5" pipe tests are characterized by:
- low mass fluxes ($\dot{G} \lesssim 600$ kg/m^{2}s)
- high void fractions ($\alpha_{typical} \approx 0.9$)
- strongly stratified flow patterns associated with considerable slip ($S \lesssim 6$ for steam-water flow at p = 40 and 75 bar)

The 3" pipe tests are characterized by:
- medium mass fluxes ($\dot{G} \lesssim 1500$ kg/m^{2}s)
- medium void fractions ($\alpha_{typical} \approx 0.65$)
- less stratified flow patterns associated with smaller slip values ($S \lesssim 3$).

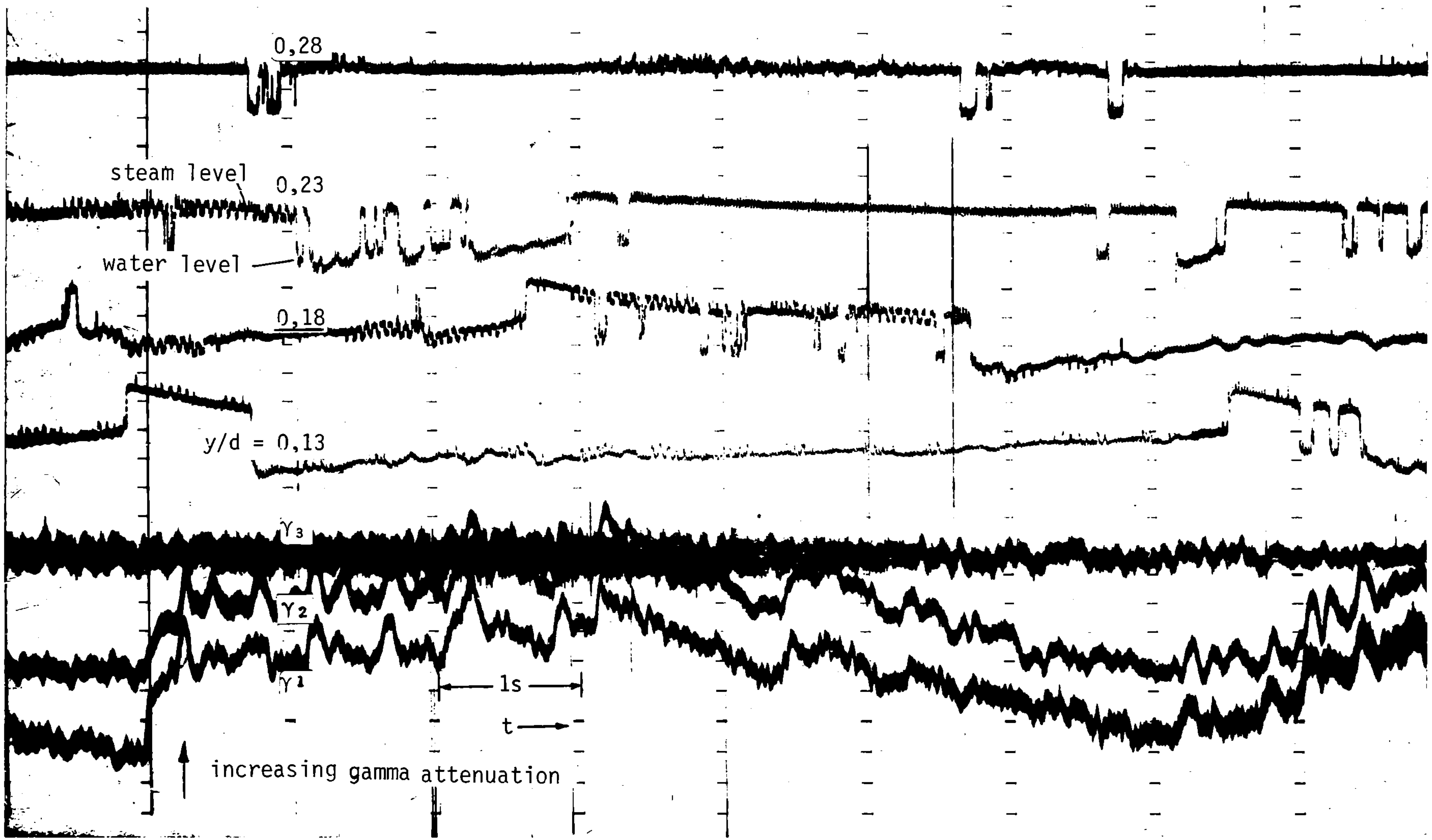

FIG. 4.1 TEST NR. 5041: IMPEDANCE PROBE AND γ-BEAM SIGNALS

(P = 40,8 BAR, V_{SG} = 0,72 M/S, V_{SL} = 0,135 M/S)

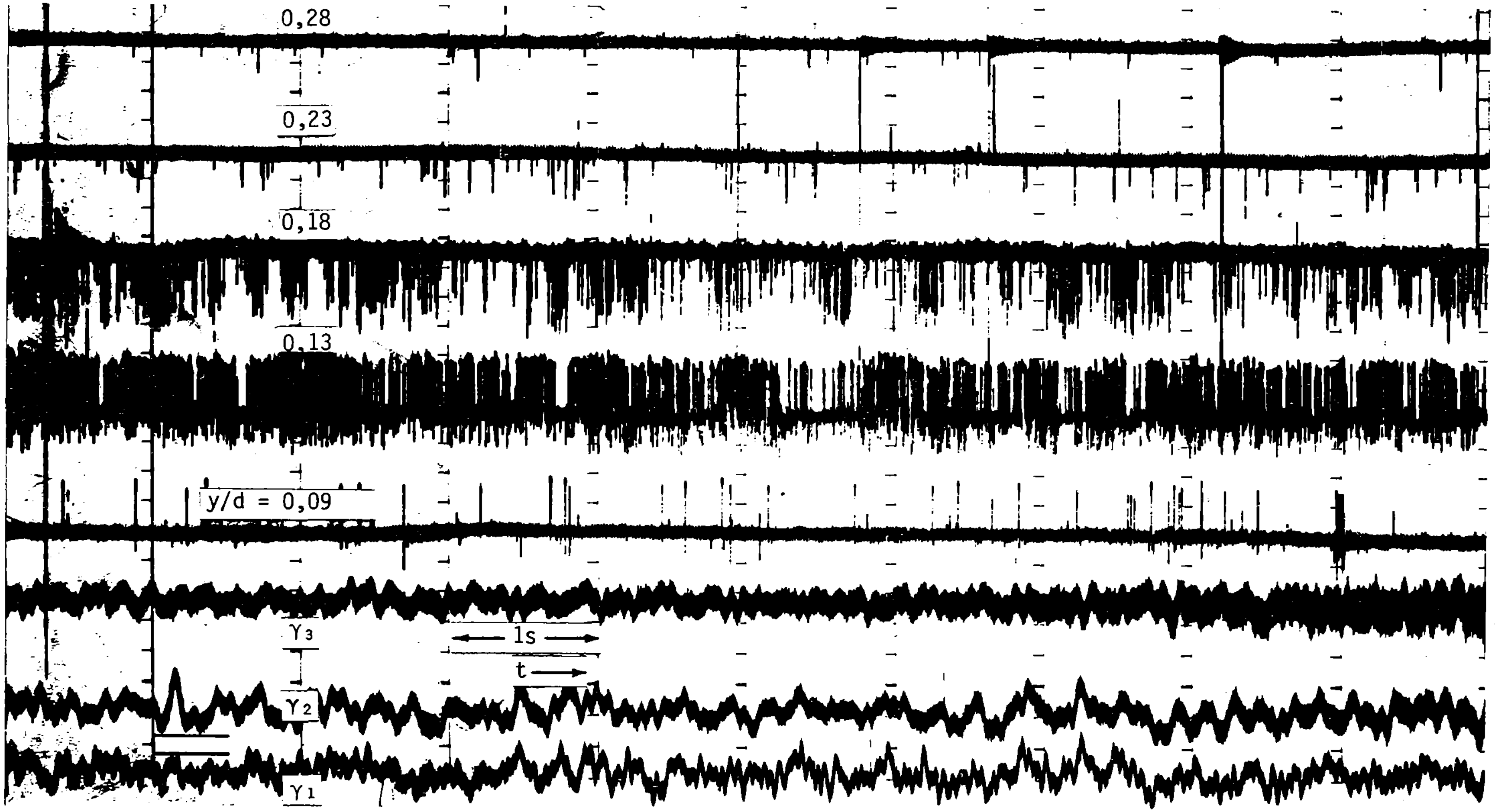

FIG. 4.2 TEST NR. 5066: IMPEDANCE PROBE AND γ-BEAM SIGNALS
(P = 75,5 BAR, V_{SG} = 4,79 M/S, V_{SL} = 0,229 M/S)

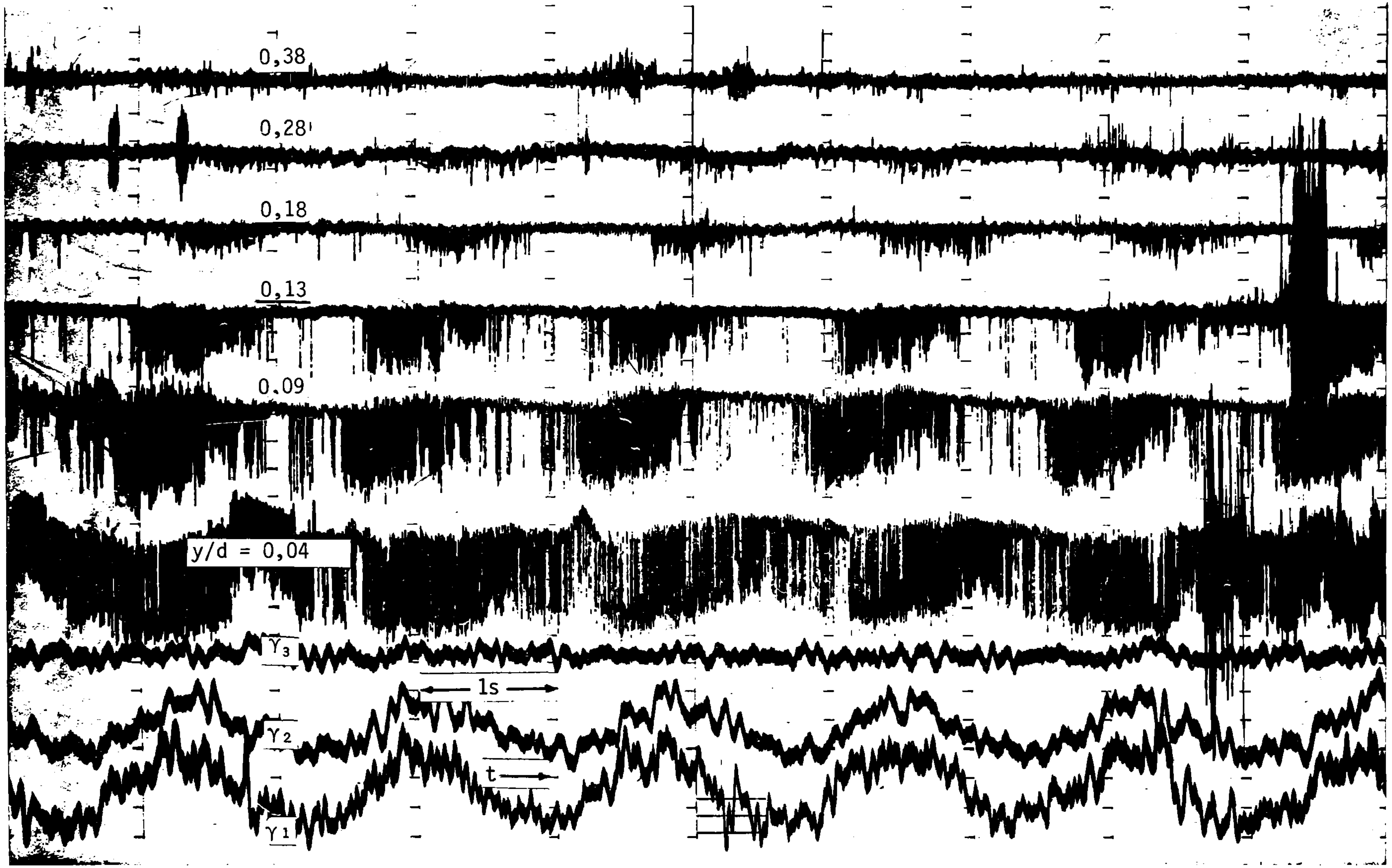

FIG. 4.3 TEST NR. 5031: IMPEDANCE PROBE AND γ-BEAM SIGNALS
(p = 4,4 BAR, v_{SG} = 5,84 M/S, v_{SL} = 0,478 M/S)

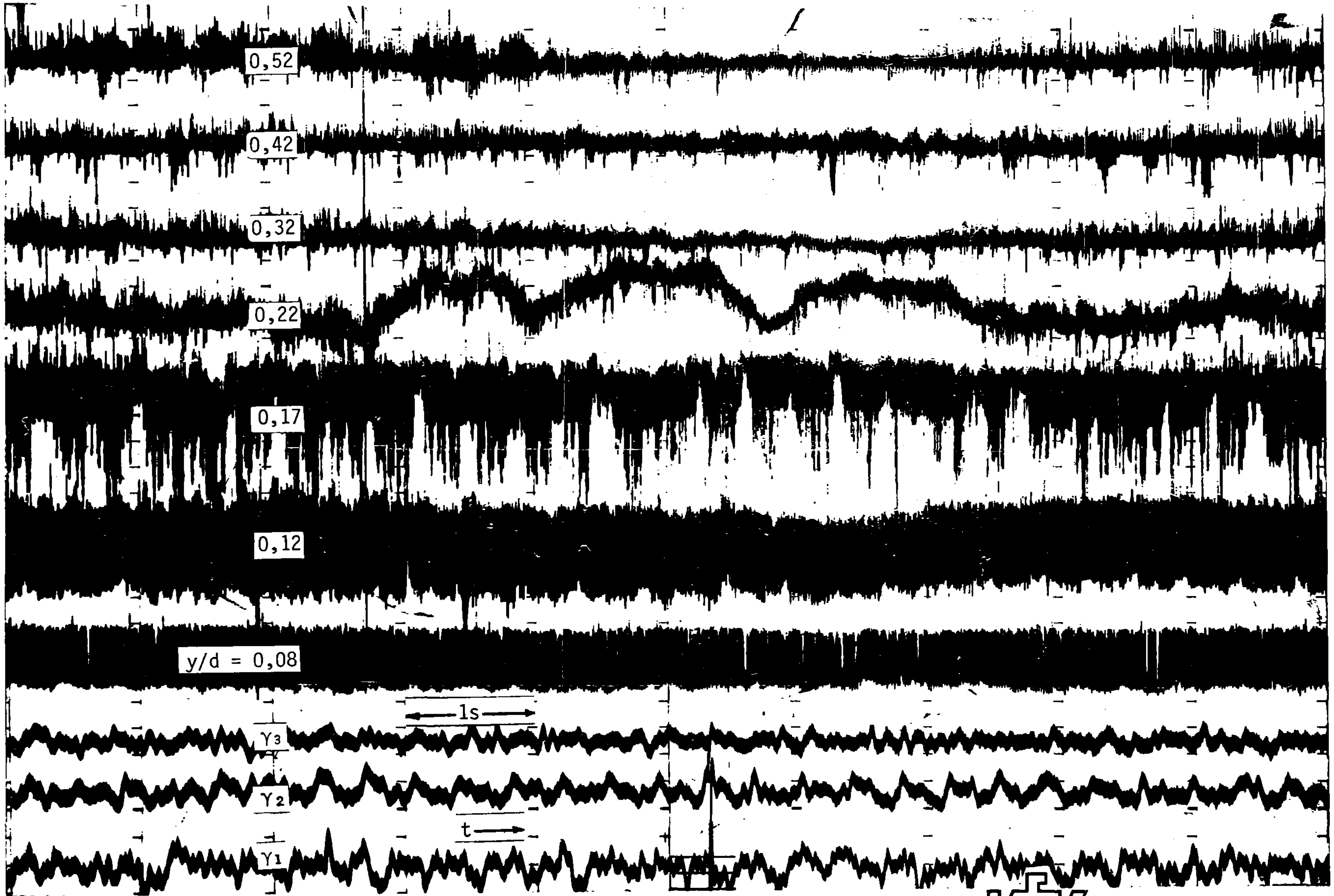

FIG. 4.4 TEST NR. 4211: IMPEDANCE PROBE AND γ-BEAM SIGNALS
(P = 2,1 BAR, V_{SG} = 10,39 M/S, V_{SL} = 0,250 M/S)

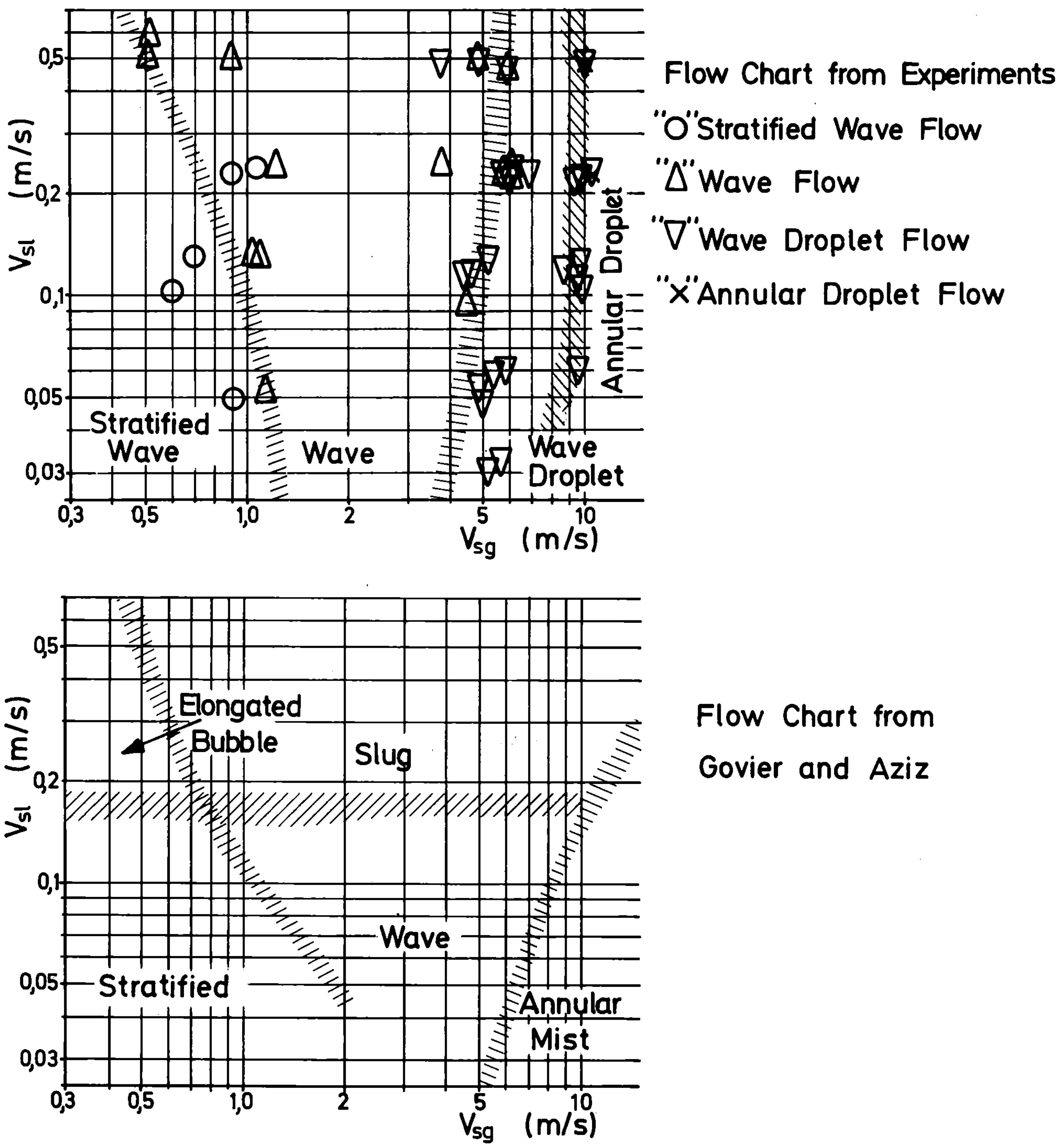

FIGURE 4.5 FLOW REGIMES IN THE 5" PIPE (50 MM DIAMETER INLET)

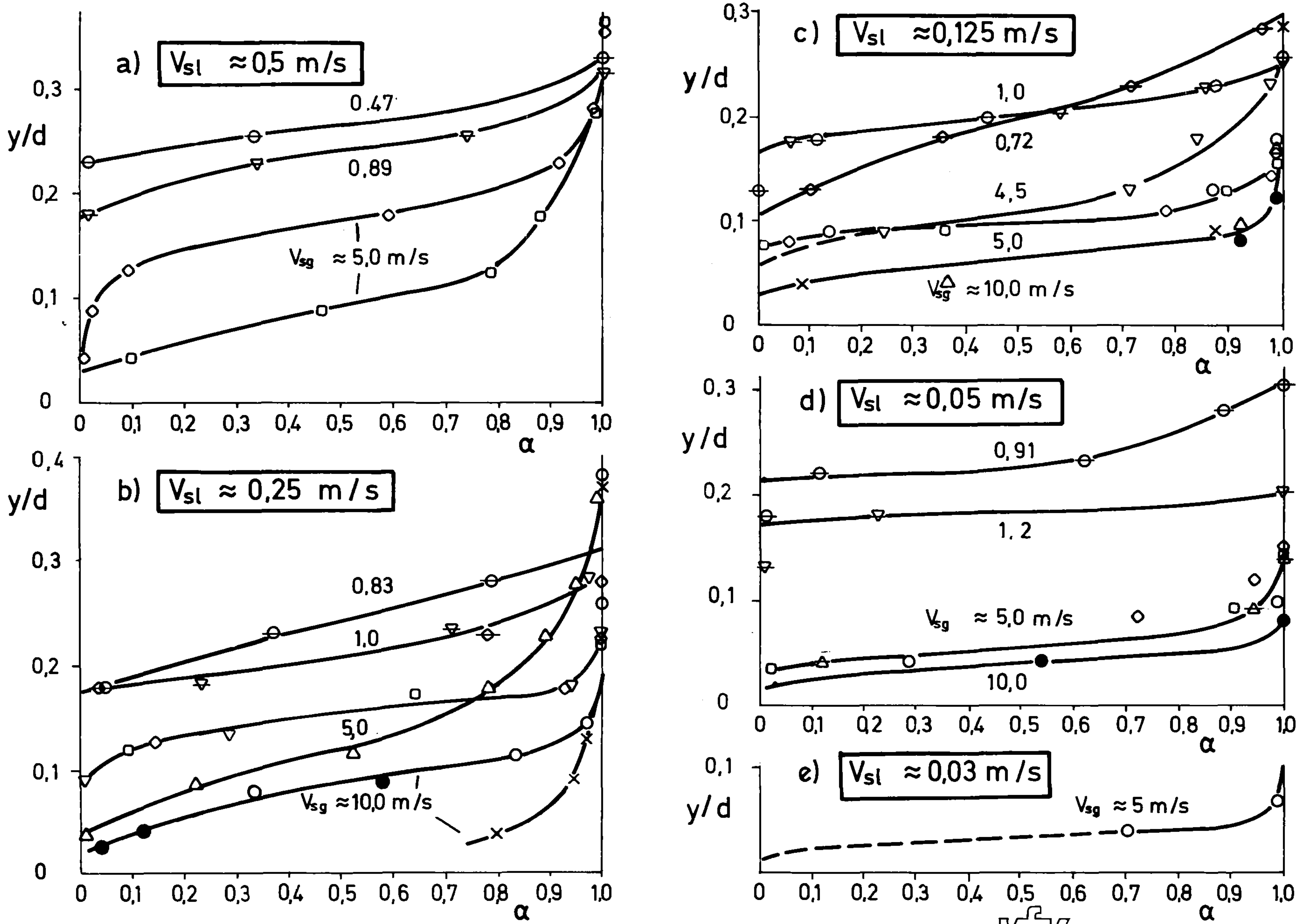

FIGURE 4.6 VOID FRACTION PROFILES FROM THE IMPEDANCE PROBE (5" PIPE TESTS)

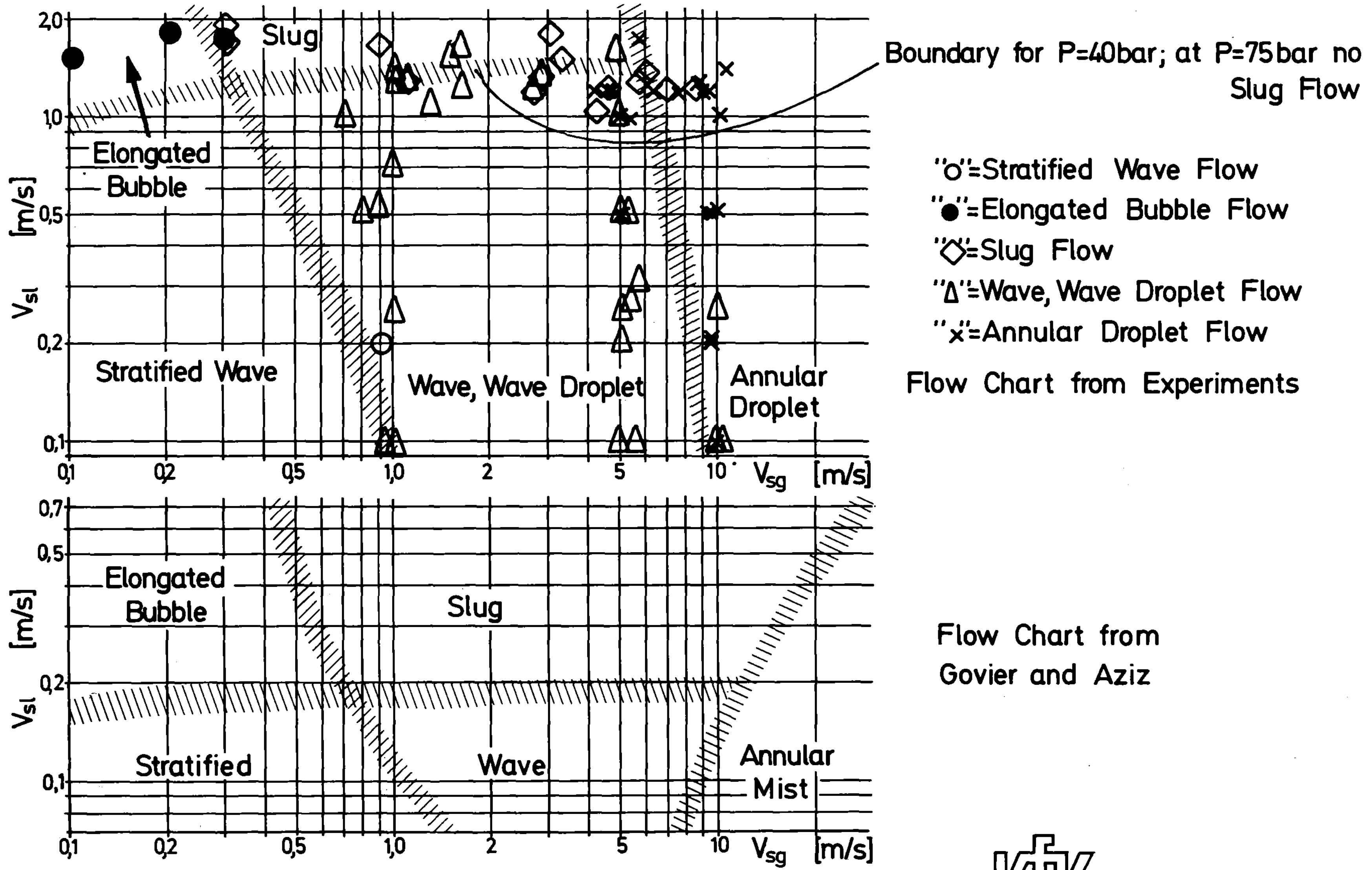

FIGURE 4.7 FLOW REGIMES IN THE 3" PIPE (50 MM DIAMETER INLET)

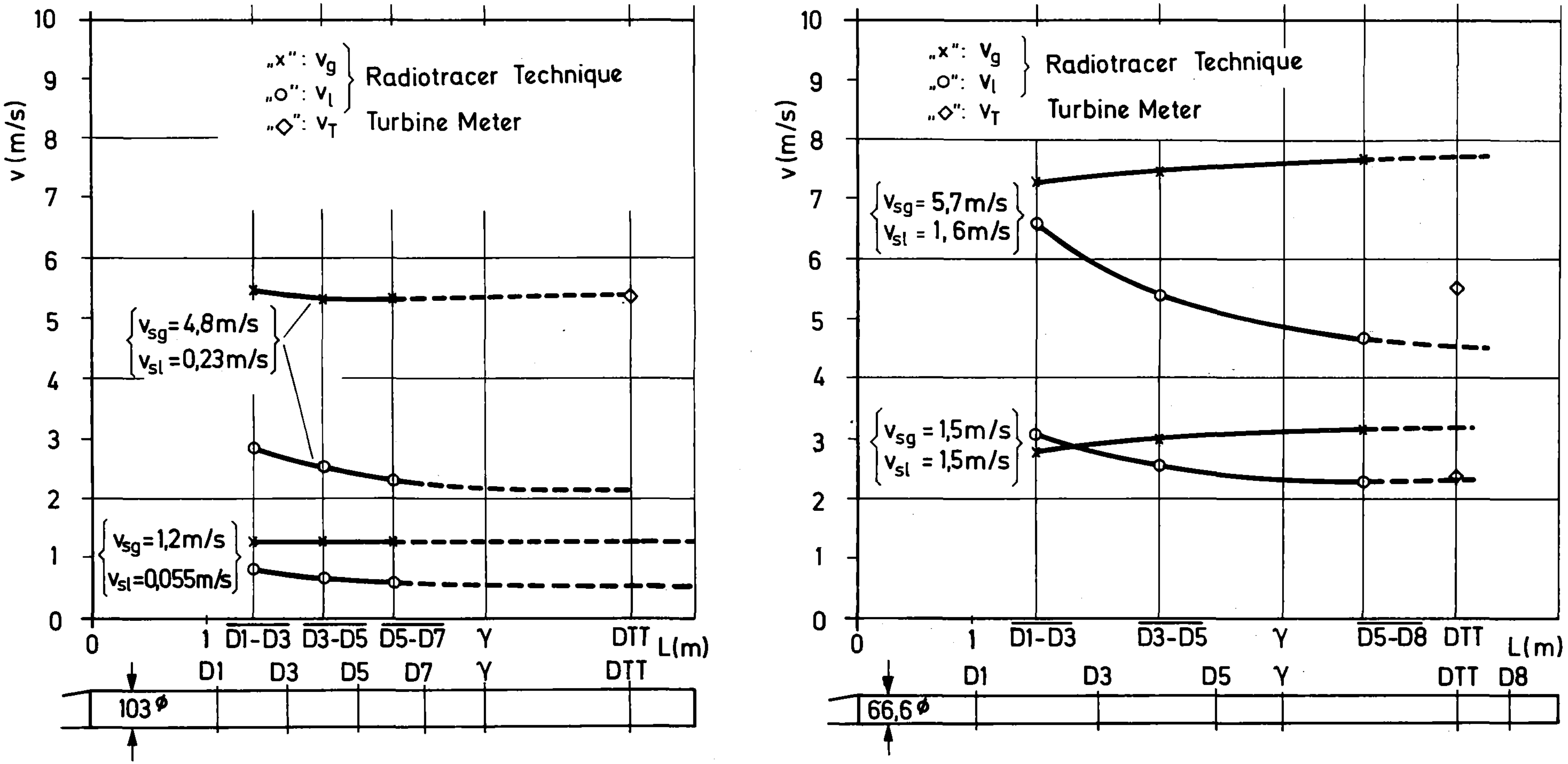

FIGURE 4.8 AXIAL DISTRIBUTION OF PHASE VELOCITIES FROM RADIOTRACER MEASUREMENTS

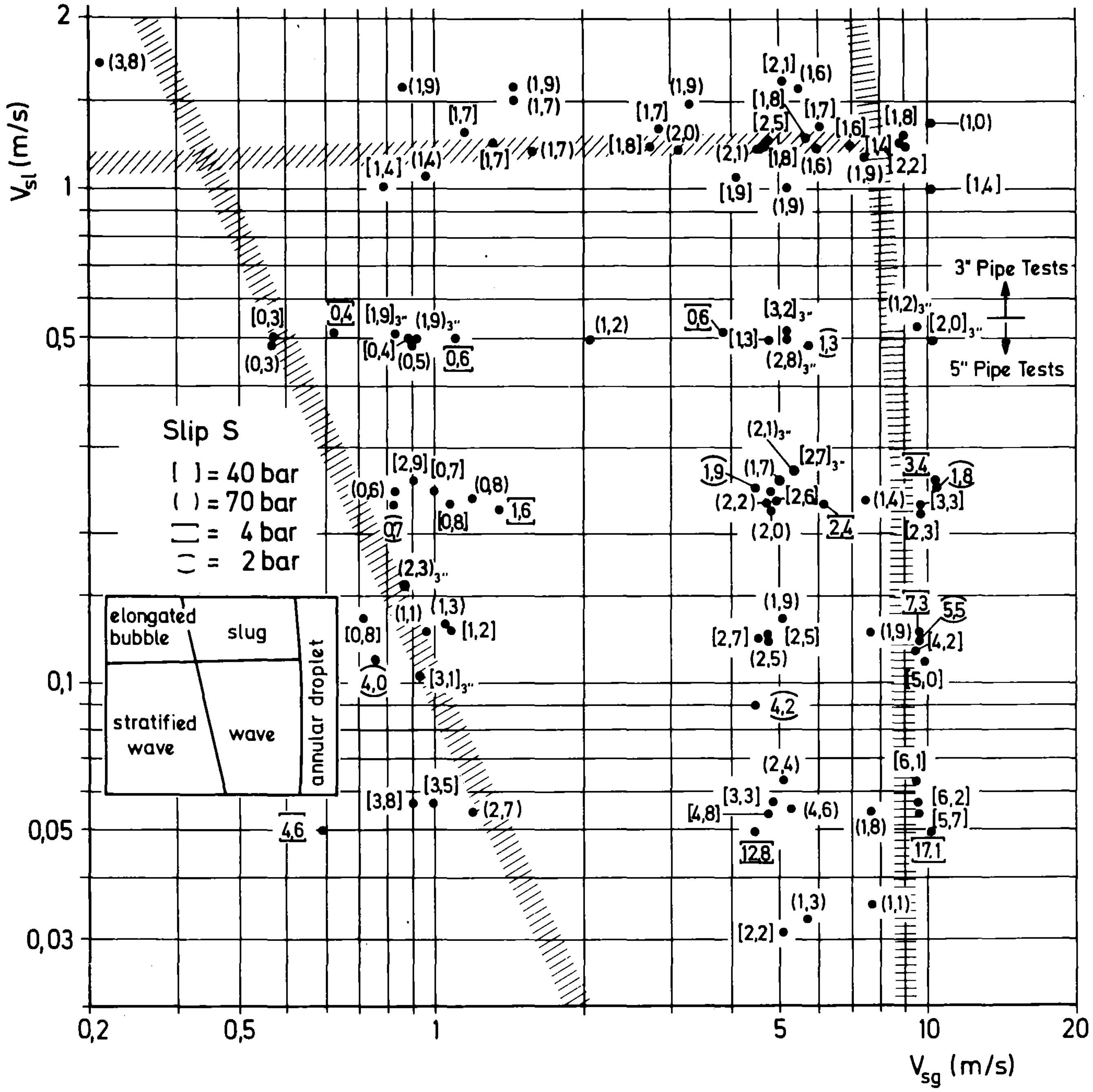

FIGURE 4.9 SLIP AS FUNCTION OF FLOW REGIME

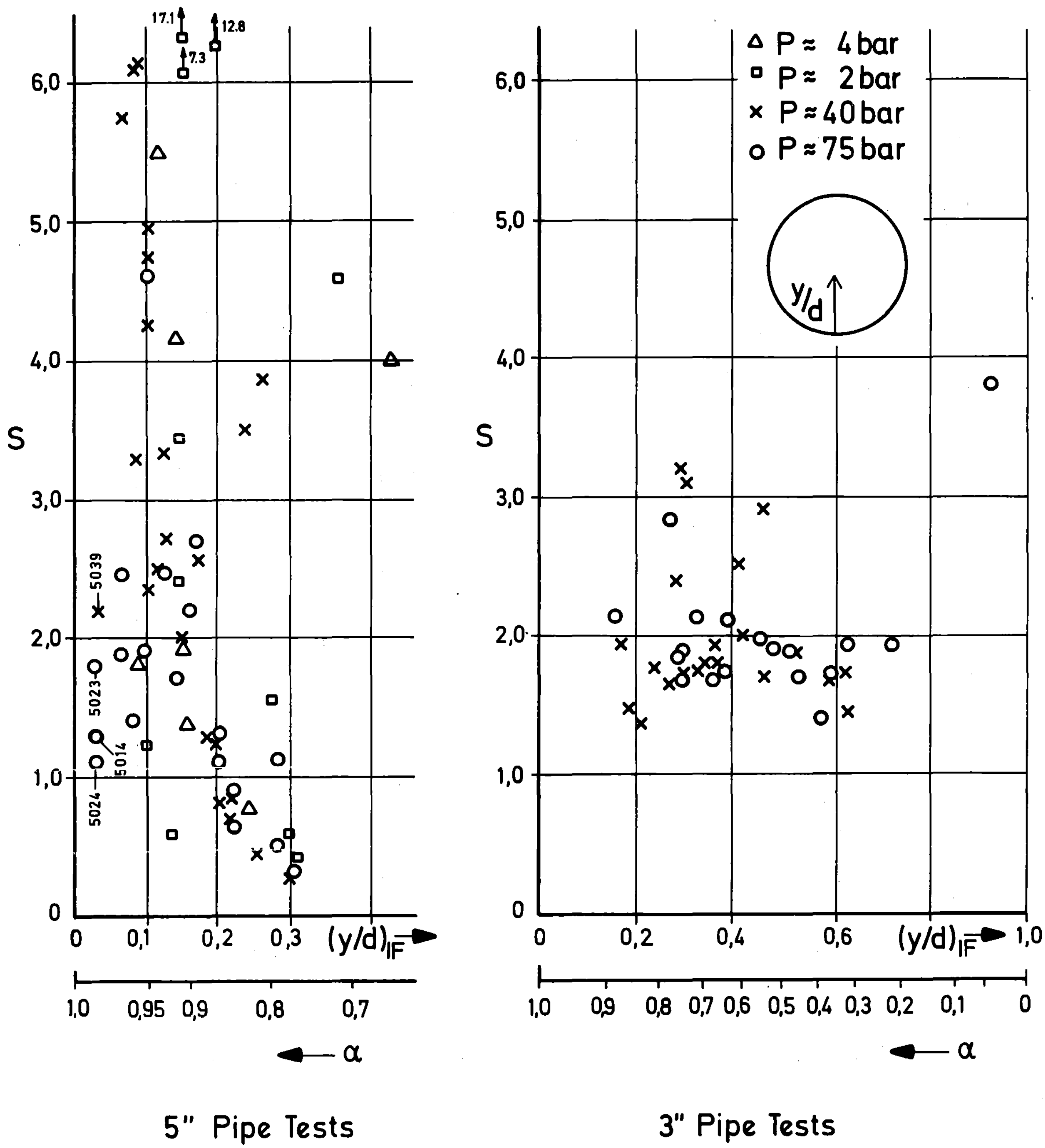

FIGURE 4.10 SLIP AS FUNCTION OF VOID FRACTION AND INTERFACE LEVEL

Fig.12	10					(y/d) Imp.Pr.			IF (%)		
Fig.	Symbol	Test Nr.	p(bar)	V_{SL}(m/s)	V_{SG}(m/s)	α ≡ 0	IF	α ≡ 1	Imp.Pr	γ-Dens.	Flow-Pattern
a	-○-	5046	39,8	0,505	0,50	0,23	0,27	0,33	-12,5	-9,0	W
		4216	2,0	0,620	0,52						W
	-▽-	5045	40,7	0,503	0,90	0,13	0,24	0,28	-20	-19,4	W
		4215	2,0	0,515	1,12						W
		4214	2,0	0,515	3,90						WD
	◇	5044	40,5	0,498	4,80	0,04	0,18	>0,48	-37	-37,3	W - WD
	□	5031	4,4	0,478	5,84	<0,04	0,13	>0,9	-50	-43,4	W - WD
		4213	2,0	0,500	10,29						WD- AD
b	-○-	5033	5,6	0,227	0,83	>0,13	0,24	<0,33	-21	-23,74	SW
	-▽-	5062	40,8	0,232	1,08	>0,13	0,21	0,28	-29	-29,33	SW - W
	-◇-	5069	75,5	0,241	1,20	>0,13	0,20	0,28	-31	-29,3	W
	△	5051	4,4	0,249	3,77	0,04	0,15	0,38	-45	-46,2	W
	▽	5066	75,5	0,229	4,80	0,09	0,15	0,28	-45	-43,4	W - WD
	◇	5055	40,1	0,228	4,80	0,09	0,15	0,28	-45	-46,3	W - WD
	□	5002	41,9	0,232	4,91	0,09	0,16	0,28	-42	-40,4	W - WD
		4212	6,0	0,230	6,25						WD
	○	5001	42,1	0,229	9,81	0,04	0,10	0,51	-58	-52,2	WD
	●	5054	40,6	0,222	9,62	<0,04	0,10	0,51	-58	-60,0	WD
	×	5032	5,6	0,238	10,4	<0,04	0,05	>0,51	-72	-63,4	WD - AD
c	△	5052	4,9	0,110	0,60	0,36	0,39	0,53	+20	+19,6	SW
	-◇-	5041	40,8	0,135	0,72	>0,10	0,10	<0,3	-35	-34,7	SW
	-▽-	5068	75,9	0,129	1,05	>0,15	0,21	<0,28	-31	-32,5	SW - W
	-○-	5060	40,0	0,127	1,08	>0,13	0,21	<0,28	-31	-37,7	SW - W
	▽	5035	4,4	0,090	4,50	<0,08	0,12	<0,28	-53	-49,1	W
	○	5037	40,0	0,125	4,77	>0,04	0,10	<0,23	-58	-55,7	WD
	□	5067	76,0	0,124	4,76	<0,08	0,10	0,23	-58	-55,7	WD
	◇	5016	75,3	0,135	5,12	<0,08	0,10	<0,23	-58	-59,8	WD
	△	5050	4,9	0,120	8,84	<0,03	0,08	<0,38	-64	-55,7	WD
	×	5059	40,0	0,116	9,44	<0,03	0,07	0,38	-66	-59,8	WD
		4209	2,1	0,125	9,73						WD
	●	5004	41,3	0,110	9,83	<0,03	0,05	<0,52	-66	-59,8	WD
d	-○-	5061	40,0	0,057	0,91	>0,18	0,25	<0,33	-18	-19,1	SW
	-▽-	5070	76,0	0,055	1,20	>0,13	0,18	0,20	-37	-40,4	W
	○	5038	40,7	0,057	4,83	<0,03	0,06	0,13	-69	-63,6	WD
	□	5057	40,8	0,054	4,78	<0,03	0,06	>0,13	-69	-59,8	WD
	◇	5015	75,0	0,063	5,12	<0,03	0,06	0,17	-69	-67,2	WD
	-△-	5071	76,1	0,055	5,36	<0,03	0,06	>0,13	-69	-59,8	WD
	●	5058	40,2	0,063	9,54	<0,03	0,04	0,13	-75	-63,6	WD
e	○	5039	40,0	0,031	5,07	<0,02	0,03	≈0,12	-77	-77,2	WD
	×	5014	75,0	0,033	5,76	<0,02	0,03	<0,18	-77	-77,2	WD

"SW" = Stratified Wave Flow; "W" = Wave Flow, "WD" = Wave Droplet Flow; "AD" = Annular Droplet Flow

TABLE 4.1 IMPEDANCE PROBE DATA FROM THE 5″ PIPE TESTS

Test-Nr.	p (MPa)	c_s (m/s)	c_w (m/s)	Upper Impedance Probe α (%)	f (Hz)	Comments	Lower Impedance Probe α (%)	f (Hz)	Comments	Flow Regime
6001	4,0	8,8	1,2	~100		droplets	~99		bs (1)	AD
2	4,0	4,2	1,2	≈110		some few droplets	9		bubbles, homogeneous	AD
3	4,0	4,7	1,2	≈100		some few droplets	11		bubbles, homogeneous	AD
4	4,0	9,3	1,2	99,3		droplets	?		bs	AD
5	4,0	9,0	1,3	98,5		droplets, splashs	?		bs	AD
6	4,0	6,0	1,6	98,5		dropelts, splashs	40		bubbles, homogeneous	S
7	4,0	0,3	1,8	≈100		elongated bubbles, slugs	0		single phase water	EB-S
8	4,0	3,0	1,8	99,5	0,36	bubble swarms, slugs	10	0,36	bubble swarms, bs	S
9	3,9	0,3	1,9	85	0,88	elongated bubbles, slugs	≈0		some few bubbles	S
13	4,0	10,2	1,0	99		some few droplets	70		bubbles, homogeneous	AD
14	4,1	4,2	1,0	~100	0,2?	droplet swarms	9	0,3	bubble swarms	S
15	4,0	0,7	1,0	100		single phase steam	0		single phase water	W
16	4,0	0,8	0,5	100		single phase steam	0		single phase water	W
17	4,0	5,2	0,5	≈100		some few droplets	≈0		some bubbles	AD
18	4,0	9,6	0,5	≈100		some droplets	73		bubbles, homogeneous	AD
19	4,0	1,1	1,3	≈100		very few droplet	~0		very few bubbles	WD-S
20	4,0	1,3	1,2	100		single phase steam	0		single phase water	WD
21	4,0	5,7	1,3	99,6	0,8	slugs?	32	0,8	bubble swarms	S
22	4,0	2,7	1,2	≈100		some few droplets	2,4	0,2	bubble swarms	WD-S
23	4,0	4,6	1,2	99,6	0,72	droplet swarms	18	0,72	bubble swarms	S
24	4,0	7,0	1,2	99,6	0,8?	droplet swarms	45		bubbles, homogeneous	S
25	4,0	8,7	1,2	98,7	0,86	droplet swarms	55		bubbles, homogeneous	S
26	4,0	6,0	1,3	99,5	0,8	droplet swarms	38		bubbles, homogeneous	S
27	4,0	2,8	1,3	≈100		some few droplets	6	0,26	bubble swarms	WD-S
35	7,8	0,2	1,8	≈0		few bubbles	0		single phase water	EB
36	7,8	0,9	1,6	≈100		some droplets (slug?)	0		single phase water	S
37	7,8	1,6	1,6	100		single phase steam	0		single phase water	WD
48	3,9	4,9	1,6	100		single phase steam	25		bubble swarms	WD
49	3,9	0,1	1,5	~2		elongated bubbles	F		single phase water	EB
51	7,5	5,5	1,0	~100		some few droplets	29		bubbles, homogeneous	AD
52	7,5	7,7	1,2	≈100		some few droplets	43		bubbles, homogeneous	AD
53	7,6	1,6	1,3	100		single phase steam	0		single phase water	WD
54	7,5	0,9	0,5	100		single phase steam	0		single phase water	WD
55	7,5	1,0	1,3	100		single phase steam	0		single phase water	WD
56	7,5	5,3	0,5	100		single phase steam	28		bubbles, homogeneous	WD
57	7,6	3,2	1,2	100		single phase steam	1,6		bubbles, homogeneous	WD
58	7,5	4,7	1,2	≈100		some few droplets	14		bubbles, homogeneous	AD
59	7,5	6,2	1,2	~100		some few droplets	36		bubbles, homogeneous	AD
60	7,6	3,4	1,5	≈100		droplets, splashs	7	0,32	bubble swarms	S
61	7,6	1,5	1,5	100		single phase steam	0		few bubbles, homogeneous	WD
62	7,5	5,7	1,6	97		droplets	29		bubbles, homogeneous	AD
63	7,6	10,6	1,4	98		droplets	70		bubbles, homogeneous	AD
64	4,0	10,5	0,1	100		single phase steam	≈100		some droplets	WD
65	4,0	5,6	0,1	100		single phase steam	≈100		some droplets	WD
66	4,0	1,0	0,1	100		single phase steam	0		single phase water	WD
67	4,0	1,0	0,25	100		single phase steam	0		single phase water	WD
68	4,0	5,0	0,25	100		single phase steam	31		bubbles, homogeneous, bs	WD
69	4,0	10,4	0,25	100		single phase steam	95		bubbles, homogeneous,	WD
70	4,0	5,4	0,26	100		single phase steam	46		bubbles, homogeneous	WD
71/72	4,0	5,0	0,1	100		single phase steam	91		droplets	WD
73/74	7,5	5,0	0,1	100		single phase steam	96		droplets	WD
75	7,5	10,0	0,1	≈100		very few droplets	≈99		droplets	WD-AD
76	7,5	9,8	0,2	≈100		very few droplets	90		droplets	AD
77	7,5	5,0	0,2	100		single phase steam	60		bubbles, homogeneous	WD
78	7,5	0,9	0,2	100		single phase steam	0		single phase water	SW
79	7,6	0,9	0,1	100		single phase steam	0		single phase water	SW-W
80	7,5	9,5	0,5	≈100		very few droplets	70		bubbles-droplets	AD
97	1,1	10,0	1,0	≈100		droplets	43		bubbles, homogeneous	AD
98	1,1	5,0	1,0	100		single phase steam	0,6	0,2	bubbles, homogeneous	WD-AD
99	1,0	1,4	1,0	100		single phase steam	0		single phase water	WD
6100	1,2	10,0	0,5	≈100		very few droplets	69	0,6	bubble swarms	AD
101	1,1	5,0	0,5	100		single phase steam	7	0,25	bubble swarms	WD
102	1,0	5,6	0,3	100		single phase steam	24	0,9	bubble swarms	WD
103	1,1	9,7	0,2	≈100		very few droplets	87		bubbles, nearly homogen.	AD

Flow Regimes: "EB" = Elongated Bubble; "SW" = Stratified Wave; "S" = Slug; "W" = Wave; "WD" = Wave Droplet; "AD" = Annular Droplet

TABLE 4.2 IMPEDANCE PROBE DATA FROM THE 3" PIPE TESTS

5. Signal Analysis of the Single Instruments

5.1 3 Beam Gamma Densitometer

The gamma densitometer is used for measuring the cross-sectional average of the mixture density (or void fraction, respectively). If the single beams measure correctly the chordal density, the mean density still may be affected by an error due to the inhomogeneous phase distribution.

In this report the averaged density (void fraction) was evaluated by weighting the single beam signals with the correponding chordal lengths, which is correct for a homogeneous distribution. The specific arrangement of the gamma beams (Figure 2.1) in the 5" pipe overemphasizes the upper portion of the tube, in the 3" pipe the lower portion is generally more strongly weighted. If the phases are totally stratified, errors occur which are shown in Table 5.1. In the 5" pipe tests with mostly very high void fractions ($\alpha_\gamma \geq 0.90$) even an ideally stratified flow should cause negligible errors. In the 3" pipe with lower void fractions ($\alpha_\gamma \simeq 0.65$) the differences are expected to be more significant. Therefore those corrections were computed and are shown as function of the length weighted void fraction in Figure 5.1.

Table 5.1 also includes the values for the vertical weighting procedure (using the vertical component of the chordal length) which gives somewhat better results than the length weighting method.

In the following, the results are often presented as function of the interface level $(y/d)_{IF}$. This interface level, assuming a totally separated flow, is computed from the length weighted void fraction by

$$(y/d)_{IF} = 0.5(1-\cos\frac{\Theta}{2})$$

with Θ from

$$\alpha_\gamma = 1- \frac{1}{2\pi}(\Theta-\sin\Theta)$$

Sometimes the interface level IF is used, which means the percent of DTT height covered by the liquid calculated by

$$IF_{3"} = \frac{6.66\ (^{y}/d)_{IF} - 1.427}{3.81} \cdot 100$$

for the 3" pipe and by

$$IF_{5"} = \frac{10.3\ (^{y}/d)_{IF} - 3.255}{3.81} \cdot 100$$

for the 5" pipe.

To check the accuracy of the 3-beam gamma densitometer measurements the densitometer void fraction is compared with the scanning densitometer void fraction α_{sc} and indirectly measured void fractions calculated from the radiotracer velocities and reference superficial velocities by

$$\alpha_{Rg} = \frac{V_{sg}}{V_{Rg}}\ ;\ \alpha_{Rl} = 1 - \frac{V_{sl}}{V_{Rl}}\ ;\ \alpha_{RS} = \left(1+S_R\,\frac{V_{sl}}{V_{sg}}\right)^{-1}$$

For this comparison the 3" pipe tests are more suitable because (i) only here some scanning densitometer data exist, and (ii) the radiotracer velocities were interpolated to the position of the gamma densitometer.

Tables 5.2 and 5.3 and Figure 5.2 show that the radiotracer void fraction values are consistent with each other which indicates a high measuring accuracy of both the radiotracer velocities and the reference values. Table 5.3 contains the mean relative errors, assuming that α_{Rl} is the correct value. There is excellent agreement between the scanning densitometer void fraction α_{sc} and α_{Rl} (deviations about 0.2%); the mean deviation of the 3 beam densitometer is -6%, and -8% for the test point where the scanning densitometer also measured. The column labeled $\alpha_{\gamma,c}$ contains the 3 beam densitometer void fraction corrected with the values from Figure 5.1. Mainly at 40 bars there are some points where the correction did not improve the agreement but the mean values show clearly the overall improvement from applying this correction. (An even better overall agreement between corrected 3 beam and scanning densitometer values existed in the tests of the Modular DTT /11/. A similar or even better improvement in accuracy should be reached by using the more sophisticated evaluation model developed by Lassahn /7/.

Figure 5.2 and Table 5.3 contain also the results for the 5" pipe tests. The mean values show good agreement although there is an increased scattering especially for the α_{Rg} values. The agreement is surprisingly good, although the radiotracer values were taken at the position $\overline{D5-D7}$ (Figure 2.1) and were not extrapolated to the densitometer position.

In the tests carried out on 11.18.77 (Test Nr. 6069-6080) the 3 beam densitometer did not give satisfactory results at least for tests 6069, 6071-76, 6080 where the C-beam obviously showed a too small density. This test series is not included in the further discussion.

It may be concluded that the LOFT 3 beam gamma densitometer, in combination with a flow model weighting procedure, is giving very precise measurements of the cross section averaged void fraction, or the apparent density.

5.2 Turbine Meter

5.2.1 Turbine Meter Models

There are different models for interpreting the signals of a full flow turbine meter:

a) Volumetric model

$$V_T = \alpha V_g + (1-\alpha) V_l = V_{sg} + V_{sl} \tag{5.1}$$

The turbine measures the volumetric velocity (total volumetric flow divided by the cross-section area).

b) Rouhani Model /8/

$$V_T = \frac{S^2 + \frac{\rho_l}{\rho_g}\frac{1-\alpha}{\alpha}}{S + \frac{\rho_l}{\rho_g}\frac{1-\alpha}{\alpha}} V_l \tag{5.2}$$

c) Aya model /9/

$$V_T = \frac{S + \left(\frac{\rho_l}{\rho_g}\frac{1-\alpha}{\alpha}\right)^{0.5}}{1 + \left(\frac{\rho_l}{\rho_g}\frac{1-\alpha}{\alpha}\right)^{0.5}} V_l \tag{5.3}$$

d) Estrada Model /10/

$$V_T = \frac{1 + \frac{\rho_l}{\rho_g} \frac{1-\alpha}{\alpha}}{1/S + \frac{\rho_l}{\rho_g} \frac{(1-\alpha)}{\alpha}} V_l \tag{5.4}$$

The Rouhani, Aya and Estrada model assume a constant phase distribution over the cross section; an assumption which is, as shown in general not valid for horizontal flow.

5.2.2 Turbine Meter in the 5" Pipe

The left part of Figure 5.3 shows the ratio of turbine velocity to the homogeneous velocities (= volumetric flux) for the high pressure experiments. The data with interface levels IF > -50% were tested under low values of V_{sg}($V_{sg} \leq 1$ m/s) in the stratified-wave flow regime (Figure 4.1), the turbine was completely surrounded by steam. For these test points the turbine is obviously below its measurement range. This fact indicates that the lower limit for the turbine shown in the single phase water calibrations ($V_{T,\ min}$= 0.46 m/s) cannot be reached if operated in gas.

The lower interface levels occurred at higher gas velocities ($V_{sg} \geq 5$ m/s). Here a wave-droplet flow existed (Figure 4.3) with no or minimal droplet entrainment in the cross-section area covered by the turbine. Under these conditions the turbine measured accurately the steam phase velocity which was only slightly higher than the homogeneous velocities (Table 5.4) in these experiments.

The right part of Figure 5.3 shows the results for the low pressure experiments. Again there are some points where the turbine operates below its measurement range. However, the turbine reading for higher values of V_{sg} is also lower than the homogeneous velocity. This could be caused by a higher bearing friction at lower temperatures or the lower momentum flux due to the lower density. These effects could be determined by performing low pressure gas calibration tests. The differences in flow pattern (higher wave amplitudes at low pressure) could contribute to this effect as well: even if the (time averaged) interface level is below the bottom of the turbine, high waves could reach the turbine and decelerate it.

Table 5.4 shows a comparison of the measured turbine velocity with the turbine velocity using the Estrada, Rouhani and Aya model. All velocities are normalized with the liquid phase velocity calculated from densitometer void fraction and superficial velocities:

$$V_l = \frac{V_{sl}}{1-\alpha_\gamma}$$

The Rouhani model describes the experiments the best but the agreement is still not satisfying.

5.2.3 Turbine Meter in the 3" Pipe

Because of the larger d_T/d ratio and the lower void fractions, the interface level was mostly above the bottom of the turbine (Figure 5.4). At low interface levels there are some test points with $V_{sg} \simeq 5$ m/s and 10 m/s and $V_{sl} \simeq 0.5$ m/s where the measured velocities are higher than the homogeneous velocities, and agree well with the 5" pipe test results. There is one test point where the liquid level was above the top of the turbine (elongated bubble flow). The data shows that the turbine again measured approximately the volumetric flux. In the rest of the experiments the turbine indicated a value of about 77% of the volumetric flux with a relatively small scatter. If the ratios V_T/V_g and V_T/V_l are plotted as function of the interface level, the ratios are decreasing with increasing interface level with a rather large data scatter. Surprisingly the ratio V_T/V_l reaches values below 1. If one assumes that the correct void fraction at the position of the DTT is slightly higher than the densitometer void fraction,this assumption should result in an even lower value of V_T/V_l. Therefore, the fact that V_T/V_l reaches values below 1 must be caused by other effects, e.g. bypassing of the DTT, influence of velocity profile on the turbine (with non-twisted blades), etc.

Table 5.4 again contains the comparisons of the measured turbine velocity with velocities calculated from the different models. The Estrada model gives turbine velocities very close to the liquid phase velocity. Therefore, the ratio V_T/V_l in Figure 5.4 is a good approximation to V_T/V_T-Estrada.

Compared to the Estrada model, the Aya model predicts somewhat better the turbine velocity, most of the values are within a $\pm$ 15% error band. The Rouhani model gives values which are between the values from the Estrada and Aya-model.

5.2.4 Turbine Meter Reading as Function of Flow Regime

Figure 5.5 shows both the 5" and 3" results drawn in the flow chart. In the high void wave and annular droplet regime the turbine measures approximately the steam phase velocity (which is close to the volumetric velocity). In the slug and wave droplet flow regime with a lower void fraction the turbine measures about 80% of the homogeneous velocity. In Figure 5.5 the line is drawn where the interface level is equal to the bottom of the turbine (3" pipe geometry, S = 2). It can be seen that this line separates fairly well the two regions where the turbine measures about 1.1 and 0.8, times of the volumetric flux.

5.3 Drag Disc

5.3.1 Drag Disc in the 5" Pipe

A drag device should measure the total two-phase momentum flux i.e. $(\rho v^2)_{tp} = \alpha\rho_g V_g^2 + (1-\alpha)\rho_l V_l^2$. A drag disc measures local momentum flux ($d_{DD}/d \simeq 0.01$). Therefore the measurement is in general not characteristic for the cross section average.

In the high pressure tests, the drag disc has always been in the steam phase with no or minimal droplet entrainment. Therefore the drag disc is expected to measure approximately the steam momentum flux $\rho_g V_g^2$. The velocity (V_{DD}-ρ_g), calculated from the drag disc reading and the steam density should agree with the turbine velocity. The ratio of (V_{DD}-ρ_g) to V_T in Table 5.5 shows that this is true as long as the drag disc is in its measuring range ($\geq$ 370 kg/m s^2). Because of the local measurement of the drag disc, the measured momentum flux may be below the measurement range even if the cross section averaged value is above.

Figure 5.6 shows the drag disc signals as a function of the interface level (only those test points where the drag disc is in the measuring range). The drag disc reading normalized with the steam momentum flux $\rho_g V_g^2$ is quite independent of the interface level. The drag disc velocity V_{DD}-ρ_g normalized with the homogeneous velocity has a value of ≈ 1.1 with an even smaller scattering.

In the low pressure experiments the drag disc should be always below its measuring range if it measured only the steam phase. Table 5.5 shows that in the steam-water experiments only for 3 test points the reading is higher but those points do not show similar tendencies as the 40 and 75 bar points shown in Figure 5.7. A behavior even more different from the high pressure tests, the air-water tests show: The drag disc reading is much higher than the gas momentum flux, sometimes considerably higher than the two-phase momentum flux. These results cannot be explained by the differences in flow regime but are thought to be caused by the greater amount of friction at low temperatures as already observed during calibration in single phase cold water. In the air-water tests the disc was sometimes stuck so severely that it had to be released by knocking.

5.3.2 Drag Disc in the 3" Pipe

Table 5.6 and Figure 5.7 show the results of the 3" pipe tests. The ratio of drag disc reading to total two-phase momentum flux $(\rho V^2)_{tp}$ was considerably below 1 when the interface level was below the bottom of the drag disc, and about 1.2 for an interface level above the top of the drag disc. The points shown in parentheses in Figure 5.7 do not indicate this characteristic behavior. These test points (starting with Test Nr. 6069) belong to a test series where a new DTT was installed. The amplifier had a considerable zero shift at the end of the test day. These data are thought to be incorrect and are not taken into account in further discussions.

The drag disc velocity (V_{DD}-ρ_g) shows a similar behavior: for $(y/d)_{IF}$ < 0.5 the value is below the homogeneous velocity (V_{DD}-ρ_g ≈ $0.57(V_{sg}+V_{sl})$, for $(y/d)_{IF}$ > 0.5 the drag disc measured about the homogeneous velocity.

5.3.3 Drag Disc Reading as Function of Flow Regime

Figure 5.8 shows the drag disc reading drawn in the flow chart. In the wave flow and annular droplet flow regime at low values of V_{sl} the two-phase momentum $(\rho V^2)_{tp}$ is approximately equal to the steam momentum flux $(\rho V^2)_g$ which is measured by the drag disc. With increasing V_{sl} the drag disc measures increasingly too low; and reduces to about a factor 0.5 in the slug flow regime. In and near the elongated bubble flow regime the interface level is above the drag disc, and the drag disc is mostly in water. Thus, the reading is higher than the cross section average. The curve $(y/d)_{IF} \equiv 0.5$ (with S = 2 assumed) clearly separates these two regions.

5.4 The Deviations of DTT Measurements from the Homogeneous Flow Parameters

The ratio of turbine reading to homogeneous velocity, the drag disc reading and phase slip were plotted vs superficial liquid velocity at constant superficial gas velocity of 5 and 10 m/s in Figure 5.9 and 5.10, respectively. In these figures, the 5" pipe and 3" pipe data fall on the same curve. The turbine reading is higher than the homogeneous velocity at low values of the superficial liquid velocities and quickly reduces below the homogeneous velocity as the superficial liquid velocity increases to a point where the interface level reaches the bottom of the turbine.

The drag disc readings are relatively constant with respect to the liquid velocity in the 5" pipe tests and increase with the steam density (or pressure) indicating that the drag disc was measuring primarily the steam flow momentum. The drag disc readings increase as the water level reaches the bottom of the DTT shroud due to the increased liquid momentum acting on the drag disc.

The slip is higher at $V_{sg} \approx 10$ m/s and decreases with increasing V_{sl}. However the slip remains relatively constant (from 1 to 3) for the data where the water level reached the turbine. Therefore, the effect of slip on DTT outputs is not apparent for these tests.

In summary, the DTT readings are dependent on the proximity of water level with respect to the turbine and can be quite different from the readings in homogeneous flow conditions.

5.5 Radiotracer Velocities

A check of the accuracy of the radiotracer velocities was already made in Chapter 5.1, evaluating in independent ways the void fraction. As shown, the values were in general very close together which means that the accuracy of the radiotracer velocity measurements is very good (assuming that the reference values are measured correctly).

Because two-phase flow often has an oscillatory behavior, the number of tracer injections must be large enough to give a satisfactory mean value. Table 5.7 shows the mean velocity values and the standard deviations for the various measuring positions together with the number of the Mn and Ar injections per point. The table shows that often the number of injections is very small. This could explain the statistical scattering of the data which is more obvious for the 5" pipe data (mean numbers of injections: $\overline{N}_{Mn} = 4.4$, $\overline{N}_{Ar} = 5.3$) than for the 3"pipe data ($\overline{N}_{Mn} = 8.3$; $\overline{N}_{Ar} = 7.3$).

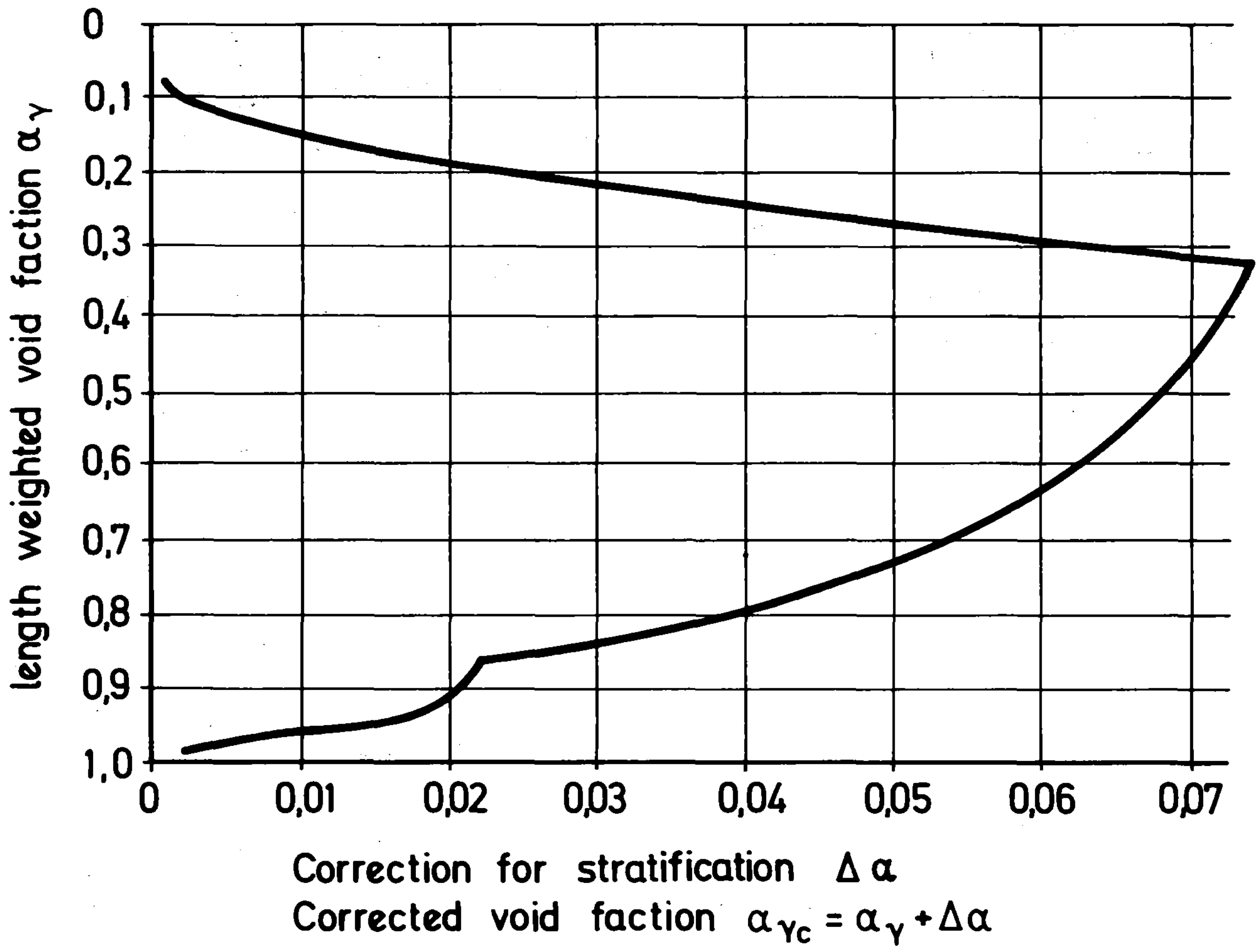

FIGURE 5.1 VOID FRACTION CORRECTION FOR TOTALLY SEPARATED FLOW (3" PIPE)

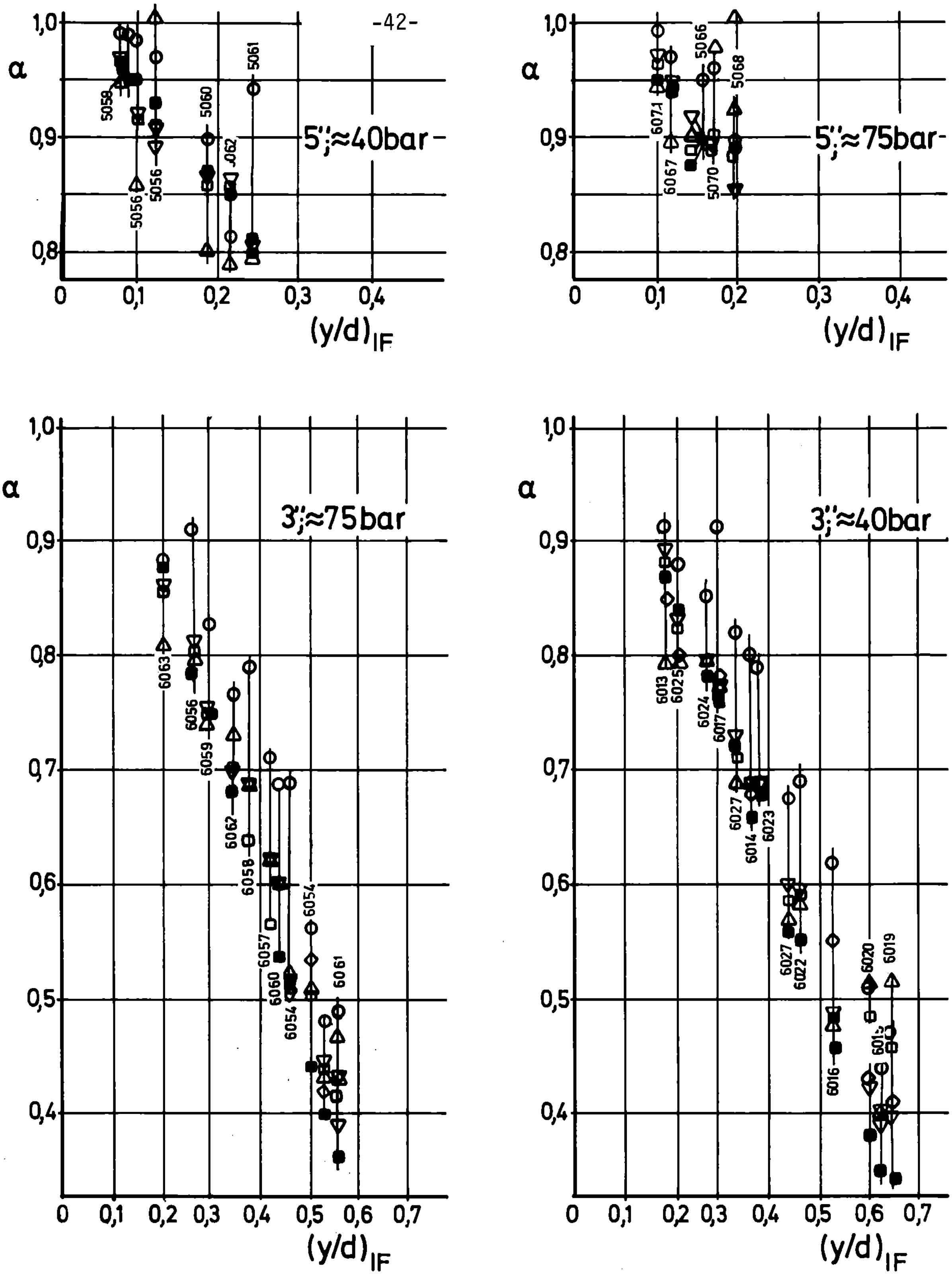

"o": $\alpha_H = V_{sg}/(V_{sg}+V_{sl})$; "■": $\alpha_{3Beam\ l.w.}$; "◇": $\alpha_{Scanning}$

"△": $\alpha_{Rg} = V_{sg}/V_g$; "▽": $\alpha_{Rl} = 1-V_{sl}/V_l$; "□": $\alpha_{Rs} = (1+(V_{sl}/V_{sg})\cdot S)^{-1}$

FIGURE 5.2 COMPARISON OF VOID FRACTION MEASUREMENTS

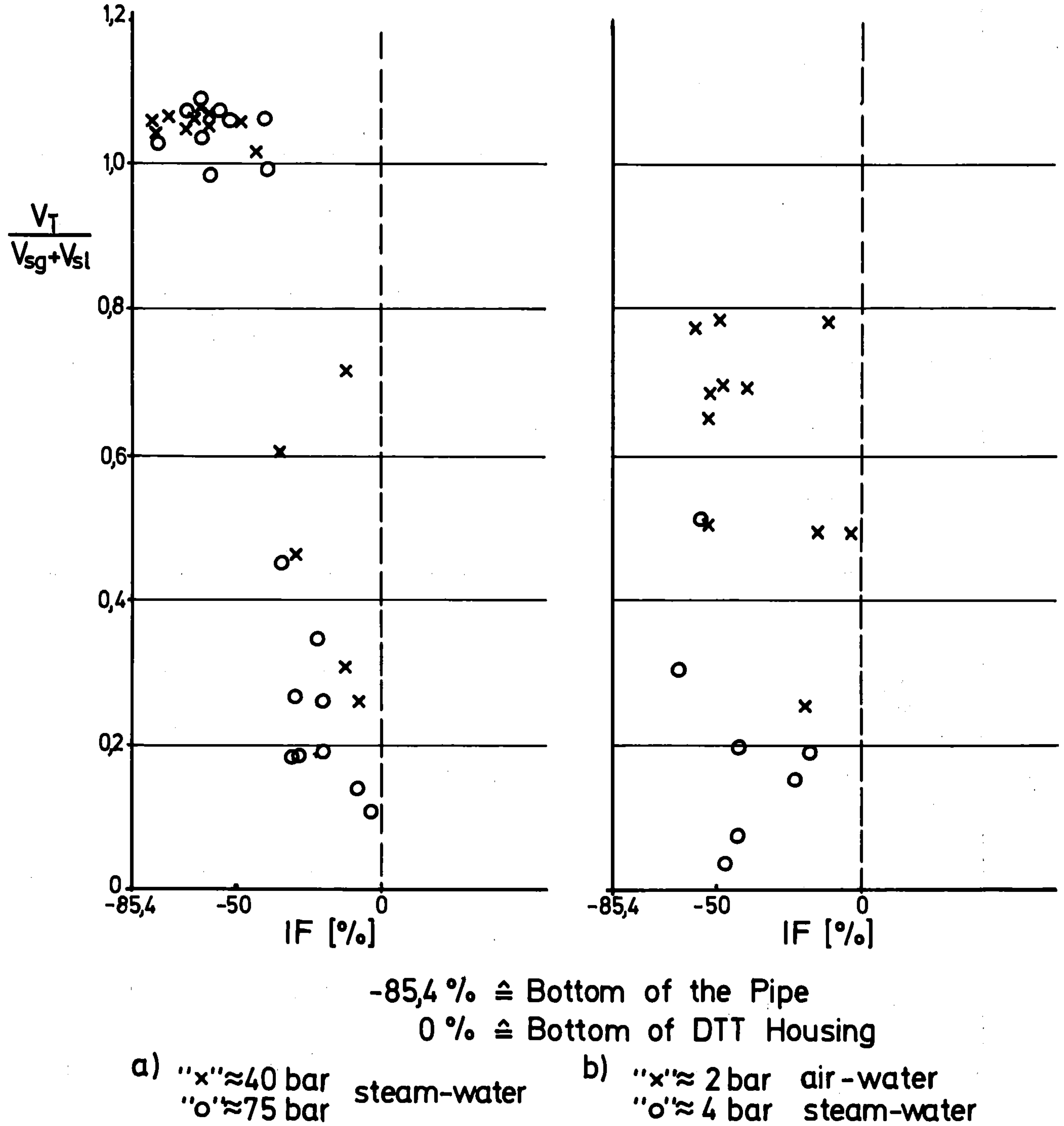

FIGURE 5.3 TURBINE METER VELOCITY AS FUNCTION OF THE INTERFACE LEVEL (5" PIPE TESTS)

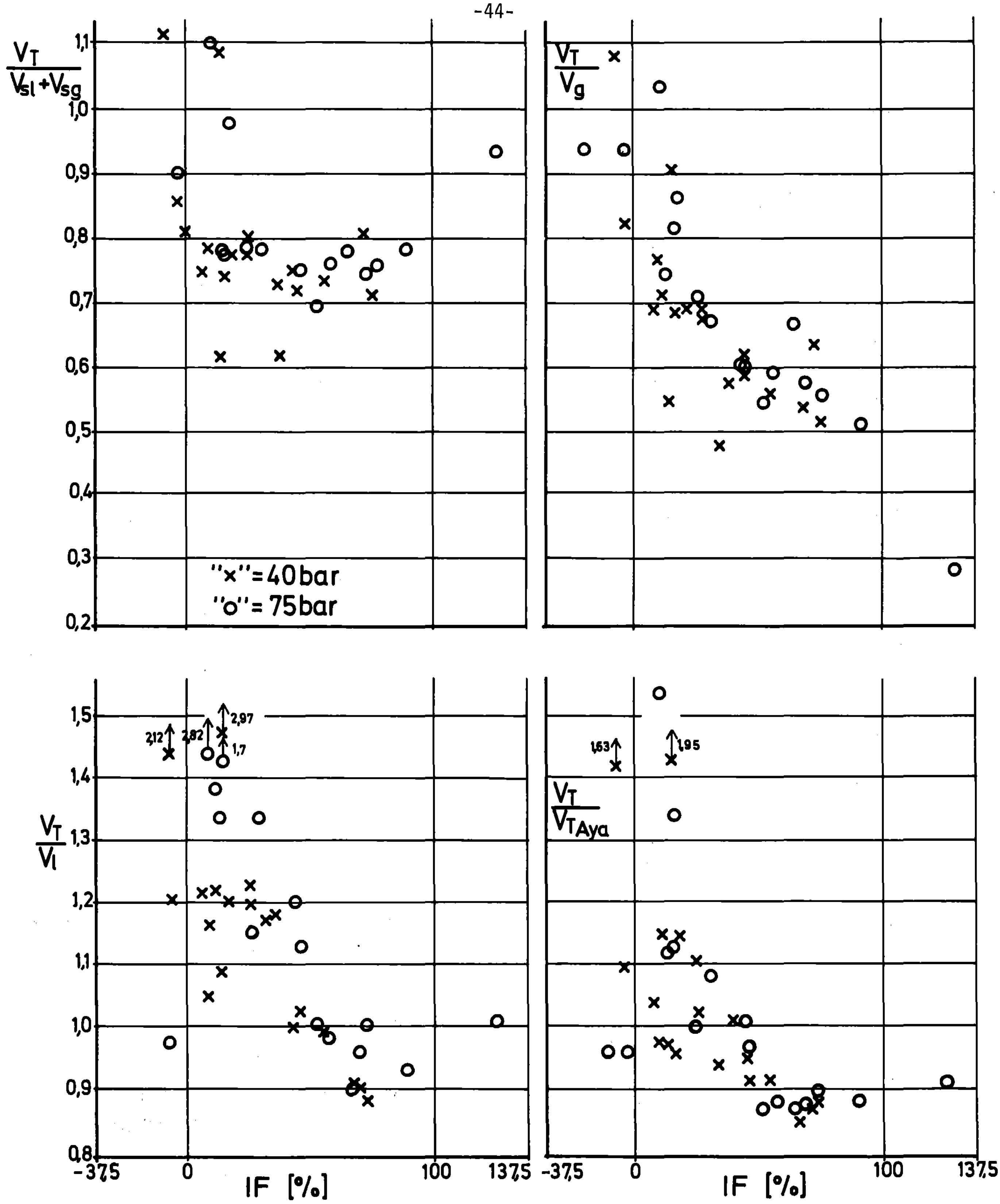

FIGURE 5.4 TURBINE METER VELOCITY AS FUNCTION OF THE INTERFACE LEVEL (3" PIPE TESTS)

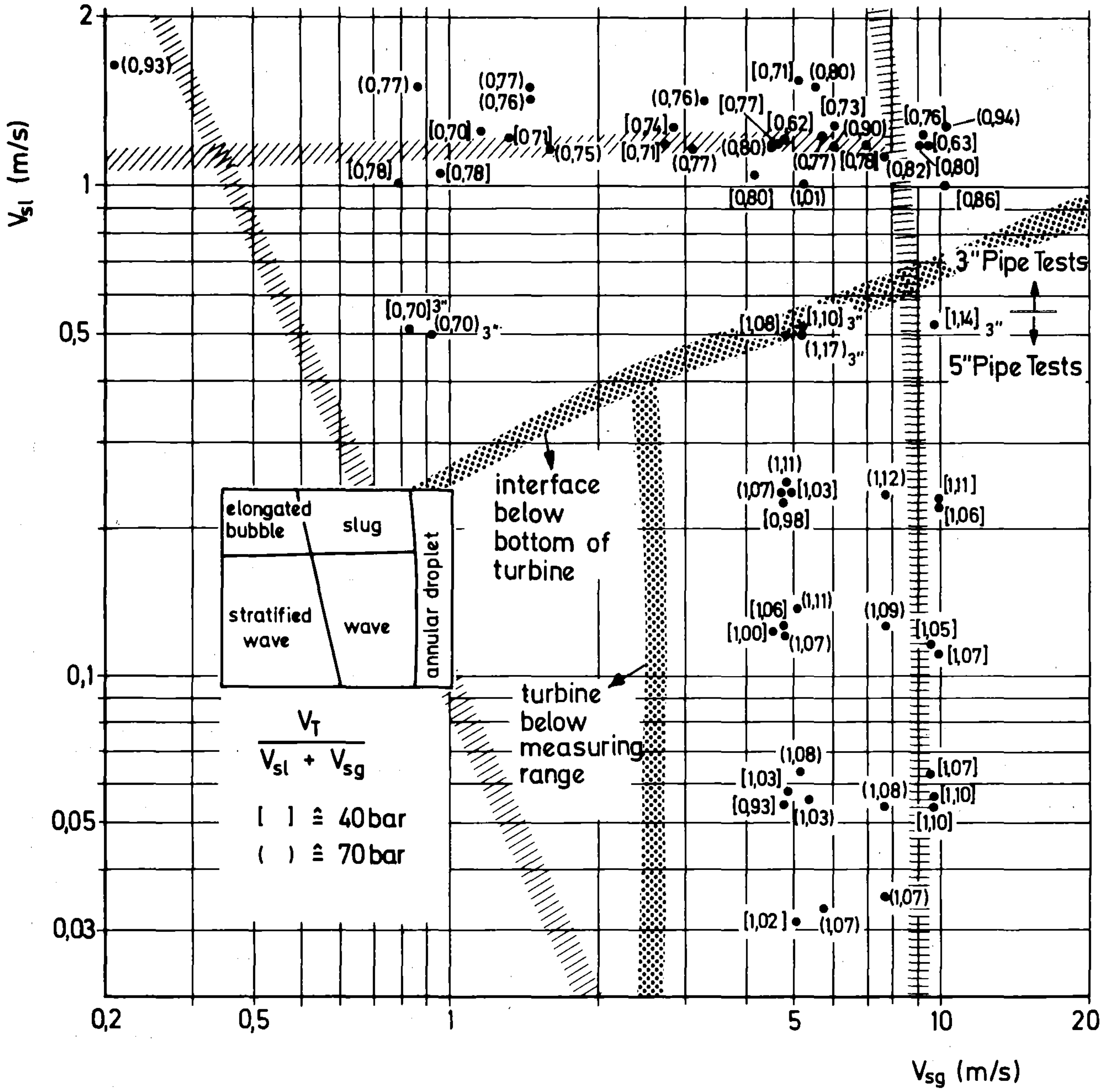

FIGURE 5.5 TURBINE METER VELOCITY AS FUNCTION OF FLOW REGIME (5" AND 3" PIPE TESTS)

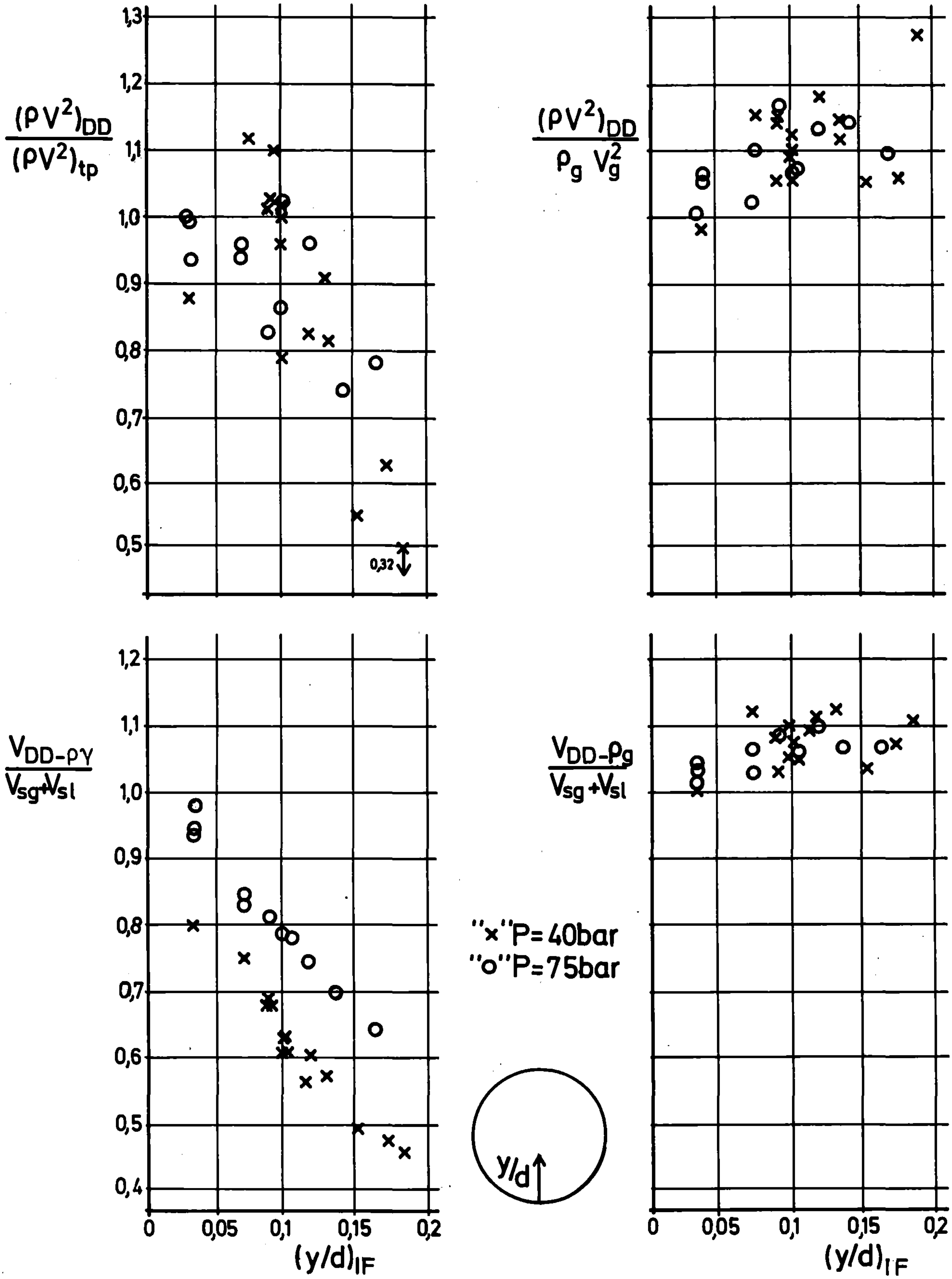

FIGURE 5.6 DRAG DISC READING AS FUNCTION OF THE INTERFACE LEVEL (5" PIPE TESTS)

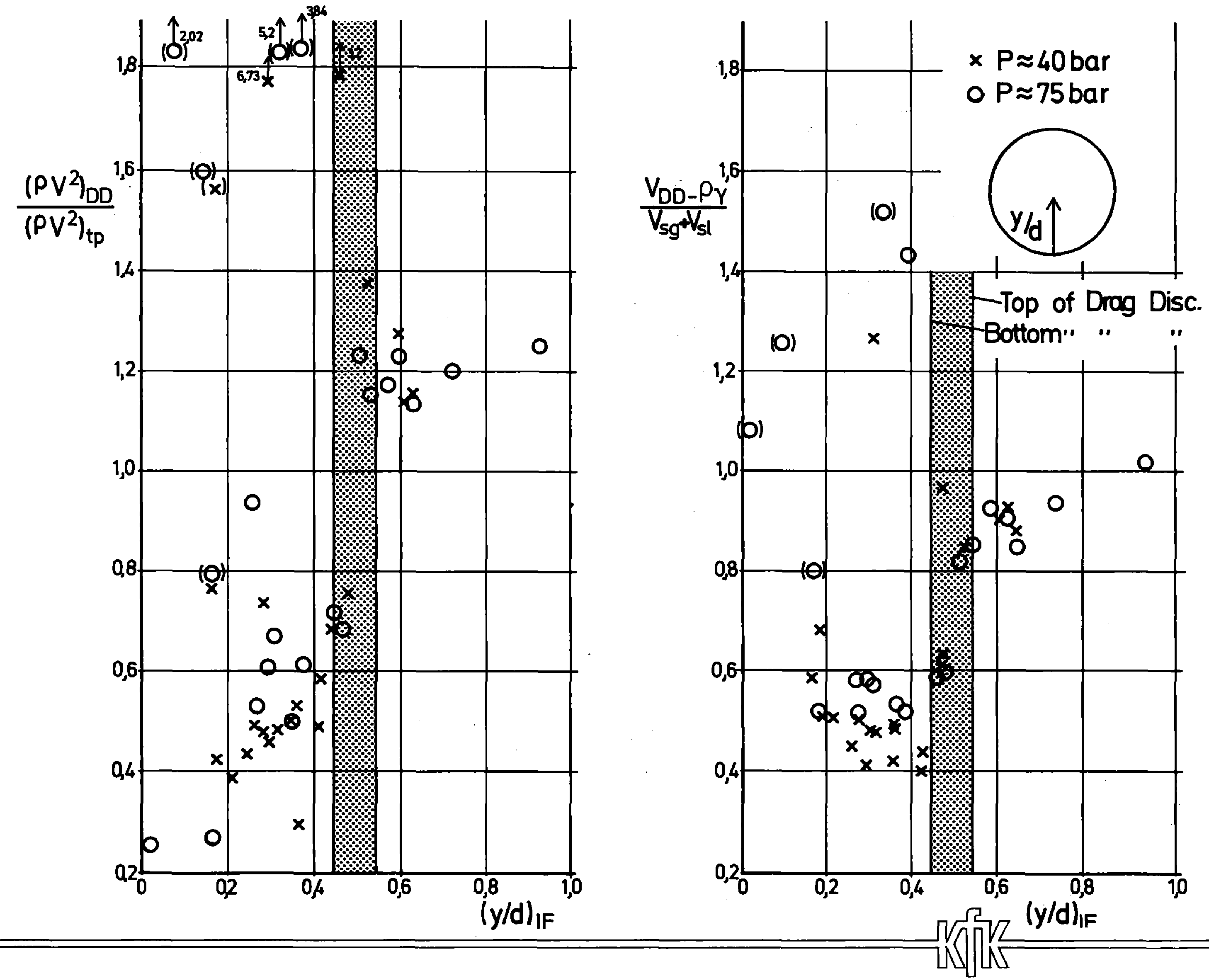

FIGURE 5.7 DRAG DISC READING AS FUNCTION OF THE INTERFACE LEVEL(3 " PIPE TESTS)

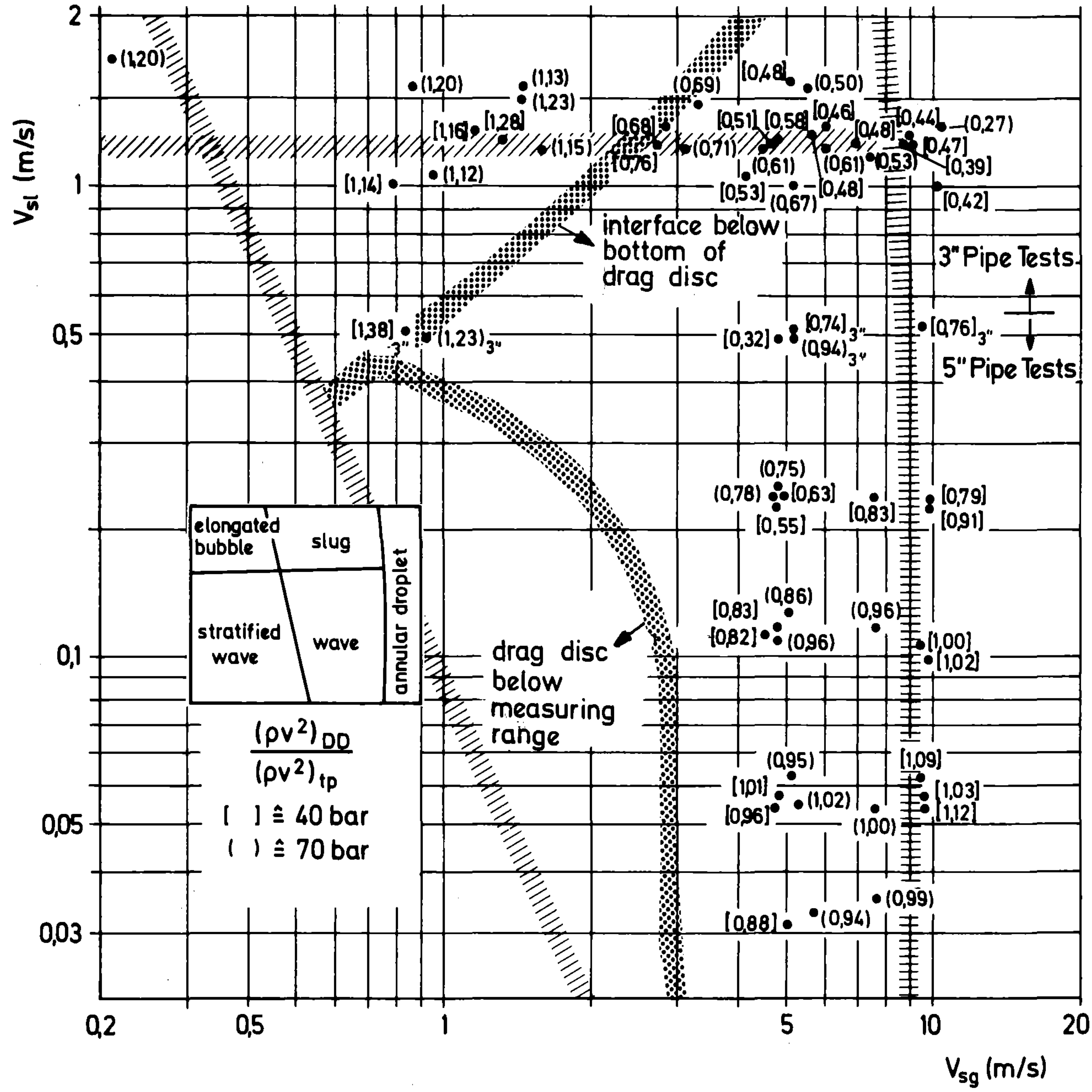

FIGURE 5.8 DRAG DISC READING AS FUNCTION OF FLOW REGIME (5" AND 3" PIPE TESTS)

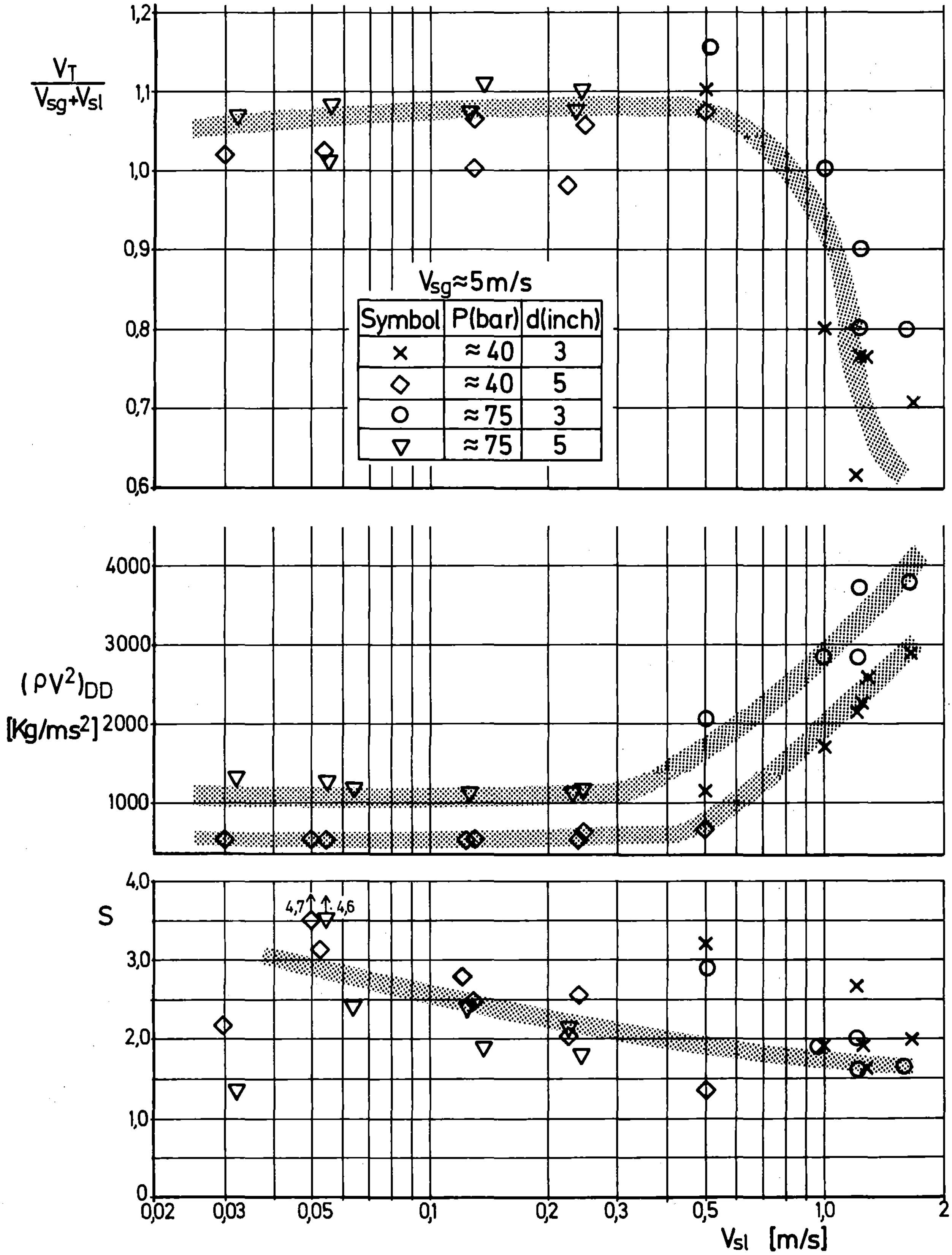

FIGURE 5.9 TURBINE METER, DRAG DISC READING AND SLIP FOR V_{SG} 5 M/S

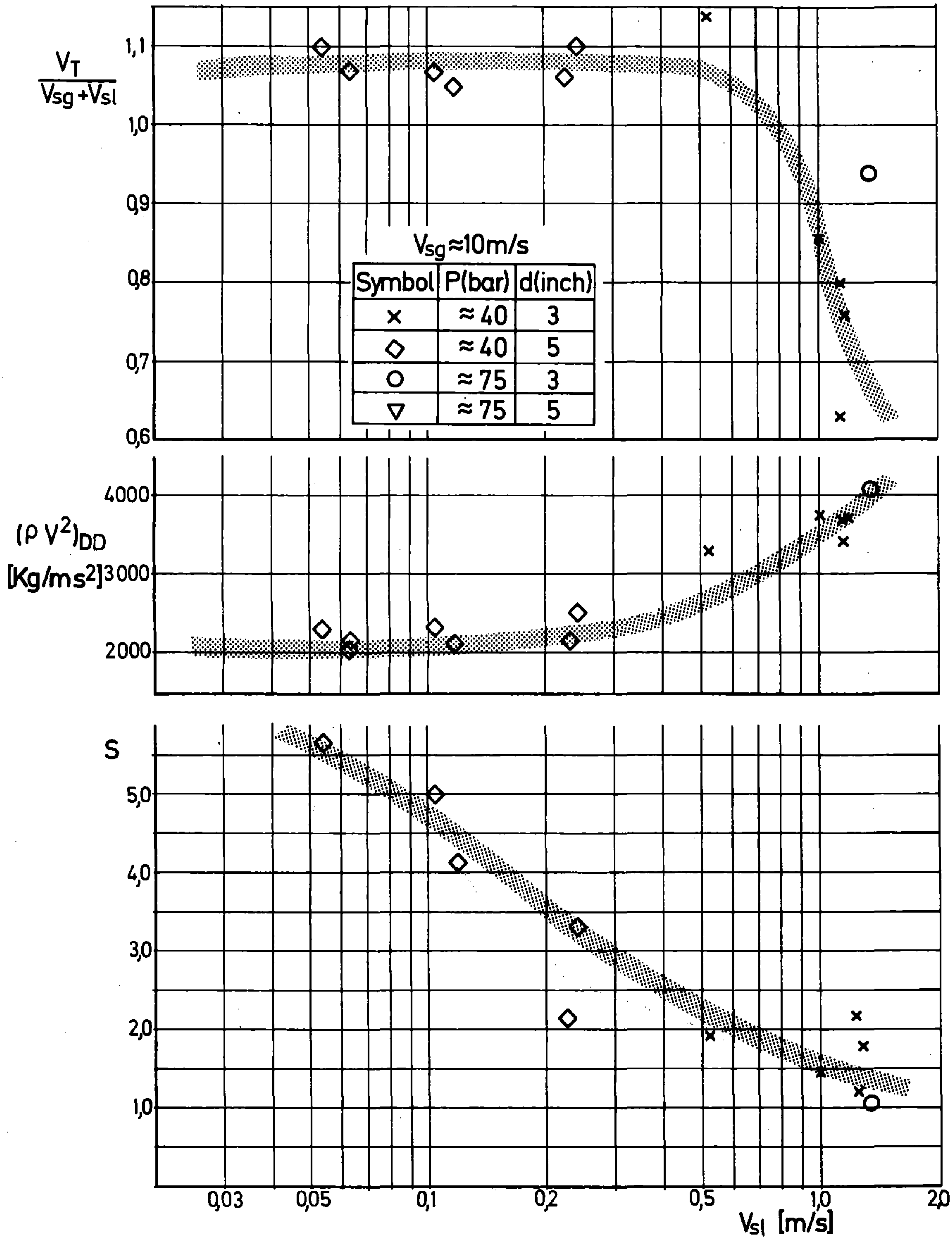

FIGURE 5.10 TURBINE METER, DRAG DISC READING AND SLIP FOR $V_{SG} \approx 10$ M/S

	5" Pipe		3" Pipe	
Void Fraction α	$(\frac{\alpha_\gamma - \alpha}{\alpha})_{lw}$	$(\frac{\alpha_\gamma - \alpha}{\alpha})_{vw}$	$(\frac{\alpha_\gamma - \alpha}{\alpha})_{lw}$	$(\frac{\alpha_\gamma - \alpha}{\alpha})_{vw}$
0,50	+0,17	+0,13	-0,14	-0,13
0,64	+0,09	+0,06	-0,10	-0,08
0,76	+0,05	+0,03	-0,07	-0,06
0,82	±0,03	±0,02	-0,04	-0,04
0,91	+0,03	+0,02	+0,01	-0,01
0,96	<0,01	<0,01	<0,04	<0,04

TABLE 5.1 MEASURING ERROR OF THE LENGTH WEIGHTED 3 BEAM DENSITOMETER VOID FRACTION FOR TOTALLY SEPARATED FLOW

			α_{R1}	$\frac{\alpha_{Rg}-\alpha_{R1}}{\alpha_{R1}}$	$\frac{\alpha_{RS}-\alpha_{R1}}{\alpha_{R1}}$	$\frac{\alpha_{3b}-\alpha_{R1}}{\alpha_{R1}}$	$\frac{\alpha_{sc}-\alpha_{R1}}{\alpha_{R1}}$	$\frac{\alpha_{3b_c}-\alpha_{R1}}{\alpha_{R1}}$
3" pipe tests (40 and 75 bars)	Mean value	a	0,65	+0,01	+0,01	-0,06		+0,03
		b	0,62	+0,03	+0,02	-0,08	<+0,01	
	Number of tests	a	←		27	→		27
		b	←		10		→	
5" pipe tests (40 and 75 bars)	Mean value	a	0,91	-0,003	0,006	0,005		
	Number of tests	a	←		14	→		

line a : all radiotracer test points

line b : test points with radiotracers and scanning densitometer

TABLE 5.3 COMPARISON OF THE MEAN VALUES OF THE DIFFERENT VOID FRACTIONS

Test Nr.	P (bar)	V_{sg} (m/s)	V_{sl} (m/s)	α_{thermo}	α_Y	α_{Y_c}	α_{sc}	α_{Rg}	α_{R1}	α_{RS}
6003		4.7	1.2	0.80	0.61	0.67				
6004		9.2	1.2	0.88	0.77	0.81				
6005		9.0	1.3	0.88	0.80	0.84				
6013		10.2	1.0	0.91	0.87	0.89	0.85	0.80	0.89	0.88
6014		4.1	1.0	0.80	0.68	0.74	0.68	0.68	0.68	0.68
6015		0.8	1.0	0.44	0.35	0.42		0.43	0.39	0.41
6016		0.8	0.5	0.62	0.46	0.53	0.55	0.48	0.50	0.48
6017		5.2	0.5	0.91	0.76	0.81	0.78	0.77	0.77	0.77
6018		9.6	0.5	0.95	0.90	0.92			0.89	
6019		1.2	1.3	0.47	0.34	0.41	0.41	0.53	0.40	0.47
6020	40	1.3	1.3	0.51	0.38	0.45	0.43	0.53	0.43	0.49
6021		5.7	1.3	0.82	0.72	0.77		0.68	0.73	0.72
6022		2.7	1.2	0.69	0.55	0.61		0.59	0.60	0.60
6023		4.7	1.2	0.79	0.68	0.73		0.70	0.68	0.69
6024		7.0	1.2	0.85	0.78	0.82		0.80	0.79	0.79
6025		8.8	1.2	0.88	0.84	0.87	0.80	0.80	0.84	0.83
6026		6.1	1.3	0.82	0.73	0.78		0.77	0.75	0.75
6027		2.8	1.3	0.68	0.56	0.62		0.56	0.61	0.59
6048		5.1	1.6	0.76	0.60	0.66				
6066		0.9	0.1	0.90	0.74	0.79				
6067		4.9	0.3	0.78	0.55	0.61				
6035		0.2	1.8	0.11	0.03		0.09			
6036		0.9	1.6	0.35	0.22	0.25	0.28			
6037		1.5	1.6	0.48	0.33	0.40	0.44			
6051		5.3	1.0	0.84	0.73	0.78	0.80			
6052		7.4	1.2	0.86	0.77	0.81		0.79	0.81	0.80
6053		1.6	1.2	0.57	0.44	0.51	0.54	0.52	0.55	0.53
6054		0.9	0.5	0.64	0.49	0.55		0.52	0.51	0.51
6055		1.0	1.1	0.48	0.40	0.47	0.43	0.44	0.46	0.45
6056		5.1	0.5	0.91	0.78	0.82		0.80	0.82	0.82
6057		3.1	1.2	0.72	0.56	0.62		0.63	0.62	0.62
6058		4.5	1.2	0.79	0.64	0.70	0.68	0.70	0.69	0.69
6059	75	6.0	1.2	0.83	0.75	0.80		0.75	0.76	0.76
6060		3.3	1.5	0.69	0.54	0.60		0.61	0.60	0.61
6061		1.5	1.5	0.49	0.36	0.43		0.44	0.45	0.44
6062		5.5	1.6	0.77	0.68	0.72		0.74	0.70	0.71
6063		10.1	1.3	0.88	0.88	0.90		0.82	0.87	0.86
6074		5.0	0.1	0.97	0.96	0.97				
6075		10.0	0.1	0.99	1.02					
6076		9.8	0.3	0.97	1.00					
6077		5.0	0.3	0.95	0.90	0.92	0.90			
6078		0.8	0.2	0.77	0.65	0.71	0.72			
6079		0.9	0.2	0.85	0.72	0.77	0.71			
6080		9.4	0.5	0.95	0.94	0.95				

TABLE 5.2 COMPARISON OF VARIOUS VOID FRACTIONS

5" Pipe, 40 bar

RUN ID TSN	TURB. VEL (M/S)	VSL+VSG (M/S)	V LIQ. G DENS (M/S)	V GAS G DENS (M/S)	V TURB / VSL+VSG	V TURB / V LIQ	V TURB / V GAS	$V\ TURB_E$ / V LIQ	$V\ TURB_A$ / V LIQ	$V\ TURB_R$ / V LIQ
5001	11.13	10.04	3.14	10.58	1.11	3.53	1.05	1.212	1.863	2.25
5002	5.28	5.13	2.14	5.50	1.03	2.46	0.96	1.11	1.48	1.53
5004	10.68	9.93	2.06	10.38	1.07	5.18	1.03	1.34	2.64	3.85
5005	10.83	9.80	1.75	10.06	1.10	6.17	1.08	1.58	3.12	4.89
5037	5.18	4.89	2.04	5.08	1.06	2.53	1.02	1.30	1.57	1.73
5038	5.05	4.88	1.52	5.01	1.03	3.27	1.00	1.35	2.00	2.52
5039	5.20	5.10	2.34	5.14	1.02	2.37	1.01	1.63	1.72	2.00
* 5040	0.37	1.04	0.33	1.18	0.35	1.10	0.31	1.08	1.64	1.75
* 5041	0.36	0.85	1.03	0.82	0.42	0.35	0.44	0.965	0.94	0.98
* 5042	0.22	1.24	1.62	1.18	0.18	0.14	0.19	0.955	0.926	0.97
5043	10.59	9.67	1.61	9.96	1.10	6.55	1.06	1.45	3.25	5.06
5044	5.74	5.31	4.07	5.49	1.08	1.41	1.04	1.04	1.10	1.07
* 5045	0.36	1.39	2.63	1.10	0.26	1.138	0.33	0.88	0.86	0.98
* 5046	0.15	0.97	2.18	0.61	0.15	0.069	0.24	0.83	0.84	0.98
5054	10.26	9.69	4.17	9.99	1.06	2.4	1.02	1.22	1.54	1.71
5055	4.92	5.02	2.60	5.26	0.98	1.89	0.94	1.11	1.34	1.34
5056	4.70	4.69	1.78	4.90	1.00	2.63	0.96	1.19	1.64	1.83
5057	4.48	4.83	1.05	5.03	0.93	4.22	0.89	1.34	1.70	3.61
5058	10.30	9.60	1.61	9.92	1.07	6.37	1.04	1.45	3.24	5.01
5059	10.20	9.55	2.36	9.92	1.05	4.31	1.03	1.32	2.30	3.13
* 5060	0.18	1.20	1.01	1.23	0.15	0.185	0.15	1.03	1.06	1.04
* 5061	0.17	0.96	0.29	1.12	0.18	0.597	0.15	1.08	1.69	1.82
* 5062	0.24	1.31	1.55	1.27	0.18	0.157	0.16	0.97	0.95	0.98

"R" = Rouhani Model; "A" = Aya Model ; "E" = Estrada Model

* Turbine Meter Below Measurement Range

3" Pipe, 40 bar

RUN ID TSN	TURB. VEL (M/S)	VSL+VSG (M/S)	V LIQ. G DENS (M/S)	V GAS G DENS (M/S)	V TURB / VSL+VSG	V TURB / V LIQ	V TURB / V GAS	$V\ TURB_E$ / V LIQ	$TURB_A$ / LIQ	$V\ TURB_R$ / V LIQ
6003	3.67	5.93	3.06	7.80	0.62	1.17	0.46	1.02	1.25	1.14
6004	6.54	10.36	5.34	11.83	0.63	1.22	0.55	1.04	1.27	1.19
6005	7.72	10.24	6.28	11.25	0.76	1.228	0.68	1.04	1.19	1.12
6013	9.60	11.17	8.04	11.62	0.86	1.2	0.83	1.05	1.10	1.09
6014	4.17	5.16	3.23	6.08	0.80	1.29	0.68	1.04	1.16	1.08
6015	1.40	1.79	1.55	2.24	0.78	0.9	0.63	1.00	1.04	1.01
6016	0.93	1.33	0.94	1.80	0.70	0.99	0.54	1.01	1.11	1.04
6017	6.33	5.74	2.13	6.89	1.10	2.97	0.91	1.05	1.52	1.46
6018	11.55	10.08	5.42	10.58	1.14	2.12	1.09	1.10	1.30	1.29
6019	1.75	2.48	1.98	3.46	0.70	0.88	0.50	1.01	1.02	1.02
6020	1.83	2.57	2.01	3.47	0.71	0.91	0.52	1.00	1.08	1.02
6021	5.35	6.96	4.47	7.94	0.77	1.19	0.68	1.03	1.15	1.08
6022	2.82	3.95	2.74	4.93	0.71	1.02	0.57	1.01	1.12	1.04
6023	4.55	5.92	3.81	6.91	0.77	1.19	0.66	1.02	1.15	1.07
6024	6.38	8.18	5.50	8.94	0.78	1.16	0.71	1.03	1.14	1.08
6025	8.02	10.02	7.61	10.48	0.80	1.05	0.76	1.02	1.10	1.06
6026	5.40	7.38	4.93	8.28	0.73	1.09	0.65	1.03	1.14	1.07
6027	3.09	4.15	3.01	5.06	0.74	1.03	0.61	1.01	1.10	1.03
6048	4.78	6.73	4.08	8.53	0.71	1.17	0.56	1.02	1.17	1.08

TABLE 5.4 TURBINE METER VELOCITY COMPARISONS FOR THE 5" AND 3" PIPE TESTS

RUN ID TSN	$(\rho V^2)_{DD}$ $\frac{kg}{ms^2}$	$(\rho V^2)_{tp}$ $\frac{kg}{ms^2}$	$(\rho V^2)_g$ $\frac{kg}{ms^2}$	$\frac{(\rho V^2)_{DD}}{(\rho V^2)_{tp}}$	$\frac{(\rho V^2)_g}{(\rho V^2)_{tp}}$	$\frac{(\rho V^2)_{DD}}{(\rho V^2)_g}$	V_{DD}-ρ_g $\frac{m}{s}$	V_{DD}-ρ_Y $\frac{m}{s}$	V_T $\frac{m}{s}$	$\frac{V_{DD}- g}{V_T}$	$\frac{V_{DD}- g}{V_{sl}+V_{sg}}$	$\frac{V_{DD}-\rho_Y}{V_{sl}+V_{sg}}$
					p ~ 40 bar							
5001	2533	2771	2196	0,91	0,79	1,15	11,25	5,73	11,13	1,01	1,12	0,57
5002	607	963	572	0,63	0,59	1,06	5,5	2,41	5,28	1,04	1,07	0,47
5004	2348	2301	2114	1,02	0,92	1,11	10,8	6,15	10,68	1,01	1,09	0,62
5005	2384	2124	2046	1,12	0,96	1,16	10,9	7,30	10,83	1,00	1,12	0,75
5037	577	691	487	0,83	0,70	1,19	5,4	2,92	5,18	1,04	1,10	0,60
5038	571	565	498	1,01	0,88	1,14	5,3	3,40	5,05	1,05	1,08	0,69
5039	514	584	524	0,88	0,90	0,98	5,1	4,10	5,20	0,98	1,00	0,80
* 5040	126	38	23	3,24	0,60	5,32	2,5	0,91	0,37	6,76	2,39	0,88
* 5041	178	122	12	1,46	0,10	14,50	3,0	1,21	0,36	8,33	3,51	1,41
* 5042	181	337	24	0,54	0,07	7,50	3,0	1,15	0,22	13,63	2,40	0,92
5043	2065	2009	1944	1,03	0,97	1,06	10,2	6,58	10,59	0,96	1,05	0,68
5044	690	2149	539	0,32	0,25	1,28	5,9	2,45	5,74	1,03	1,11	0,46
* 5045	217	1067	20	0,20	0,02	10,80	3,3	1,13	0,36	9,16	2,35	0,81
* 5046	183	880	6	0,21	0,01	31,70	3,0	0,95	0,15	20,00	3,07	0,97
5054	2121	2694	1933	0,79	0,72	1,09	10,2	5,90	10,26	0,99	1,05	0,61
5055	537	982	511	0,55	0,52	1,05	5,2	2,46	4,92	1,05	1,03	0,49
5056	516	632	461	0,82	0,73	1,12	5,1	2,65	4,70	1,08	1,09	0,56
5057	519	539	493	0,96	0,91	1,05	5,1	2,95	4,48	1,14	1,05	0,61
5058	2169	1998	1920	1,09	0,96	1,13	10,4	6,56	10,30	1,01	1,08	0,68
5059	2106	2100	1886	1,00	0,90	1,11	10,2	6,02	10,20	1,00	1,07	0,63
* 5060	107	128	27	0,83	0,21	3,96	2,3	0,95	0,18	12,77	1,90	0,79
* 5061	92	33	20	2,72	0,60	4,60	2,1	0,73	0,17	12,35	2,17	0,75
* 5062	85	312	28	0,27	0,09	3,00	2,0	0,78	0,24	8,33	1,52	0,59
					p ≈ 75 bar							
5014	1334	1423	1315	0,94	0,93	1,01	5,84	5,48	6,19	0,94	1,01	0,95
5015	1104	1165	1065	0,95	0,91	1,03	5,32	4,30	5,61	0,95	1,03	0,83
5016	1183	1372	1090	0,86	0,79	1,08	5,5	4,04	5,83	0,94	1,05	0,77
* 5017	61	137	43	0,44	0,31	1,42	1,25	0,69	0,67	1,86	1,13	0,62
* 5019	99	325	32	0,30	0,01	3,09	1,59	0,83	0,51	3,12	1,49	0,77
5021	2777	3332	2369	0,83	0,71	1,17	8,43	6,38	8,73	0,97	1,08	0,81
5022	2689	2800	2417	0,96	0,86	1,11	8,30	6,67	8,58	0,97	1,06	0,85
5023	2523	2522	2351	1,00	0,93	1,07	8,04	7,25	8,35	0,96	1,04	0,93
5024	2475	2505	2336	0,99	0,93	1,06	7,97	7,58	8,20	0,97	1,03	0,98
5025	1155	1537	1000	0,75	0,65	1,15	5,44	3,48	5,59	0,97	1,07	0,69
* 5047	350	1049	213	0,33	0,20	1,64	3,00	1,35	1,87	1,60	1,16	0,52
* 5048	192	892	39	0,21	0,44	4,92	2,21	1,01	0,46	4,82	1,60	0,73
* 5049	152	768	11	0,20	0,01	13,82	1,97	0,86	0,25	7,90	2,05	0,89
5066	1106	1414	1010	0,78	0,71	1,09	5,32	3,23	5,34	1,00	1,06	0,64
5067	1102	1152	967	0,96	0,84	1,13	5,31	3,66	5,22	1,02	1,09	0,75
* 5068	86	141	51	0,61	0,36	1,68	1,48	0,80	0,52	2,85	1,26	0,68
* 5069	110	358	65	0,30	0,18	1,69	1,68	0,88	0,30	5,59	1,18	0,62
* 5070	147	84	65	1,75	0,77	2,26	1,94	1,12	0,71	2,73	1,55	0,90
5071	1291	1256	1207	1,02	0,96	1,07	5,75	4,24	5,59	1,03	1,06	0,78
					p ≈ 4 bar							
5031	494	2236	89	0,22	0,04	5,55	14,60	2,31	1,13	2,04	2,31	0,36
5032	603	1681	332	0,36	0,20	1,82	14,30	3,98	3,74	1,06	1,34	0,37
* 5033	69	280	2	0,25	0,01	34,50	4,84	0,66	0,16	4,12	4,60	0,64
5034	283								0,44			
* 5035	133	146	52	0,91	0,35	2,56	7,56	1,33	0,15	8,86	1,65	0,29
5050	784	464	254	1,69	0,55	3,09	17,90	3,62	4,65	0,77	1,75	0,36
* 5051	206	657	52	0,31	0,07	3,96	9,50	1,53	0,29	5,27	1,99	0,32
* 5052	288	32	2		0,07	144,00	10,50	0,92	0,14	6,57	12,08	1,06
					Air-Water Flow, p ≈ 2 bar (TSN 4208, 4212 : p ≈ 6 bar)							
o 4208	582	260	14	2,24	0,05	41,00	3,75	1,75	0,39	9,63	2,37	1,11
o 4209	827	387	207	2,15	0,54	4,00	18,56	3,18	6,75	2,96	1,89	0,32
o 4210	595	266	233	2,24	0,88	2,55	15,74	2,88	7,10	2,21	1,50	0,27
o 4211	1315	1060	235	1,24	0,22	5,60	23,40	4,30	6,86	3,41	2,20	0,40
o 4212	587	903	253	0,65	0,28	2,32	9,02	2,76	5,10	1,77	1,40	0,47
o 4213	2209	4693	222	0,47	0,05	9,95	30,33	6,45	7,54	4,02	2,80	0,60
o 4214	874	3565	2	0,25	<0,01	406,00	19,08	3,51	2,65	7,20	4,34	0,80
o 4215	1016	1067	3	0,95	<0,01	311,00	20,50	2,23	0,77	26,72	12,57	1,35
o 4216	1218	1138	1	1,07	<0,01	1268,00	22,53	2,36	0,89	25,31	19,93	2,10

"*" Drag Disc below Measuring Range ; "o" Drag Disc sticked

$$(\rho V^2)_{tp} = G_g V_g + G_l V_l = G_g V_{sg}/\alpha + G_l V_{sl}/(1-\alpha) = \alpha \rho_g V_g^{\,2} + (1-\alpha)\rho_l V_l^{\,2}$$

$$V_{DD}\text{-}\rho_g = ((\rho V^2)_{DD}/\rho_g)^{0.5} \quad ; \quad V_{DD}\text{-}\rho_Y = ((\rho V^2)_{DD}/\rho_Y)^{0.5}$$

TABLE 5.5 COMPARISON USING THE DRAG DISC READING (5" PIPE TESTS)

	RUN ID TSN	$(\rho v^2)_{DD}$ (kg/ms^2)	$(\rho v^2)_{tp}$ (kg/ms^2)	$(\rho v^2)_h$ (kg/ms^2)	$\frac{(\rho v^2)_{DD}}{(\rho v^2)_{tp}}$	$\frac{(\rho v^2)_{DD}}{(\rho v^2)_h}$	$v_{DD-\rho_\gamma}$ (m/s)	$\frac{v_{DD-\rho_\gamma}}{v_{sg}+v_{sl}}$	$\frac{v_{DD-\rho_\gamma}}{v_T}$
					3 INCH	40 BAR			
	6003	2125	3693	6268	0.58	0.34	2.55	0.43	0.69
	6004	3484	7347	11890	0.47	0.29	4.22	0.41	0.64
	6005	3716	8408	12221	0.44	0.30	4.58	0.45	0.59
	6013	3755	8879	11308	0.42	0.33	5.64	0.51	0.59
	6014	1713	3201	4721	0.53	0.36	2.51	0.49	0.60
	6015	1459	1276	1463	1.14	1.00	1.67	0.93	1.19
	6016	565	409	560	1.38	1.01	1.13	0.85	1.21
	6017	1189	1604	2959	0.74	0.40	2.39	0.42	0.38
	6018	3281	4319	6170	0.76	0.53	5.86	0.58	0.51
	6019	2524	2163	2658	1.16	0.95	2.17	0.88	1.24
	6020	2697	2097	2623	1.28	1.03	2.32	0.90	1.26
	6021	2618	5390	7774	0.48	0.34	3.31	0.48	0.62
	6022	2257	2964	4088	0.76	0.55	2.47	0.63	0.88
	6023	2250	4375	6332	0.51	0.35	2.89	0.49	0.64
	6024	3209	6608	9091	0.48	0.35	4.09	0.50	0.65
	6025	3721	9314	11596	0.39	0.32	5.05	0.50	0.63
	6026	2874	6229	8702	0.46	0.33	3.54	0.48	0.65
	6027	2360	3451	4603	0.68	0.51	2.56	0.61	0.83
	6048	2966	6214	9517	0.48	0.31	2.98	0.44	0.63
	6066	377	56	104	6.73	3.62	1.31	1.27	
	6067	463	145	257	3.19	1.80	1.12	0.97	
2)	6068	901	-	1526		0.59			
1) 2)	6069	4749	-	4388	-	1.08			
1)	6070	1744	1108	1785	1.57	0.98	3.86	0.69	
1) 2)	6071	1401	-	1034		1.35			
					3 INCH	75 BAR			
	6035	2943	2442	2600	1.20	1.13	2.03	1.02	1.09
	6036	3150	2621	3051	1.20	1.03	2.33	0.94	1.21
	6037	3402	3014	3745	1.13	0.91	2.59	0.85	1.10
	6051	2866	4259	5917	0.67	0.48	3.57	0.57	0.56
	6052	3851	7254	9957	0.53	0.39	4.37	0.51	0.62
	6053	2507	2174	2710	1.15	0.93	2.41	0.85	1.13
	6054	538	436	578	1.23	0.93	1.16	0.82	1.17
	6055	1649	1468	1660	1.12	0.99	1.89	0.93	1.19
	6056	2070	2198	3241	0.94	0.64	3.27	0.58	0.50
	6057	2222	3114	4350	0.71	0.51	2.53	0.59	0.77
	6058	2626	4292	6133	0.61	0.43	3.01	0.52	0.65
	6059	3762	6186	8072	0.61	0.47	4.19	0.59	0.65
	6060	2995	4329	5876	0.69	0.51	2.87	0.60	0.80
	6061	3434	2781	3385	1.23	1.01	2.65	0.91	1.18
	6062	3863	7702	10004	0.50	0.38	3.82	0.54	0.67
	6063	4162	15398	15779	0.27	0.26	5.80	0.51	0.54
1)	6074	2772	1370	1520	2.02	1.82	6.42	1.25	
1)	6075	5360	3181	5047	1.68	1.06	14.60	1.43	
1)	6076	5456	20709	5798	0.26	0.94	11.47	1.09	
1)	6077	2544	1582	2034	1.60	1.25	4.80	0.78	
1)	6078	585	152	203	3.84	2.88	1.44	1.44	
1)	6079	559	103	149	5.42	3.75	1.53	1.52	
1)	6080	5465	7024	7647	0.78	0.71	8.03	0.80	

1) Drag Disc Shifted 2) Densitometer Reading not Correct

TABLE 5.6 COMPARISON USING THE DRAG DISC READING (3" PIPE TESTS)

TSN	V_g (m/s)	V_l (m/s)	S (1)	N_{Mn}	N_{Ar}	σ_{V_g} (m/s)	σ_{V_e} (m/s)	V_g (m/s)	V_l (m/s)	S (1)	N_{Mn}	N_{Ar}	σ_{V_g} (m/s)	σ_{V_l} (m/s)	V_g (m/s)	V_l (m/s)	S (1)	N_{Mn}	N_{Ar}	σ_{V_g} (m/s)	σ_{V_l} (m/s)	V_g^* (m/s)	V_l^* (m/s)
5" Pipe Tests:	$\overline{D1-D3}$							$\overline{D3-D5}$							$\overline{D5-D7}$								
5054	10.40	3.50	2.97	6	5	0.88	0.21	11.00	3.56	3.09	6	5	1.10	0,48	11.00	2.98	3.69	6	5	1.10	0.44		
5056	5.0	1.3	3.85	6	5	0.00	0.10	4.70	1.29	3.64	2	5	0.30	0.06	4.45	1.33	3.35	6	5	0.47	0.06		
5057	5.00	1.36	3.68	3	2	0.00	0.09	5.00	1.36	3.68	3	2	0.00	0.04	5.45	7.27	4.29	3	2	0.00	0.06		
5058	10.67	2.83	3.77	4	3	1,15	0.20	10.00	2.49	4.02	4	3	0.00	0.32	10.00	2.32	4.31	4	3	0.00	0.19		
5059	11.00	3.16	3.48	3	2	1.41	0.17	10.00	2.86	3.50	3	2	0.00	0.14	10.00	2.52	3.97	3	2	0.00	0.27		
5060	1.21	1.21	1.00	5	4	0.08	0.09	1.23	1.06	1.16	5	4	0.09	0.10	1.35	1.00	1.35	5	4	0.14	0.07		
5061	1.08	0.59	1.83	4	3	0.10	0.05	1.20	0.30	4.00	4	3	0.02	0.02	1.15	0.31	3.71	4	3	0.04	0.02		
5062	1.35	2.08	0.65	6	4	0.10	0.07	1.39	1.94	0.72	6	4	0.09	0.17	1.36	1.83	0.74	6	4	0.08	0.22		
5066	5.43	2.95	1.84	11	10	0.41	0.44	5.27	2.59	2.03	7	10	0.23	0.58	5.27	2.27	2.32	3	10	0.23	0.67		
5067	5.21	3.36	1.55	8	9	0.31	1.21	5.11	2.96	1.73	7	9	0.28	0.83	5.25	2.51	2.09	5	9	0.24	0.41		
5068	1.00	1.30	0.77	3	1	0.00	0.06	1.02	1.16	0.88	3	1	0.00	0.05	1.03	0.96	1.07	3	1	0.00	0.05		
5069	1.17	1.91	0.61	7	5	0.06	0.07	1.18	1.80	0.66	7	5	0.07	0.23	1.20	1.57	0.76	7	5	0.09	0.12		
5070	1.21	0.76	1.59	4	3	0.01	0.10	1.30	0.62	2.10	4	3	0.20	0.03	1.22	0.50	2.44	4	3	0.05	0.05		
5071	5.55	2.86	1.94	5	18	0.32	0.84	5.64	2.4	2.35	4	18	0.31	1.30	5.65	1.87	3.02	3	18	0.42	0.31		
3" Pipe Tests:	$\overline{D1-D3}$							$\overline{D3-D5}$							$\overline{D5-D8}$							V_g^* (m/s)	V_l^* (m/s)
6013	1.24	11.61	1.07	7	6	0,44	1.20	12.61	9.77	1.29	7	6	0.24	2.78	12.93	9.12	1.42	7	6	0.30	3.29	12.77	9.45
6014	5.56	4.59	1.21	7	6	0,57	0,90	6,09	3.70	1.65	7	6	0.84	0.51	6.26	2.99	2.08	7	6	0.86	0.41	6.18	3.35
6015	1.56	2.19	0.71	6	5	0.20	0,09	1.70	1.87	0.91	6	5	0.19	0.12	2.12	1.50	1.41	6	5	0.85	0.11	1.91	1.69
6016	1.47	1.45	1.01	3	3	0.00	0.10	1.61	1.08	1.49	3	1	0.00	0.06	1.83	0.89	2.06	3	1	0.00	0.11	1.72	0.99
6017	6.67	2.81	2.66	3	1	0.00	0.12	7.14	2.34	3,05	3	1	0.00	0.25	6.51	2.20	2.96	3	1	0.00	0.06	6.83	2.27
6018	10.56	6.20	1.70	3	2	0,78	1,85	10,56	5.45	1,93	3	2	0.78		10.72	4.04	2.65	3	2	0.33		10.64	4.75
6019	1.96	2.83	0.69	3	2	0.06	0.05	2.11	2.27	0,93	3	2	0.16	0.06	2.37	2.03	1.17	3	2	0.13	0.08	2.24	2.15
6020	1.94	2.75	0.71	4	2	0,21	0.18	2.21	2.33	0,95	4	2	0.18	0.12	2.71	2.03	1.33	4	2	0.00	0.11	2.46	2.52
6021	7.62	7.18	1,06	5	4	0.80	1.37	8.15	5,44	1.50	5	4	0.94	0.69	8.61	4.00	2.15	5	4	0.62	0.34	8.38	4.72
6022	3.79	4.11	0.92	5	3	0.71	0,64	4.13	3.35	1.23	5	3	0.73	0.5	4.76	2.77	1.72	5	3	1.10	0.52	4.45	3.06
6023	6.13	5.69	1.08	8	7	0.52	0,82	6.78	4.08	1.66	8	7	0.92	0.23	6.86	3.63	1.89	8	7	0.79	0.42	6.82	3.86
6024	9.02	8.16	1.10	12	11	0.79	0,59	8.98	6.40	1.40	12	11	0.87	0.71	8.94	5.01	1.78	12	11	0.43	0.60	8.96	5.71
6025	11.02	10.01	1.10	10	9	0,71	1,00	11.04	9.06	1.22	10	9	0.45	1.38	10.96	6.50	1.69	10	9	0.42	1.0	11.00	7.78
6026	8.05	7.13	1.13	9	7	0.90	0.58	7,89	5.66	1.39	9	7	0.94	0.65	7.85	4.82	1.63	9	7	1.05	0.34	7.87	5.24
6027	4.66	4.46	1.04	20	19	0.77	0.52	4.92	3.63	1.36	20	19	0.75	0.43	5.20	3.09	1.69	7	19	0.94	0.37	5.06	3.36

* = Phase Velocities interpolated on LOFT densitometer position: $V^* = \frac{V_{\overline{D3-D6}} + V_{\overline{D5-D8}}}{2}$

TABLE 5.7 MEAN VALUES AND STANDARD DEVIATIONS OF THE RADIOTRACER VELOCITY MEASUREMENTS

6. Discussion of Mass Flow Rates (Pipe Averaged Mass Fluxes) Using Two Parameter Equations

6.1 Discussion of the Two Parameter Equations

In the existing mass flux measurement model mass fluxes are calculated combining two instrument readings in the following manner:

$$\dot{G}_{\gamma\text{-}T} = \rho_\gamma V_T \tag{6.1}$$

$$G_{\gamma\text{-}DD} = (\rho_\gamma(\rho V^2)_{DD})^{0.5} \tag{6.2}$$

$$\dot{G}_{T\text{-}DD} = (\rho V^2)_{DD}/V_T \tag{6.3}$$

In the following, the equations using two instrument readings are called "two parameter equations". These equations are only correct for slip $S \equiv 1$ (compare e.g. Reimann /11/).

An equation which is correct for arbitriary values of slip is

$$\dot{G} = \alpha\rho_g V_g + (1-\alpha)\rho_l V_l \tag{6.4}$$

This equation, using three measurements (α, V_g and V_l, the densities are assumed to be known) is called a "three parameter equation".

In the following, characteristic errors are computed using a two parameter equation instead of eq. (6.4):
If the following assumptions are made:

i: the gamma densitometer measures the cross section averaged apparent density:

$$\rho_\gamma = \alpha\rho_g + (1-\alpha)\rho_l \tag{6.5}$$

ii: the turbine meter measures the total volume flow rate per unit area (total volume flux):

$$V_T = \alpha V_g + (1-\alpha)V_l \tag{6.6}$$

iii: the drag disc measures the cross section average of the two-phase momentum flux:

$$(\rho V^2)_{DD} = (\rho V^2)_{tp} = \alpha\rho_g V_g^2 + (1-\alpha)\rho_l V_l^2 \tag{6.7}$$

then the following ratios may be formed by inserting (6.5) - (6.7) in

(6.1) - (6.3) and deviding by (6.4):

$$\left(\frac{\dot{G}_{\gamma-T}}{G}\right)_{th} = \frac{\left(\alpha \frac{\rho_g}{\rho_l} + 1-\alpha\right)(\alpha S + 1-\alpha)}{\alpha \frac{\rho_g}{\rho_l} S + 1-\alpha} \tag{6.8}$$

$$\left(\frac{\dot{G}_{\gamma-DD}}{G}\right)_{th} = \frac{\left(\left(\alpha \frac{\rho_g}{\rho_l} + 1-\alpha\right)\left(\alpha \frac{\rho_g}{\rho_l} S^2 + 1-\alpha\right)\right)^{0.5}}{\alpha \frac{\rho_g}{\rho_l} S + 1-\alpha} \tag{6.9}$$

$$\left(\frac{\dot{G}_{T-DD}}{G}\right)_{th} = \frac{\alpha \frac{\rho_g}{\rho_l} \cdot S^2 + 1-\alpha}{(\alpha S + 1-\alpha)\left(\frac{\alpha\rho_g}{\rho_l} \cdot S + 1-\alpha\right)} \tag{6.10}$$

These ratios are labled with a "th" (= theoretical) to differ from the measured ratios which are discussed later.

The Figures 6.1 and 6.2 show these ratios for typical values of α as function of slip for steam-water flow at 40 and $\approx$ 75 bars. Equation (6.8) gives considerably high values even at low slip. Equation (6.9) calculates higher calues for slip $S>1$ but the deviations from the correct value are small compared with equation (6.8). Equation (6.10) using the turbine meter and drag disc reading gives too small values. With increasing pressure the deviations in using the equations (6.8) to (6.10) become smaller.

In the following the measured mass fluxes (using the instrument readings and equations (6.1) - (6.3) and the measured reference mass fluxes are compared. If these mass fluxes are not equal the difference is caused by

i) the equations (6.1) - 6.3)

ii) the single instrument readings, not giving the cross section averaged values

These two error sources will be discussed in detail.

6.2 Discussion of the 5" Pipe Tests

6.2.1 Mass Flow Rate from Gamma Densitometer and Turbine Meter

As shown previously the low pressure experiments with the 5" pipe did not give satisfactory results because the DTT reading was not satisfactory. Therefore, in the following only the experiments at ≈ 40 and ≈ 75 bars are discussed and only test points where the DTT was in the measuring range. Unlike Figure 3.1 where the results were presented as function of mass flux, Figure 6.3 shows the results as function of the interface level. Table 6.1 contains a comparison of the various ratios: the measured ratios using eq. (6.1) - (6.3) are presented in the columns (1) - (3) and the calculated ratios from (6.8) - (6.10) are shown in the columns (4), (6) and (8). As shown, in section 5 the DTT was measuring mostly steam flow in the 5" pipe experiments. Therefore the assumptions (6.6) and (6.7) are not quite correct. At these experiments, better assumptions are:

i) the turbine was measuring the phase velocity of steam

$$V_T = V_g \tag{6.11}$$

ii) the drag disc was measuring the momentum flux of the steam phase

$$(\rho V^2)_{DD} = \rho_g V_g^2 \tag{6.12}$$

If (6.11) and (6.12) are used in the equations (6.1) - (6.3), the following ratios may be formed:

$$\left(\frac{\dot{G}_{\gamma-T}}{\dot{G}}\right)_{th} = \frac{\alpha \frac{\rho_g}{\rho_l} + 1-\alpha}{\alpha \frac{\rho_g}{\rho_l} + (1-\alpha)/S} \tag{6.13}$$

$$\left(\frac{\dot{G}_{\gamma-DD}}{\dot{G}}\right)_{th} = \frac{\left(\alpha+(1-\alpha)\frac{\rho_l}{\rho_g}\right)^{0.5}}{\alpha+(1-\alpha)\frac{\rho_l}{\rho_g}\cdot\frac{1}{S}} \tag{6.14}$$

$$\left(\frac{\dot{G}_{T-DD}}{\dot{G}}\right)th = \frac{1}{\alpha + \frac{1-\alpha}{S}\frac{\rho_l}{\rho_g}} \tag{6.15}$$

The corresponding values from these equations are contained in the columns 5, 7 and 9.

Column 1 shows that the ratio $G_{\gamma-T}/G_{Ref}$ is mostly considerably above 1, often by a factor 2. The values are even higher than the values in column 4 because the turbine velocity was about 10% higher than the volumentric flux. The agreement between column 1 and 5 is very good.

It can be summarized that in high void fraction tests where the turbine measured approximately the volumetric flux, very high deviation are caused by the use of the two parameter equation (6.1).

6.2.2 Mass Flow Rate from Gamma Densitometer and Drag Disc

The results are shown in the Figures 3.2 and 6.3. Column 2 of Table 6.1 shows that the values of the ratio $G_{\gamma-DD}/G_{Ref}$ are in general much closer to 1 than the values in column 1. This is mainly caused by the fact that equation (6.9) (column 6 and Figs. 6.1 and 6.2) is only weakly dependent on slip. The values of the column 2 are in general lower than the corresponding values in column 6 because the measured steam momentum flux was smaller than the total two-phase momentum flux. The agreement between columns 2 and 7 is very good also at test points, where the values are considerably below 1 (e.g. Test Nr. 6044 and 5047).

To sum up, it can be stated that the combination of densitometer and drag disc gave much better results than the combination of densitometer and turbine meter. The reason for this is that equation (6.2) gives values which are only slightly too high even at high slip values. There errors are sometimes compensated somewhat by the drag disc reading which was in general too low. Large errors occurred when the measured steam momentum flux was considerably lower than the total momentum flux $(\rho V^2)_{tp}$.

6.2.3 Mass Flow Rate from Turbine Meter and Drag Disc

The Figures 3.3 and 6.3 contain the results. The measured ratio G_{T-DD}/G_{Ref} (column 3) is always too low due to the fact that

i) equation (6.10) gives too low values
ii) the measured momentum flux is lower than the total momentum flux and the turbine meter velocity is higher than the volumetric flux.

The comparison of the column 3 to the columns 8 and 9 show these effects. For most of the test points the errors are mainly caused by i) and not by ii).

6.3 Discussion of the 3" Pipe Tests

6.3.1 Mass Flow Rate from Gamma Densitometer and Turbine Meter

Table 6.2 again shows the measured and calculated ratios for the various combinations. For the computed values eq. (6.8) - (6.10) were taken using the assumptions (6.5) - (6.7). It was shown in Chapter 5 that these assumptions are not as fulfilled as for the 5" pipe tests. Therefore the deviations between the corresponding columns are larger.

The Tables 6.2 and 3.1 and the Figures 3.1 - 3.3 and 6.2 show that the results for the combination gamma densitometer-turbine meter have a much higher accuracy in the 3" pipe tests than in the 5" pipe tests.

The reason for this is

i) the slip is lower and because of this ratio $(G_{\gamma-T}/G)_{th}$ is not as high as in the 5" tests.
ii) the turbine in general did not read higher than the volumetric velocity but only about $0.8 \cdot (V_{sl}+V_{sg})$ (Figure 5.6). This tends to compensate the error of i).

However there are some test runs (6017, 18, 56) with $V_{sl} \approx 0.5$ m/s and $V_{sg} \geq 5$ m/s which are similar to the 5" pipe tests. These test points were situated in the wave droplet flow regime with relatively low droplet entrainment. Therefore the turbine measured about the phase velocity of steam, the ratio $(G_{\gamma-T}/G_{Ref})$ is much higher than 1 and even higher then $(G_{\gamma-T}/G)_{th}$.

If these points are not taken into account the mean values and standard deviation are as follows

p(bar)	$(G_{\gamma-T}/G_{Ref})$	σ
40	1.05	0.1
75	1.07	0.17
40 + 75	1.06	0.11

Fig. 6.4 shows $(G_{\gamma-T}/G_{Ref})$ as function of the interface level. The ratio increases with decreasing interface level. This tendency is caused by the fact that with decreasing interface level the slip increases and thus the ratio $(G_{\gamma-T}/G)_{th}$ increases.

To sum up, it can be stated that the measurements using turbine and gamma densitometer had a good accuracy if the interface level was in the turbine. Large errors occurred at low values of V_{sl} ($V_{sl} \lesssim 0.5$ m/s) and high void fraction (interface level near the bottom of the turbine or below).

6.3.2 Mass Flow Rate from Gamma Densitometer and Drag Disc

The equation (6.2) introduces only small errors for the slip range which exists in the 3" pipe tests as the column $(G_{\gamma\text{-}DD}/G)_{th}$ in Table 6.2 shows. Therefore, the mass flux ratios in Figure 6.4 show the same tendency as the momentum flux ratios in Figure 5.7. Because the mass flux is evaluated with the square root of the drag disc reading, the deviations in Figure 6.4 are about half of the deviations in Figure 5.7.

To sum up, it can be stated that the deviations in mass flux are caused by the local measurement of the drag disc which in general is not characteristic for the cross section averaged value.

6.3.3. Mass Flow Rate from Turbine Meter and Drag Disc

The deviations are caused by the following effects:

i) the accuracy of the equation (6.3) is quite sensitive to slip and gives in general too low values

ii) the drag disc reading which is too low for $(y/d)_{IF} < 0.5$ and too high for $(y/d)_{IF} > 0.5$

iii) the turbine meter reading which is about 0.8 $(V_{sg}+V_{sl})$ for an interface level in the turbine and about $(V_{sg}+V_{sl})$ for an interface level below or near the bottom of the turbine.

These effects are superimposed and cause the large scattering of data.

6.4 Influence of the Axial Distance between Gamma Densitometer and DTT Position

Up to now the length weighted densitometer density (void fraction) was used for evaluating the mass fluxes although it was shown in 5.1 that a correction for stratification improved the agreement between the 3 beam densitometer and the radiotracer void fractions. The length weighted void fraction was smaller than the corrected value and gave a higher value for the slip. On the other hand the axial distribution of radiotracer velocities (Figure 4.8) showed that even at the instrument position an axial change of phase velocities could still exist with the tendency that slip increased with increasing pipe length. Therefore the too high slip evaluated from the upstream densitometer was compensated somewhat by the fact that at the DTT position slip has increased due to the velocity rearrangement between the two positions.

To examine this effect, the axial radiotracer void fraction distributions evaluated from $\alpha_{Rl} = 1 - V_{sl}/V_{Rl}$ were extrapolated to the DTT position (Figure 6.5) and the corresponding densities were used for the equations (6.1) and (6.2). Table 6.3 shows that the mean values are nearly the same which justifies the assumptions that the two different effects compensate each other.

6.5 Mass Fluxes as Function of Flow Regime

As it was done for the reading of the single instruments, in the Figures6.6 - 6.8 the mass fluxes are drawn in the flow regime map. The mass flux $G_{\gamma-T}$ has the least error in the slug flow regime and large errors in the wave flow regime and the transition to annular droplet flow. The accuracy of the mass flux $G_{\gamma-DD}$ is quite good in the wave and transition to annular droplet flow regime and in the transition from slug to elongated bubble flow. However in the slug regime the results are to low. The values of G_{T-DD} are mostly too low except those in the transition from slug to elongated bubble flow.

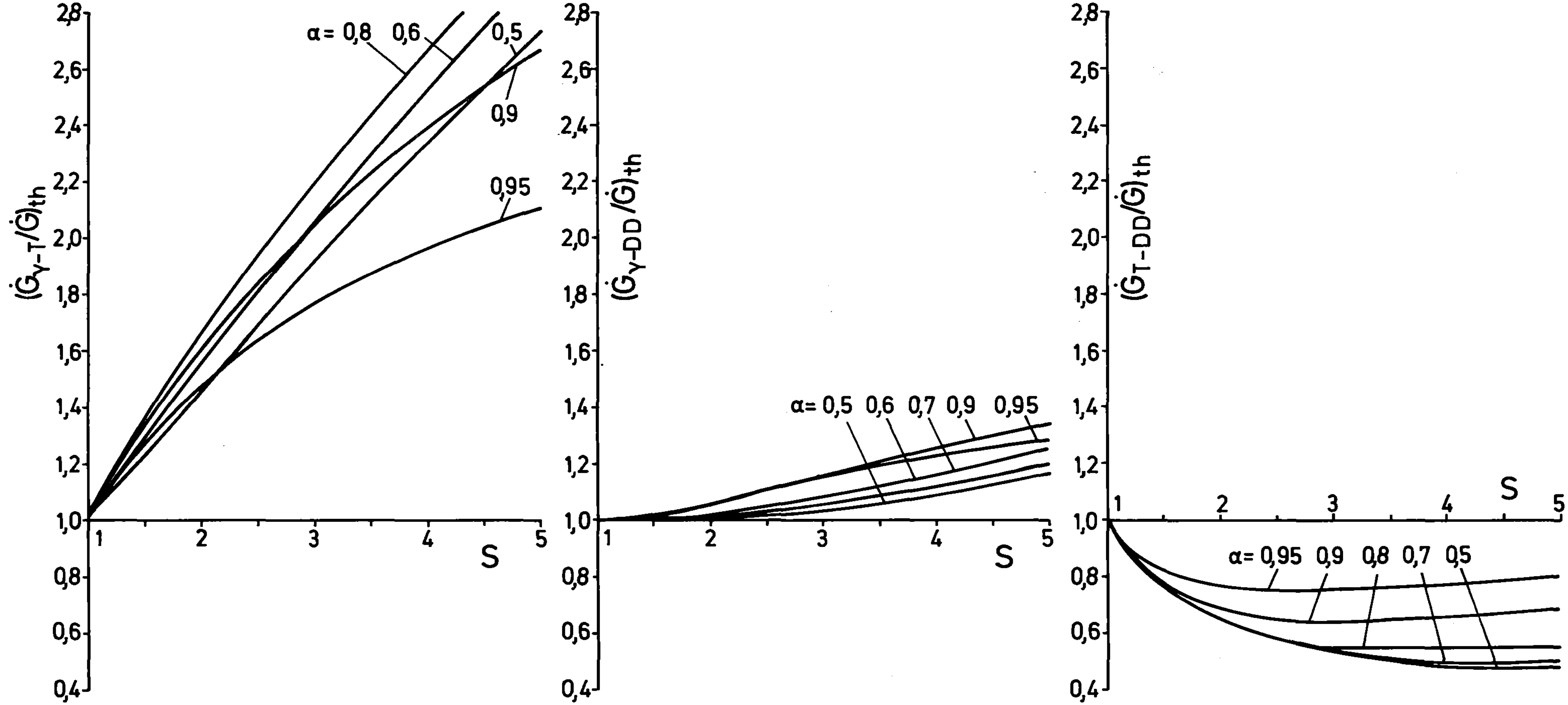

FIGURE 6.1 RATIOS OF THE TWO PARAMETER MASS FLOW RATE EQUATIONS TO THE EXACT EQUATION AS FUNCTION OF SLIP (STEAM-WATER FLOW, P = 40 BAR)

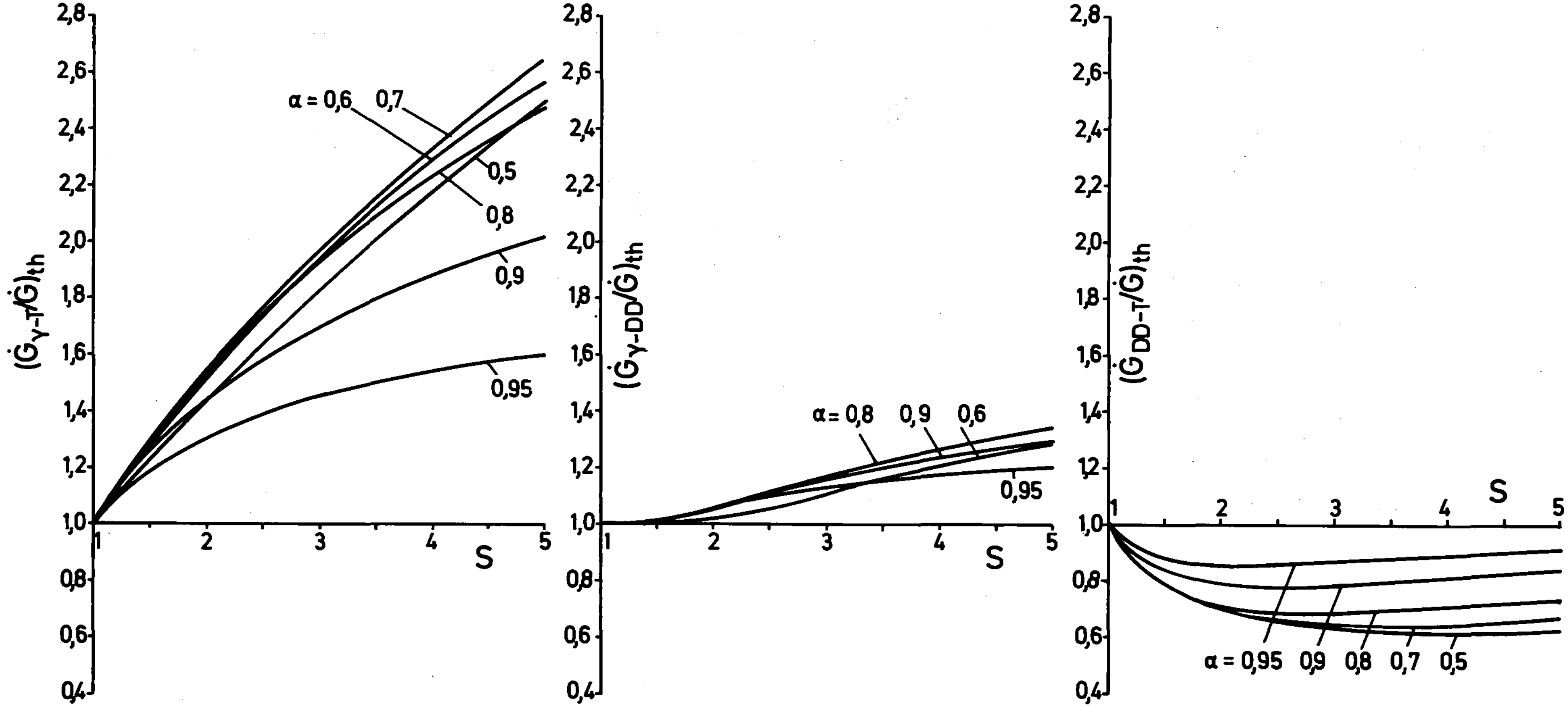

FIGURE 6.2 RATIOS OF THE TWO PARAMETER MASS FLOW RATE EQUATIONS TO THE EXACT EQUATION AS FUNCTION OF SLIP (STEAM-WATER FLOW, P = 75 BAR)

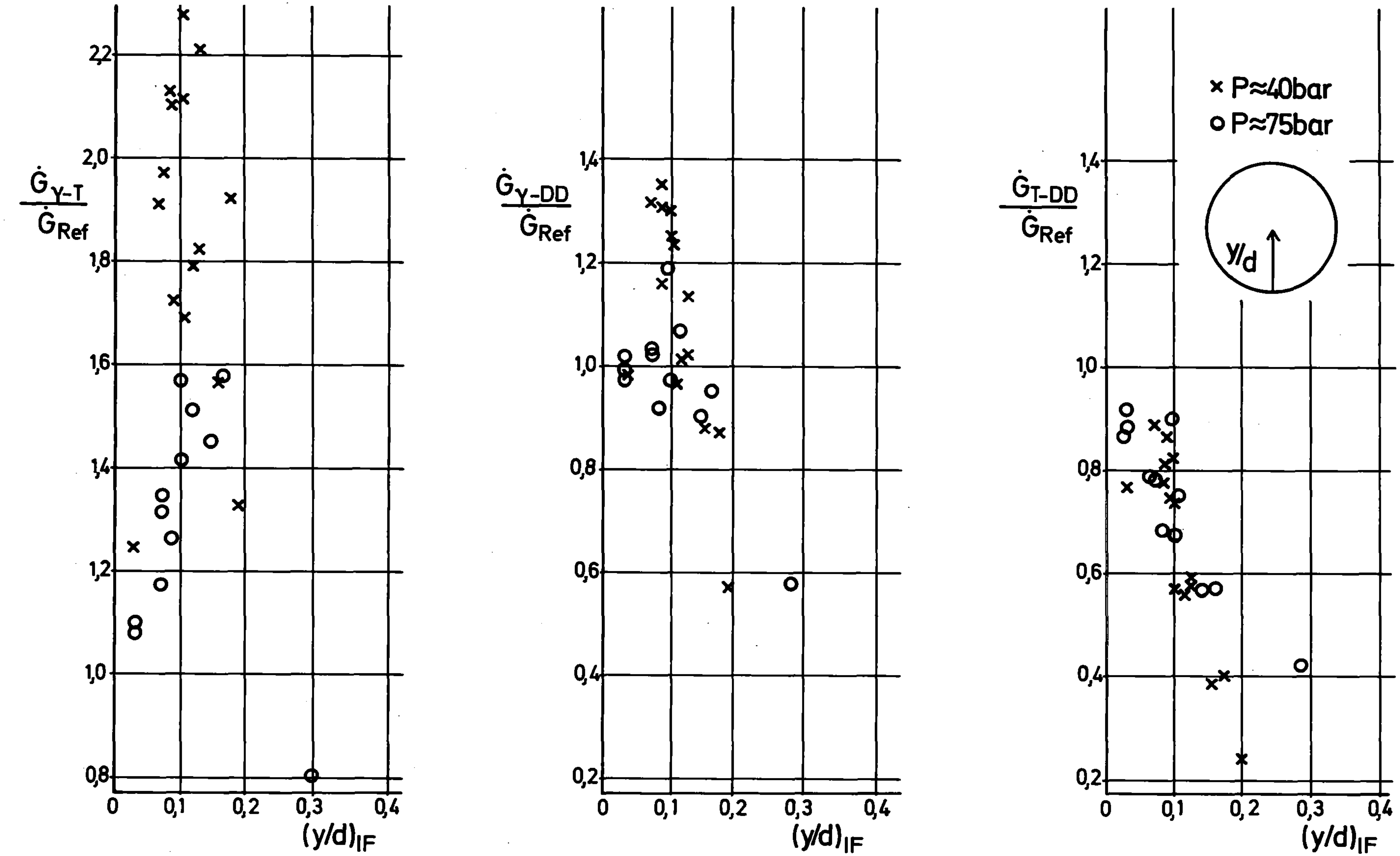

FIGURE 6.3 TWO PARAMETER MASS FLOW RATES AS FUNCTION OF THE INTERFACE LEVEL (5 " PIPE TESTS)

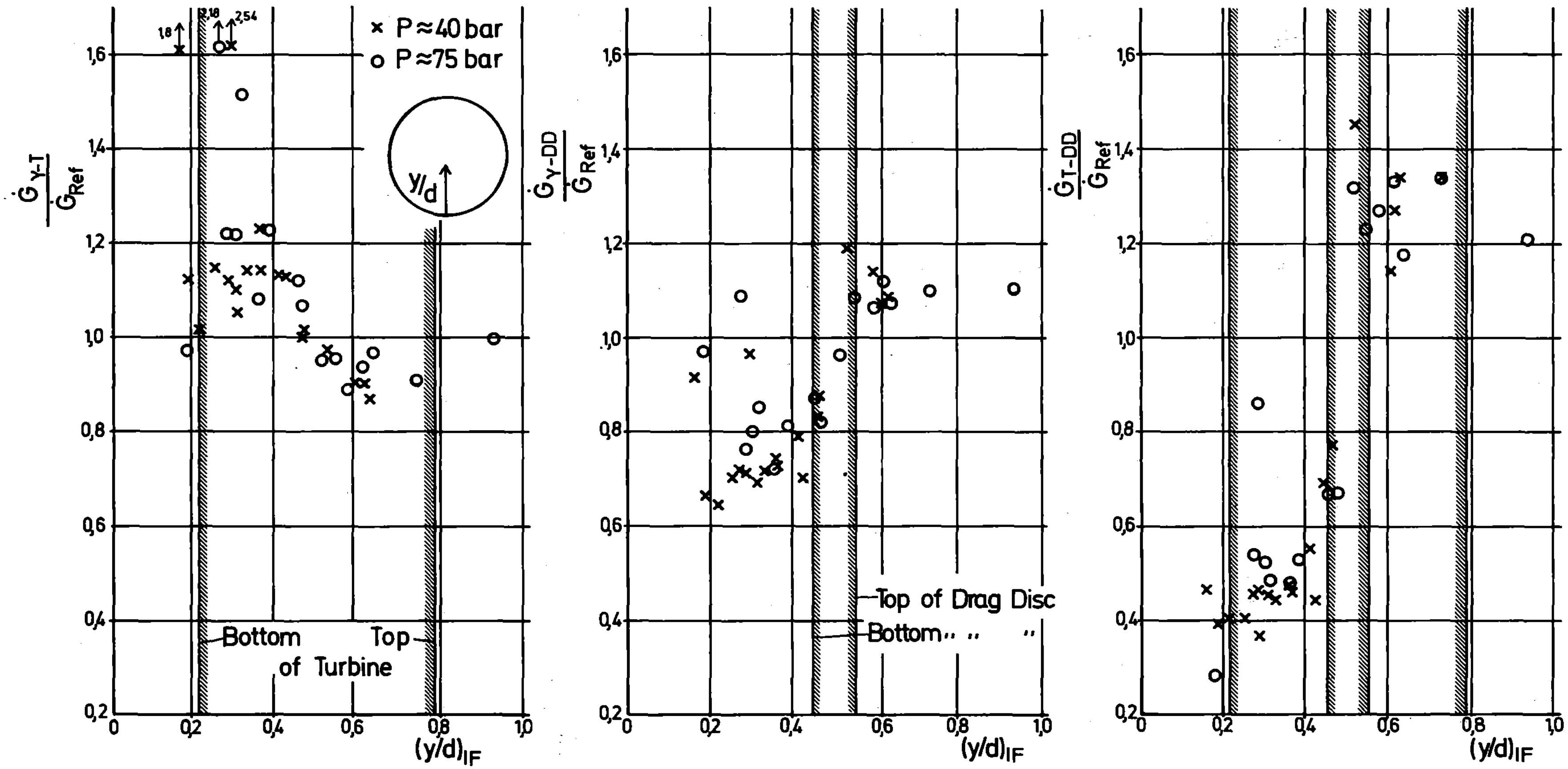

FIGURE 6.4 TWO PARAMETER MASS FLOW RATES AS FUNCTION OF THE INTERFACE LEVEL (3" PIPE TESTS)

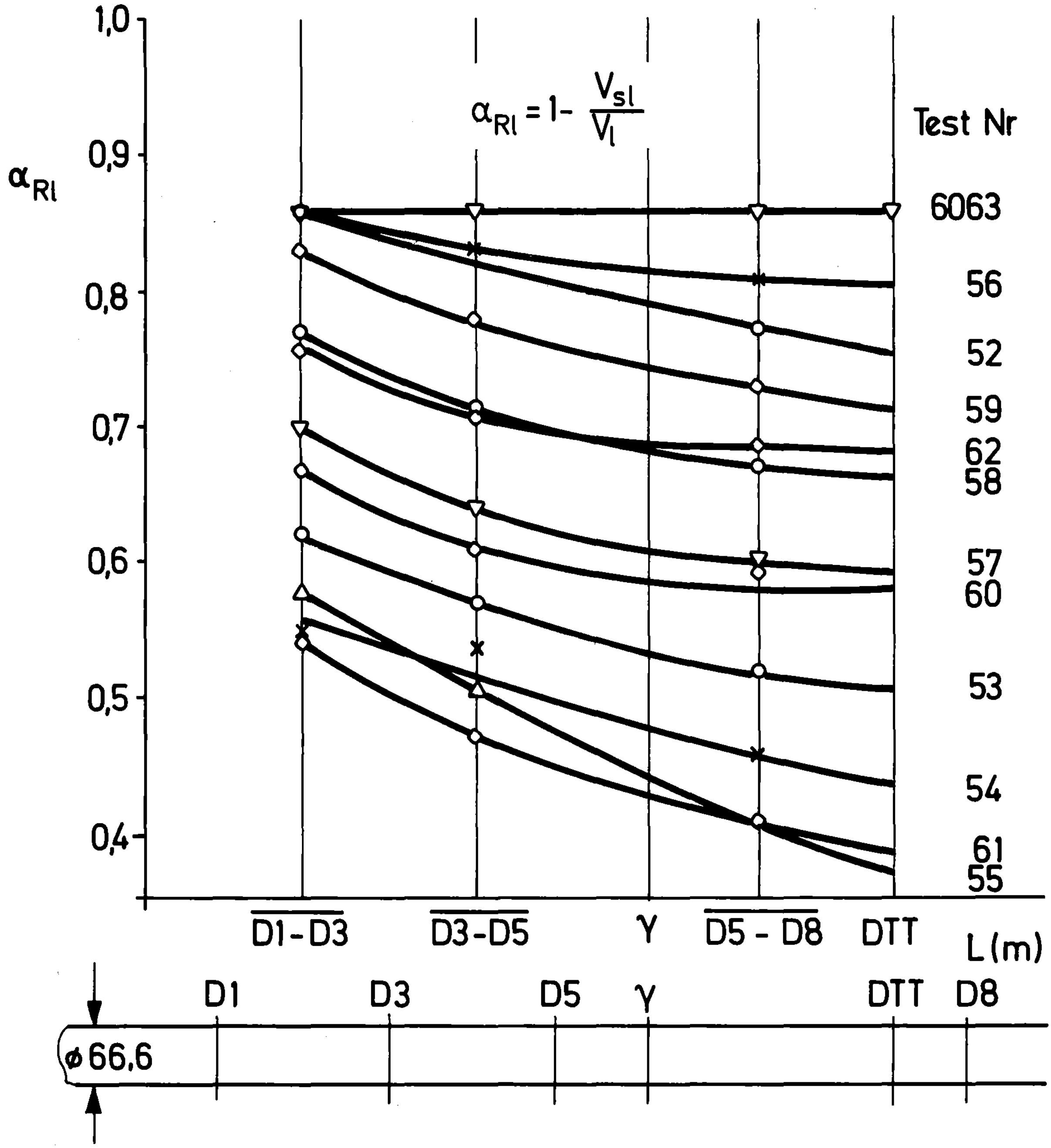

FIGURE 6.5 AXIAL DISTRIBUTION OF VOID FRACTION FROM RADIOTRACER MEASUREMENTS
(STEAM-WATER FLOW, P = 75 BAR, 3" PIPE TESTS)

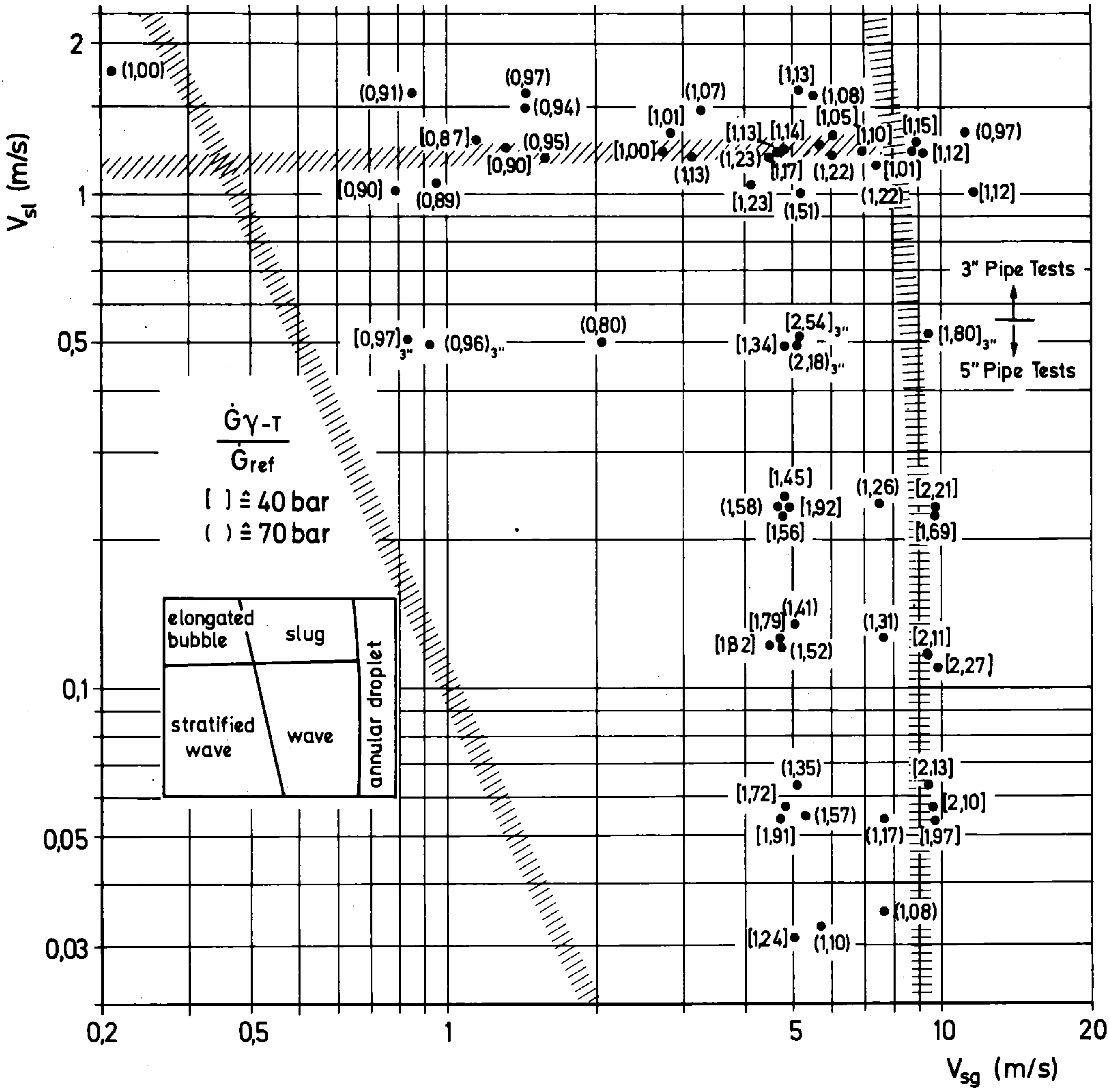

FIGURE 6.6 GAMMA DENSITOMETER-TURBINE MASS FLOW RATES AS FUNCTION OF FLOW REGIME (5" AND 3" PIPE TESTS)

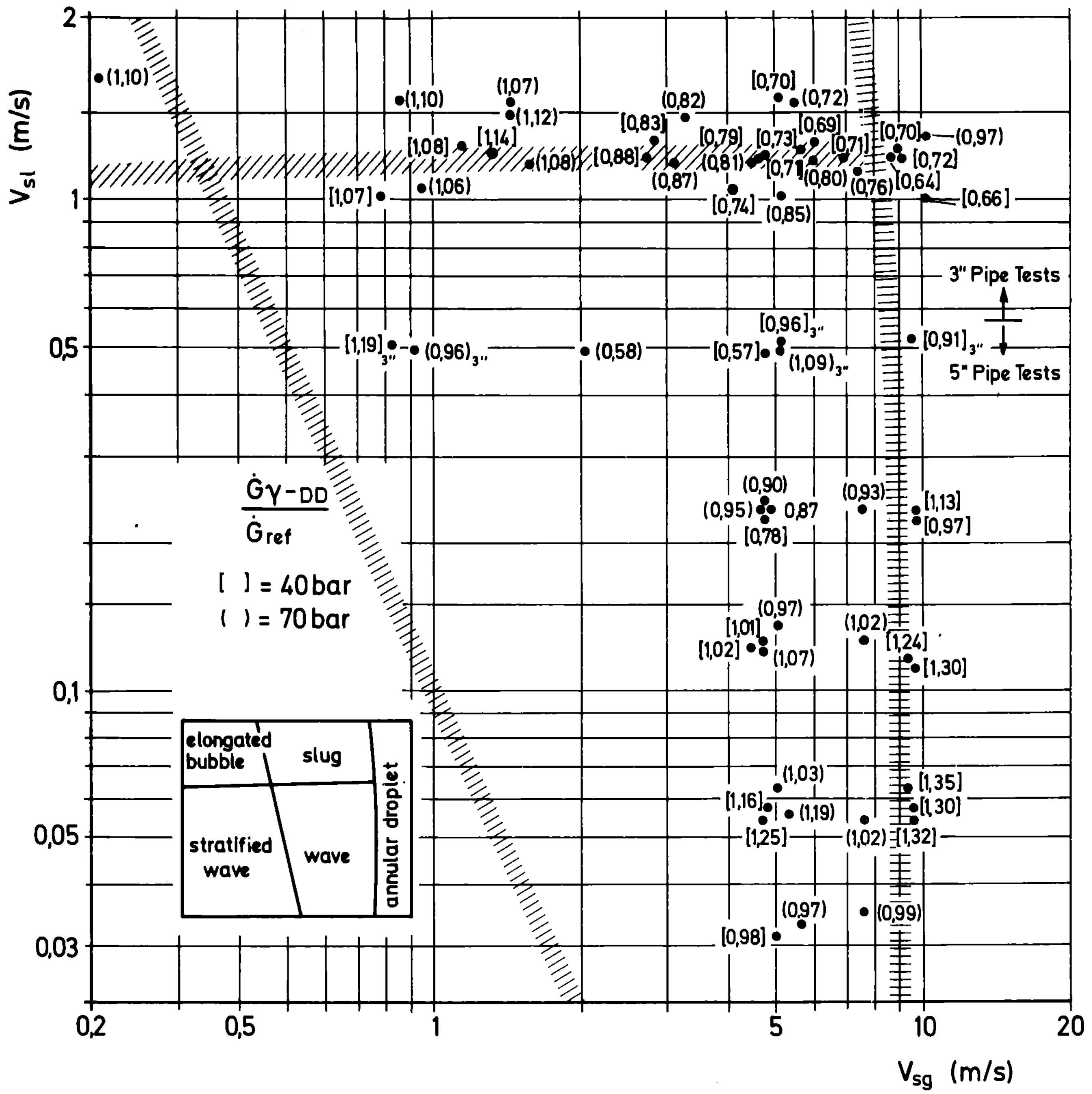

FIGURE 6.7. GAMMA DENSITOMETER-DRAG DISC MASS FLOW RATES AS FUNCTION OF FLOW REGIME (5" AND 3" PIPE TESTS)

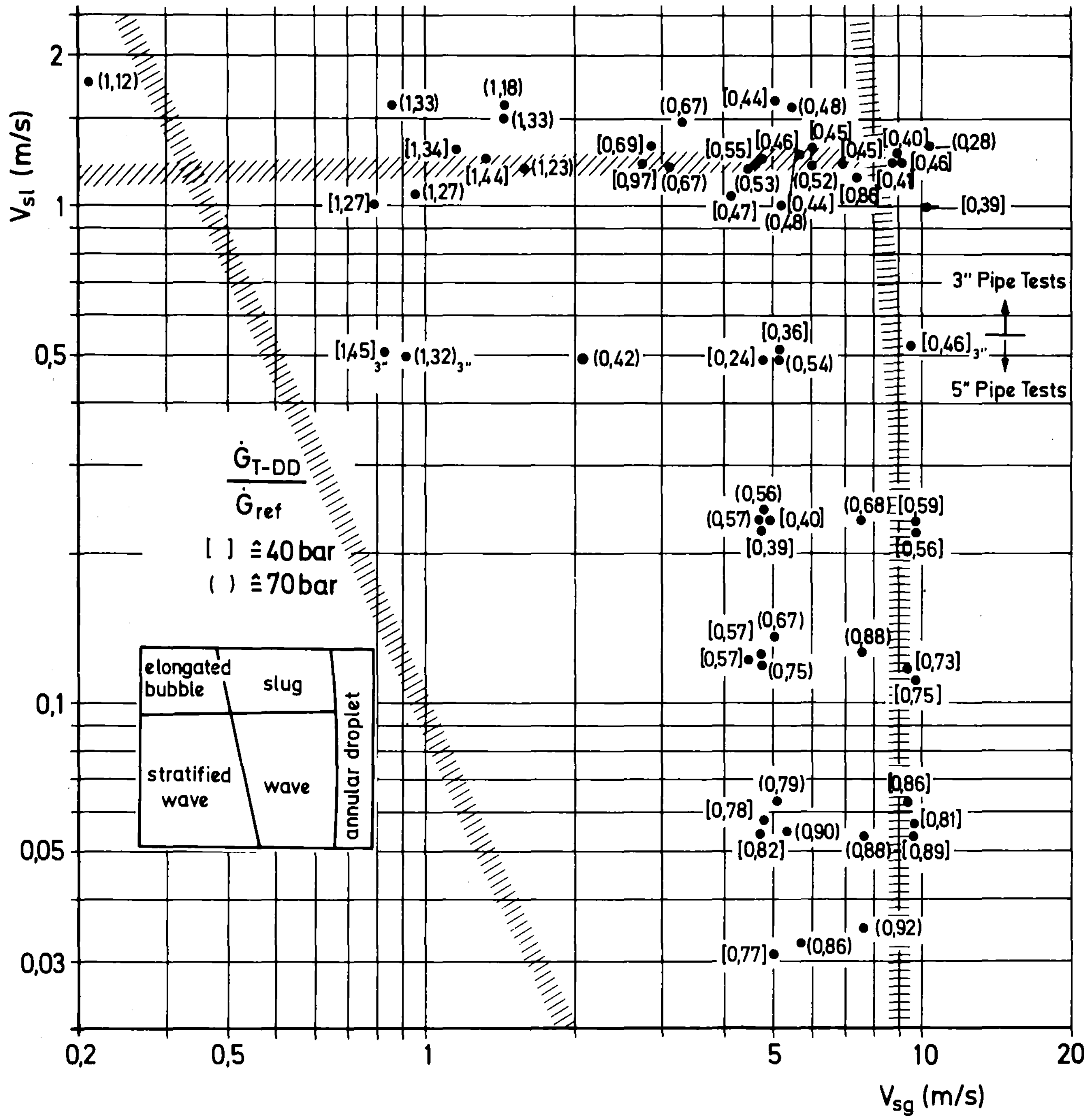

FIGURE 6.8 TURBINE METER - DRAG DISC MASS FLOW RATES AS FUNCTION OF FLOW REGIME (5" AND 3" PIPE TESTS)

Test Nr.	Measurements			Calculated Values					
	$\frac{G_{\gamma-T}}{G_{Ref}}$	$\frac{G_{\gamma-DD}}{G_{Ref}}$	$\frac{G_{T-DD}}{G_{Ref}}$	$(\frac{G_{\gamma-T}}{G})_{th}$		$(\frac{G_{\gamma}-DD}{G})_{th}$		$(\frac{G_{T-DD}}{G})_{th}$	
	1	2	3	4*	5**	6 *	7**	8*	9**
				p ≈ 40 bar					
5001	2,21	1,13	0,59	2,02	2,12	1,18	1,09	0,70	0,56
5002	1,92	0,87	0,40	1,89	2,03	1,10	0,88	0,64	0,38
5004	2,27	1,30	0,75	2,11	2,21	1,29	1,28	0,79	0,74
5005	1,97	1,32	0,89	1,80	1,85	1,26	1,25	0,87	0,85
5037	1,79	1,01	0,57	1,69	1,76	1,10	0,96	0,72	0,52
5038	1,72	1,16	0,78	1,72	1,78	1,16	1,11	0,79	0,69
5039	1,24	0,98	0,77	1,18	1,19	1,04	1,00	0,92	0,85
5043	2,10	1,30	0,81	2,04	2,11	1,32	1,31	0,85	0,82
5044	1,34	0,57	0,24	1,23	1,27	1,01	0,53	0,82	0,22
5054	1,69	0,97	0,56	1,59	1,64	1,09	0,95	0,75	0,55
5055	1,56	0,78	0,39	1,60	1,68	1,06	0,78	0,70	0,37
5056	1,82	1,02	0,57	1,83	1,92	1,13	0,99	0,70	0,51
5057	1,91	1,25	0,82	2,08	2,16	1,28	1,25	0,79	0,73
5058	2,13	1,35	0,86	2,04	2,11	1,31	1,31	0,85	0,82
5059	2,11	1,24	0,73			1,24	1,20	0,77	0,70
$\bar{x}$	1,85	1,08	0,65	1,78	1,84	1,17	1,06	0,77	0,62
σ	0,30	0,22	0,19	0,30	0,32	0,10	0,22	0,08	0,20
				p ≈ 75 bar					
5014	1,10	0,97	0,86	1,033	1,035	1,00	0,95	0,97	0,89
5015	1,35	1,03	0,79	1,252	1,27	1,06	1,03	0,90	0,83
5016	1,41	0,97	0,67	1,27	1,30	1,05	0,95	0,86	0,69
5021	1,26	0,93	0,68	1,13	1,14	1,01	0,87	0,91	0,67
5022	1,31	1,02	0,79	1,20	1,21	1,04	0,98	0,90	0,79
5023	1,17	1,02	0,88	1,07	1,08	1,02	0,99	0,96	0,91
5024	1,08	0,99	0,92	1,02	1,02	1,00	0,94	0,98	0,87
5025	1.45	0,90	0,56	1,30	1,36	1,04	0,87	0,82	0,56
5066	1,58	0,95	0,57	1,50	1,58	1,08	0,95	0,78	0,57
5067	1,52	1,07	0,75	1,43	1,48	1,09	1,03	0,83	0,72
5071	1,57	1,19	0,90	1,97	1,64	1,19	1,19	0,90	0,87
$\bar{x}$	1,30	0,97	0,73	1,27	1,27	1,05	0,95	0,89	0,72
σ	0,23	0,14	0,16	0,27	0,21	0,05	0,14	0,06	0,20
				p ≈ 40 ± 75 bar					
$\bar{x}$	1,60	1,03	0,69	1,55	1,58	1,12	1,01	0,82	0,66
σ	0,39	0,20	0,18	0,38	0,40	0,10	0,20	0,09	0,20

$* : \quad V_T = V_{sg}+V_{sl} \;; \quad (\rho V^2)_{DD} = \alpha\rho_g V_g{}^2 + (1-\alpha)\rho_l V_l{}^2$

$** : \quad V_T = V_g \;; \quad (\rho V^2)_{DD} = \rho_g V_g{}^2$

TABLE 6.1 COMPARISON OF MEASURED MASS FLUX RATIOS TO CALCULATED RATIOS (5" PIPE TESTS)

Test Nr.	Measured Values $\frac{G_{\gamma-T}}{G_{Ref}}$	$\frac{G_{\gamma-DD}}{G_{Ref}}$	$\frac{G_{T-DD}}{G_{Ref}}$	Calculated Values $\left(\frac{G_{\gamma-T}}{G}\right)_{th}$	$\left(\frac{G_{\gamma-DD}}{G}\right)_{th}$	$\left(\frac{G_{T-DD}}{G}\right)_{th}$
				p ≈ 40 bar		
6003	1,13	0,79	0,55	1,85	1,04	0,59
6004	1,12	0,72	0,46	1,77	1,04	0,61
6005	1,15	0,70	0,40	1,52	1,02	0,69
6013	1,12	0,66	0,39	1,30	1,01	0,78
6014	1,23	0,74	0,45	1,53	1,02	0,67
6015	0,90	1,07	1,27	1,14	1,00	0,87
6016	0,97	1,19	1,45	1,39	1,01	0,73
6017	2,54	0,96	0,36	2,30	1,12	0,54
6018	1,80	0,91	0,46	1,58	1,05	0,69
6019	0,89	1,08	1,34	1,24	1,00	0,81
6020	0,90	1,14	1,44	1,26	1,00	0,80
6021	1,14	0,71	0,44	1,48	1,02	0,69
6022	1,00	0,88	0,77	1,40	1,01	0,73
6023	1,14	0,73	0,46	1,49	1,01	0,69
6024	1,10	0,71	0,45	1,41	1,01	0,73
6025	1,01	0,64	0,40	1,26	1,01	0,81
6026	1,05	0,69	0,45	1,43	1,01	0,71
6027	1,01	0,83	0,69	1,35	1,01	0,75
6048	1,13	0,70	0,44	1,59	1,02	0,65
$\bar{x}$	1,18	0,83	0,67	1,49	1,02	0,71
σ	0,39	0,18	0,39	0,26	0,03	0,08
				p ≈ 75 bar		
6035	1,00	1,10	1,21	1,08	1,00	0,94
6036	0,91	1,10	1,33	1,18	1,01	0,86
6037	0,97	1,07	1,18	1,27	1,01	0,80
6051	1,51	0,85	0,48	1,50	1,04	0,62
6052	1,22	0,76	0,86	1,48	1,04	0,72
6053	0,95	1,08	1,23	1,27	1,01	0,80
6054	0,96	0,96	1,32	1,37	1,02	0,75
6055	0,89	1,06	1,27	1,14	1,00	0,88
6056	2,18	1,09	0,54	1,88	1,25	0,67
6057	1,13	0,87	0,67	1,47	1,03	0,71
6058	1,23	0,81	0,33	1,54	1,04	0,70
6059	1,22	0,80	0,52	1,36	1,02	0,76
6060	1,07	0,82	0,67	1,41	1,02	0,74
6061	0,94	1,12	1,33	1,23	1,00	0,82
6062	1,08	0,72	0,48	1,34	1,01	0,77
6063	0,97	0,52	0,28	1,02	1,00	0,98
x	1,14	0,92	0,87			
σ	0,32	0,18	0,38			
				p ≈ 40 + 75 bar		
$\bar{x}$	1,16	0,87	0,76			
σ	0,35	0,18	0,40			

TABLE 6.2 COMPARISON OF MEASURED MASS FLUX RATIOS TO CALCULATED RATIOS (3" PIPE TESTS)

Test Nr.	length weighted densitometer density $\frac{G_{\gamma-T}}{G_{Ref}}$	$\frac{G_{\gamma-DD}}{G_{Ref}}$	radionuclide density at DTT position $\frac{G_{\gamma-T}}{G_{Ref}}$	$\frac{G_{\gamma-DD}}{G_{Ref}}$
		$p \approx 40$ bar		
6013	1,12	0,66	1,00	0,62
6014	1,23	0,74	1,43	0,80
6015	0,90	1,07	1,00	1,13
6016	0,97	1,19	1,08	1,25
6017	2,54	0,96	2,50	0,95
6018	1,80	0,91	2,37	1,05
6019	0,87	1,08	0,87	1,09
6020	0,90	1,14	0,97	1,19
6021	1,14	0,71	1,41	0,79
6022	1,00	0,88	1,07	0,91
6023	1,14	0,73	1,25	0,76
6024	1,10	0,71	1,23	0,75
6025	1,01	0,64	1,25	0,71
6026	1,05	0,69	1,13	0,71
6027	1,01	0,83	1,02	0,84
$\overline{x}$	1,19	0,86	1,31	0,90
σ	0,44	0,19	0,49	0,20
		$p \approx 75$ bar		
6052	1,22	0,76	1,26	0,77
6053	0,95	1,08	0,95	1,08
6054	0,96	0,96	1,04	1,18
6055	0,89	1,06	0,92	1,08
6056	2,18	1,09	1,99	1,04
6057	1,13	0,87	1,07	0,84
6058	1,23	0,81	1,19	0,80
6059	1,22	0,80	1,34	0,83
6060	1,07	0,82	0,98	0,81
6061	0,94	1,12	0,93	1,11
6062	1,08	0,72	1,07	0,72
6063	0,97	0,52	1,02	0,53
$\overline{x}$	1,16	0,87	1,13	0,90
σ	0,36	0,18	0,31	0,20
		$p \approx 40 + 75$ bar		
$\overline{x}$	1,17	0,87	1,23	0,90
σ	0,40	0,18	0,41	0,19

TABLE 6.3 MASS FLUXES EVALUATED WITH DIFFERENT DENSITIES

7. Mass Flow Rates using Various Turbine Models (Three-Parameter Equations)

The equation (6.4) for mass flow rate shows that there are 3 independent variables: α, V and S if the densities are assumed to be known. On the other hand, there are 3 independent measurements ρ_γ, V_T and $(\rho V^2)_{DD}$ which can be used to calculate these variables. For doing this, it is assumed that

i) the gamma densitometer measures the apparent density ρ (eq. 6.5) with this equation the void fraction α can be directly computed

$$\alpha = \frac{\rho_l - \rho}{\rho_l - \rho_g}$$

In the following the length weighted 3 beam densitometer void fraction is used.

ii) the drag disc measures the two-phases momentum flux (eq. 6.7)) assuming that the single phase drag coefficients are equal 1. From this equation it follows for slip

$$S = (((\rho V^2)_{DD} - (1-\alpha)\rho_l V_l^2)/\alpha \rho_g V_l^2)^{0.5} \tag{7.1}$$

iii) for the turbine reading the expression from the void fraction, Rouhani, Aya or Estrada model is used (eq(5.1)-(5.4).

Transforming these equations, the liquid velocity V_l is expressed by

Void Fraction Model

$$V_l = \frac{(1-\alpha)}{p} V_T + \left(\frac{(1-\alpha)^2 V_T^2}{p^2} + \frac{\alpha(\rho V^2)_{DD}/\rho_g - V_T^2}{p}\right)^{0.5} \tag{7.2}$$

with $p = (1-\alpha)^2 + \alpha(1-\alpha)\rho_l/\rho_g$

Estrada Model

$$\alpha y(1+y)^2 \rho_g V_l^4 - 2\alpha y^2(1+y)\rho_g V_T V_l^3 + (\alpha \rho_g V_T^2 + \alpha y^3 \rho_g V_T^2 \tag{7.3}$$

$$- (1-y)^2 (\rho V^2)_{DD}) V_l^2 + 2y(1+y) V_T (\rho V^2)_{DD} V_l - y^2 (\rho V^2)_{DD} V_T^2 = 0$$

with $y = \frac{1-\alpha}{\alpha} \frac{\rho_l}{\rho_g}$

eq. (7.3) has to be solved iteratively.

Aya Model

$$V_l = \frac{1}{2}p + \left(\frac{(\rho V^2)_{DD}}{\alpha\rho_g 2y} - \frac{1}{4}p^2\right)^{0.5} \tag{7.4}$$

with $p = \frac{1 + y^{0.5}}{y^{0.5}} V_T$, $y = \frac{1-\alpha}{\alpha} \frac{\rho_l}{\rho_g}$

By inserting V_l in eq (7.1) S is computed and then $\dot{G}$ from

$$\dot{G} = (\alpha\rho_g S + (1-\alpha)\rho_l)V_l \tag{7.5}$$

With the Rouhani Model first slip S is computed iteratively by

$$(1- (\rho V^2)_{DD}/(V_T^2\alpha\rho_g))S^4+2yS^3 + (y^2+y - 2y(\rho V^2)_{DD}/(V_T^2\alpha\rho_g))S^2$$
$$+ 2y^2S + (y^3- y^2(\rho V^2)_{DD}/(V_T^2\alpha\rho_g)) = 0 \tag{7.6}$$

with $y \frac{1-\alpha}{\alpha} \frac{\rho_l}{\rho_g}$

and then inserted in eq (5.2) to obtain V_l

Table 7.1 shows the results for the 5" pipe tests: The void fraction model does not give a real value for V_l for most of the test points although in the 5" pipe experiments the assumption of this model for the turbine reading is quite well fulfilled. The reason for the negative radical in equation 7.2 is the too small drag disc reading. The points where a real solution for V_l exists belong to test points with a low liquid input where the steam momentum flux $(\rho V^2)_{gg}$ is about the total momentum flux $(\rho V^2)_{tp}$. The liquid velocity is predicted too low, the slip to high.

The other models fail totally because the measured turbine reading S is essentially higher than the predicted value. This gives rise to either a a complex solution for V_l (Aya model) or a negative slip (Estrada and Rouhani model).

For the 3" pipe tests (Table 7.2) the void fraction model gives a real solution for all test points except one. The accuracy of the mass flow evaluation is worse than using the two parameter equation (2) combining the densitometer and drag disc reading. Slip is described quite well. The Aya and Estrada model give only for a part of the experiments a meaningful solution. The Rouhani model again gives always values $S<0$.

Summarizing the 5" and 3" pipe tests if can be stated that no model was applicable for all test points. If a solution existed the mean accuracy of the computed mass fluxes was not improved compared to the drag disc-densitometer mass fluxes. Therefore there is no advantage in applying these models in a strongly stratified horizontal two-phase flow because the assumptions of constant void and velocity distribution in the cross section are not fulfilled.

Test Nr.	p bar	γ-Densitometer + Ref.-Values V_1 (m/s)	S (1)	Void Fraction Model V_1 (m/s)	S (1)	G_{VF}/G_{Ref} (1)
5001		3.14	3.35	R<0		
5002		2.14	2.56	"		
5004		2.06	5.03	"		
5005		1.75	5.73	"		
5037		2.04	2.48	0.45	12,1	0,64
5038	40	1.52	3.29	1.25	4,16	0.97
5039		2.34	2.19	R<0		
5043		1.61	6.15	"		
5044		4.07	1.34	"		
5054		4.27	2.34	"		
5055		2.60	2.02	0.43	12.46	0.46
5056		1.78	2.74	0.99	5.03	0.78
5057		1.05	4.76	1.67	2.76	1.10
5058		1.61	6.14	R<0		
5059		2.36	4.19	"		
5014		4.56	1.27	R<0		
5015		2.18	2.41	"		
5016		2.85	1.88	"		
5021		5.62	1.40	"		
5022	75	4.16	1.91	"		
5023		4.33	1.79	"		
5024		6.72	1.14	"		
5025		3.02	1.73	"		
5066		2.40	2.20	"		
5067		2.04	2.48	"		
5071		1.21	4.62	0.88	6.65	0,97

Mean Values	Void Fraction Model		
p (bar)	40	75	40 + 75
$V_{1\ Model}/V_1$	0.67	0,73	0,68
σ	0.58	-	0,52
S_{Model}/S	2.95	1.44	2.69
σ	2.44	-	2.27
G_{Model}/G_{Ref}	0,79	0,97	0,82
σ	0.25	-	0,24
N/N_{total}	5/15	I/II	6/26

Table 7.1 Results from Void Fraction Model (5" Pipe Tests)

Test Nr.	p (bar)	γ-Densitom. +Ref.-Values V_1 (m/s)	S (1)	Void Fraction Model V_1 (m/s)	S (1)	G_{VF}/G_{Ref} (1)	Aya Model V_1 (m/s)	S (1)	G_A/G_{Ref}	Estrada Model V_1 (m/s)	S (1)	G_R/G_{Ref}
6003		3.07	2.54	2.46	1.81	0.78						
6004		5.34	2.21	3.79	1.94	0.71						
6005		6.29	1.79	3.97	2.18	0.65						
6013		8.04	1.44	4.24	2.46	0.61						
6014		3.23	1.88	2.31	2.19	0.72						
6015		1.55	1.44	1.67	0.54	1.07	1.67	0.56	1.07	1.38	5.87	0.95
6016		0.94	1.91	1.14	0.60	1.19	1.14	0.45	1.19	0.91	5.14	1.04
6017	40	2.13	3.23	1.07	7.50	0.63						
6018		5.43	1.95	2.33	5.39	0.68						
6019		1.99	1.74	2.18	0.42	1.08	2.17	0.92	1.08	1.73	6.79	0.93
6020		2.02	1.72	2.33	0.44	1.14	2.32	0.91	1.14	1.81	6.59	0.97
6021		4.47	1.77	3.03	2.07	0.69						
6022		2.75	1.79	2.44	1.28	0.88	2.28	2.59	0.85			
6023		3.81	1.81	2.69	2.02	0.71						
6024		5.51	1.62	3.70	1.93	0.69						
6025		7.61	1.37	4.37	2.0	0.61						
6026		4.94	1.67	3.27	1.89	0.68						
6027		3.01	1.68	2.51	1.42	0.83	1.95	4.88	0.72			
6048		4.08	2.09	2.80	2.18	0.69						
6035		1.83	3.83	2.03	1.78	1.11	2.03	1.17	1.11	1.86	11.05	1.83
6036		2.10	1.89	2.35	0.19	1.10	2.34	0.61	1.10	1.91	5.89	0.97
6037		2.36	1.92	2.61	0.70	1.07	2.63	0.26	1.07	2.32	3.33	1.02
6051		3.75	1.92	2.37	3.31	0.74						
6052		5.10	1.88	3.32	2.46	0.69						
6053		2.16	1.70	2.45	0.70	1.08	2.47	0.17	1.07	2.06	3.25	1.00
6054	75	0.99	1.88	1.18	0.67	1.12	1.20	0.06	1.10	0.96	3.34	1.03
6055		1.76	1.38	1.93	0.56	1.05	1.94	0.13	1.04	1.55	4.00	0.95
6056		2.31	2.82									
6057		2.74	2.02	2.41	1.66	0.86						
6058		3.39	2.06	2.62	2.18	0.78						
6059		4.84	1.64	3.42	2.18	0.75						
6060		3.22	1.95	2.78	1.56	0.84						
6061		2.33	1.73	2.69	0.53	1.12	2.70	0.16	1.11	2.19	4.21	1.01
6062		5.00	1.63	3.34	2.06	0.69						

Mean Values	Void Fraction Model			Aya Model			Estrada Model		
p(bar)	40	75	40 + 75	40	75	40 + 75	40	75	40 + 75
$V_{1_{Model}}/V_1$	0.77	0.93	0.84	1.0	1.14	1.07	0.91	0.95	0.93
σ	0.23	0.22	0.23	0,22	0,04	0,16	0.04	0.05	0.05
S_{Model}/S	1.09	0.77	0.95	1.01	0.15	0.55	3.63	2.39	3.04
σ	0.66	0.50	0.61	1,02	0.11	0.80	0.63	0.59	0.60
G_{Model}/G_{Ref}	0.79	0.93	0.85	1,01	1.09	1.05	0.97	1.0	0.98
σ	0.19	0.18	0.19	0.18	0.03	0.13	0.05	0.03	0.04
N/N_{total}	19/19	14/15	33/34	6/19	7/15	13/34	19/19	16/15	35/34

Table 7.2 Results from Void Fraction, Aya and Estrada Model (3" Pipe Tests)

8. Calibration of the LOFT Mass Flow Rate Instrumentation

8.1 Possibilities of Calibration

As it was shown, the accuracy of the combination of DTT and gamma densitometer is quite dependent on the phase and velocity distribution in the cross section. Using calibration coefficients, obtained from these steady-state tests, should improve the accuracy in other (transient) experiments if

i) mass flux, quality and pressure ranges are the same
ii) the geometry is the same (diameters, arrangement of the single instruments, pipe geometry upstream the instrumentation etc).
iii) the transient does not affect the phase distribution

Compared with the measurement condition in the LOFT experiments these conditions are only partly fullfilled. These experiments were made at quite moderate mass fluxes compared to mass fluxes occuring at the beginning of a full area break blowdown, the use of calibration coefficients therefore should be limited to the mass fluxes investigated. At these relatively low mass fluxes, more typical for the end of a large area break blowdown or a small area break blowdown, the transient effects should be of minor influence. Different geometries e.g. elbows not far away upstream of the instrument position are influencing very much the phase and velocity distribution. Thus an extrapolation of calibration results is quite doubtful.

Because the tested instrumentation is sensitive to phase and velocities distribution, a calibration procedure should be based on these distributions. The 3 beam gamma densitometer can give the information on phase distribution and flow regime. Using calibration factors for each instrument, different for each flow regime, the mass flux can be evaluated with three parameter equations. Using a two parameter equation, the mass flux as a function of flow regime should be looked at and the corresponding calibration factors should be determined directly from such a map. However, such a calibration is advantageous only if exactly these flow regimes (with the same slip values etc.) exist in other experiments. In general this is not ensured. Because of this a simple calibration procedure is presented which is believed to be more generally applicable. This procedure uses the height of the interface level evaluated from the densitometer void fraction to set up different calibration factors as function of this height.

8.2 Pipe Averaged Mass Flux from Calibrated Gamma Densitometer and Drag Disc (Two-Parameter Equation)

If a two-parameter equation is used, the equation combining the momentum flux and density is the most applicable because this combination is least sensitive to slip.

As it was shown in Figure 5.9 in the 3" pipe tests the ratio of drag disc reading to total two-phase momentum flux was clearly different if the interface level was below or above the drag disc:

3" pipe tests

for $(y/d)_{IF} > 0.5$: $(\rho V^2)_{DD} = 1.2(\rho V^2)_{tp}$

for $(y/d)_{IF} < 0.5$: $(\rho V^2)_{DD} = 0.57(\rho V^2)_{tp}$

If the two-phase momentum flux mainly consisted of the gas momentum flux which is connected with low interface levels (5" pipe tests, Figure 5.8), the drag disc was measuring about the total momentum flux:

5" pipe tests:

for $(y/d)_{IF} < 0.2$: $(\rho V^2)_{DD} = (\rho V^2)_{tp}$

The density (void fraction) from the 3 beam gamma densitometer should be evaluated with a flow model (Lassahn /7/). If the length weighted method is used a correction for stratification should be applied as shown in 5.2.1 depending on the beam orientations. In the following analyses this correction is not applied because the density error from the length weighting procedure was nearly compensated by the change of flow distribution between the positions of the densitometer and the DTT.

Therefore the following procedure is proposed

$$G_{\gamma\text{-}DD} = C\ (\rho_\gamma(\rho V^2)_{DD})^{0.5}$$

with

$C = 0.91$ for $(y/d)_{IF} > 0.5$

$C = 1.32$ for $0.5 > (y/d)_{IF} > 0.2$

$C = 1.0$ for $0.2 > (y/d)_{IF}$

Table 8.1 shows a comparison of results with and without calibration factors for the 3" pipe tests. An improvement is clearly seen. The factor C is equal to 1 for the 5" pipe tests; that means the original two parameter equation is used, the results (shown again in Table 7.2) were very satisfying.

Similar calibration procedures for the other instrument combination are useful only for small ranges of parameters because of the large slip sensitivity of the corresponding equations.

Looking at the turbine-gamma densitometer combination in the 3" pipe tests the positive error in the mean value of the data calculated from the two parameter equation was fairly well compensated by the too low turbine reading (Table 6.2) as long as the interface level was not below or near the bottom of the turbine. Of course this compensation worked only well for small values of slip. In the 5" pipe tests the higher slip caused higher errors by the equation itself. Here, obtaining a calibration factor is not possible.

Regarding the turbine-drag disc combination, a similar procedure proposed for the drag disc could be made for the turbine. This should improve the mass flow rates for the small slip values in the 3" pipe tests for $0<IF\lesssim100$ but would not work for the 5" pipe tests. The reliability of such a procedure is very restricted and is not discussed in detail.

The disadvantage of two-parameter equations is that phase velocities and slip cannot be evaluated. This can only be done by using three-parameter equations. Such a model using calibration factors is discussed in the following.

8.3 Mass Flow Rate using Three-Parameter Equations with Calibration Factors

The correct equation for mass flow rate contains three parameters α, V_l and V_g or α, S and V_l which can be computed from three independent measurements. The model used in chapter 7 were not very successful because for horizontal two-phase flow the drag disc and turbine reading were not modeled satisfactorily for both the 5" and 3" pipe tests.

In the model presented the readings of the single instruments are corrected by calibration factors which are a function of the interface level.

It is assumed that

i) the gamma densitometer measures the mean density ρ and void fraction α, respectively. The density (void fraction) is evaluated according to the method by Lassahn (/7/) or if a length weighted method is used with a correction similar as it was presented in 5.1

ii) Using a single phase calibration curve (thus assuming that the drag coefficients in single phase and in two-phase flow are equal) the drag disc measures

$$(\rho V^2)_{DD} = (\alpha\rho_g S^2 + A(1-\alpha)\rho_l)V_l^{\,2} \tag{8.1}$$

iii) Using a single phase calibration curve the turbine measures

$$V_T = B(\alpha S + (1-\alpha))V_l \tag{8.2}$$

From (8.1) and (8.2) it follows

$$V_l = \frac{1-\alpha}{p} \frac{V_T}{B} + (\frac{(1-\alpha)^2}{p^2} \frac{V_T{}^2}{B^2} + \frac{\alpha(\rho V^2)_{DD}/\rho_g - V_T^2/B^2}{p} \tag{8.3}$$

where $p = \alpha(1-\alpha)\ A\rho_l/\rho_g + (1-\alpha)$

and
$$S = \frac{V_T/B-(1-\alpha)V_l}{\alpha V_l} \tag{8.4}$$

A and B are taken from the experiments.

$A = 1.2$ for IF > 50 %.

$A = 0.5$ for IF < 50 %

$B = 0.8$ for IF > $(y/d)_{\text{bottom of turbine}}$

$B = 1.1$ for IF < $(y/d)_{\text{bottom of turbine}}$.

The pipe averaged mass flux is evaluated from

$$\dot{G} = (\alpha\rho_g S + (1-\alpha)\rho_l)V_l \tag{8.5}$$

Table 8.1 and 8.2 also contain the results obtained with this method. For the 5" pipe tests the accuracy for mass flux is slightly reduced compared with that from the two-parameter equation but slip and phase velocities are described better than from any other three parameter models. In the 3" pipe tests the accuracy of this method is considerably higher compared to the other three parameter models both in mass flow rate, slip and phase velocity. If the information on slip and phase velocity is not of great importance the combination of gamma densitometer and drag disc should be used together with the calibration factors which gives the best accuracy for the mass flow rate.

Test Nr.	p (bar)	TPE* $\frac{G_{\gamma\text{-DD}}}{G_{Ref}}$	γ-Densitometer + Ref.-Values V_1 (m/s)	S (1)	Three Parameter Equations with Calibration Factors V_1 (m/s)	S (1)	$\frac{\dot{G}_{3P_c}}{\dot{G}_{Ref}}$
5001		1.13	3.14	3.35	3.80	2.78	1.06
5002		0.87	2.14	2.56	1.61	3.24	0.82
5004		1.30	2.06	5.03	4.55	2.19	1.28
5005		1.32	1.75	5.73	5.85	1.70	1.36
5037		1.01	2.04	2.48	2.22	2.20	1.01
5038	40	1.16	1.52	3.29	2.96	1.57	1.28
5039		0.98	2.34	2.19	3.94	1.20	0.99
5043		1.30	1.61	6.15	3.21	3.08	1.23
5044		0.57	4.07	1.34	1.46	3.94	0.49
5054		0.97	4.27	2.34	4.07	2.36	0.93
5055		0.78	2.60	2.02	1.80	2.63	0.78
5056		1.02	1.78	2.74	2.22	2.00	1.09
5057		1.25	1.05	4.76	2.98	1.39	1.41
5058		1.35	1.61	6.14	4.85	1.97	1.39
5059		1.24	2.36	4.19	4.13	2.31	1.23
5014		0.97	4.56	1.27	5.20	1.08	1.02
5015		1.03	2.18	2.41	2.75	1.88	1.03
5016		0.97	2.85	1.88	1.86	2.94	0.90
5021		0.93	5.62	1.40	4.55	1.78	0.93
5022	75	1.02	4.16	1.91	5.41	1.45	1.05
5023		1.02	4.33	1.79	8.60	0.88	1.04
5024		0.99	6.72	1.14	9.09	0.82	1.08
5025		0.90	3.02	1.73	1.99	2.69	0.84
5066		0.95	2.40	2.20	2.02	2.57	0.92
5067		1.07	2.04	2.48	3.13	1.55	1.12
5071		1.19	1.21	4.62	3.93	1.31	1.31

Mean Values	* Two-Parameter Equation			Three Parameter Equations with Calibration Factors		
p (bar)	40	75	40 + 75	40	75	40 + 75
$V_{1\ Model}/V_1$	-	-	-	1.67	1.34	1.53
σ	-	-	-	0.89	0.75	0.84
S_{Model}/S	-	-	-	0.83	0.94	0.87
σ	-	-	-	0.67	0.40	0.56
G_{Model}/G_{Ref}	1.08	1.00	1.05	1.09	1.03	1.06
σ	0.23	0.08	0.18	0.26	0.13	0.21
N/N_{total}	15/15	11/11	26/26	15/15	11/11	26/26

TABLE 8.1 Mass Flow Rate Evaluation with Calibration Factors (5" Pipe Tests)

TABLE 8.2 Mass Flow Rate Evaluation with Calibration Factors (3" Pipe Tests)

Test Nr.	p (bar)	TPE* $\dot{G}_{\gamma-DD}/\dot{G}_{Ref}$	TPE^{**}_c $(\dot{G}_{\gamma-DD})_c/\dot{G}_{Ref}$	γ-Densitometer +Ref.-Values V_1 (m/s)	γ-Densitometer +Ref.-Values S (1)	Three Par. Equations with Cal Factors V_1 (m/s)	Three Par. Equations with Cal Factors S (1)	$\dot{G}_{3P_c}/\dot{G}_{Ref}$
6003		0.79	0.05	3.07	2.54	3.20	1.71	1.01
6004		0.72	0.95	5.34	2.21	4.63	2.00	0.87
6005		0.70	0.93	6.29	1.79	4.53	2.41	0.76
6013		0.66	0.87	8.04	1.44	6.36	1.43	0.81
6014		0.74	0.99	3.23	1.88	2.88	2.20	0.90
6015		1.07	0.97	1.55	1.44	1.51	1.45	0.98
6016		1.19	1.08	0.94	1.91	1.03	1.28	1.09
6017	40	0.96	1.27	2.13	3.23	2.09	3.30	0.99
6018		0.91	1.20	5.43	1.95	4.89	2.27	0.97
6019		1.08	0.98	1.99	1.74	1.98	1.31	0.99
6020		1.14	1.04	2.02	1.72	2.11	1.22	1.05
6021		0.71	0.94	4.47	1.77	3.75	2.09	0.85
6022		0.88	1.17	2.75	1.79	3.26	1.15	1.17
6023		0.73	0.97	3.81	1.81	3.75	1.20	0.95
6024		0.71	0.94	5.51	1.62	4.50	1.99	0.84
6025		0.64	0.90	7.61	1.37	4.87	2.25	0.70
6026		0.69	0.91	4.94	1.67	4.11	1.88	0.85
6027		0.83	1.10	3.01	1.68	3.33	1.29	1.10
6048		0.70	0.93	4.08	2.09	3.60	2.11	0.88
6035		1.10	1.00	1.83	3.83	1.57	1.70	0.88
6036		1.10	1.00	2.10	1.89	2.10	1.66	1.01
6037		1.07	0.97	2.36	1.92	2.32	1.83	0.98
6051		0.85	1.12	3.75	1.92	3.91	1.66	1.02
6052		0.76	1.01	5.10	1.88	5.16	1.31	0.92
6053		1.08	1.98	2.16	1.70	2.17	1.50	0.99
6054	75	0.96	0.87	0.99	1.88	1.05	1.36	1.03
6055		1.06	0.96	1.76	1.38	1.72	1.39	0.97
6056		1.09	1.44	2.31	2.82	2.66	2.59	1.11
6057		0.87	1.15	2.74	2.02	3.08	1.60	1.09
6058		0.81	1.07	3.39	2.06	2.98	2.45	0.91
6059		0.80	1.06	4.84	1.64	3.19	3.03	0.77
6060		0.82	1.09	3.22	1.95	3.59	1.48	1.08
6061		1.12	1.01	2.33	1.73	2.41	1.46	1.02
6062		0.72	0.95	5.00	1.63	3.75	2.34	0.79

Mean Values	* Two-Par. Equation			** Two-Par. Equation with Cal. Factor			Three-Par. Equations with Cal. Factors		
p (bar)	40	75	40 + 75	40	75	40 + 75	40	75	40 + 75
$V_{1_{Model}}/V_1$	-	-	-	-	-	-	1.02	0.98	1.00
σ							0.40	0.14	0.31
S_{Model}/S	-	-	-	-	-	-	0.99	1.12	0.99
σ							0.27	0.34	0.27
$\dot{G}_{Model}/\dot{G}_{Ref}$	0.83	0.92	0.87	1.01	1.02	1.02	0.93	0.97	0.95
σ	0.18	0.18	0.18	0.11	0.15	0.13	0.12	0.10	0.11
N/N_{total}	19/19	15/15	34/34	19/19	15/15	34/34	19/19	15/15	34/34

9. Discussion of the Local Behavior of the DTT

9.1 Model for the Local Measurement

In the previous chapters it was discussed how turbine and drag disc readings differed from the pipe average values. Now it will be shown that the DTT readings are consistent for the pipe section covered by the DTT.

In the following a model is used which is demonstrated in Figure 9.1:

- The phase velocities upstream of the DTT entrance (plane 0) are assumed to be identical with the pipe average values. The void fraction integrated over the DTT area is different from the pipe average void fraction.

- The entrance grid of the DTT causes a certain homogenization of the phases but only negligibly effects the phase velocities.

- The flow impinges on the drag disc and a wake behind the drag disc is formed. The two-phase flow is further homogenized by the impingement and wake interaction such that the flow at turbine location is homogeneous.

These assumptions imply that the phase velocities at the planes 0 and 1 are about the same. The density or void fraction is different in all planes. The only way to calculate a local density is

$$\rho_{DTT} = (\rho V^2)_{DD}/V_T^2 \tag{9.1}$$

and with this the corresponding void fraction

$$\alpha_{DTT} = (\rho_{DTT} - \rho_l)/(\rho_g - \rho_l) \tag{9.2}$$

The way to calculate this density is only exactly valid for $S \equiv 1$. It is assumed that this density approximately represents the density at all planes.

9.2 Density Comparison

To compare the local density (void fraction) with the pipe average value, the interface level is used. Similar to Chapter 5.1 α_{DTT} is converted to a liquid level in the DTT with the equations

$$\alpha_{DTT} = 1-\frac{1}{2\pi}(\Theta - \sin\Theta) \qquad (9.3)$$

$$\frac{h}{d_{DTT}} = \frac{1}{2}(1-\cos\frac{\Theta}{2}) \qquad (9.4)$$

$(y/d)_{IF\ DTT}$ is obtained by adding the distance between the DTT and the pipe bottom to h and deviding this sum by the pipe diameter. From the gamma densitometer readings the interface level is, in contrast to section 5.1 evaluated by calculating the interface level of the single beams, converting this to a void fraction and then calculating $(y/d)_{\gamma,c}$. The same value is obtained by using the length average value and the correction for totally stratified flow from Figure 5.1. Both interface levels are compared in Figure 9.2. For the tests where the water level indicated by the gamma densitometer was above the lower edge of the drag disc, the DTT indicated a higher interface level than the gamma densitometer. For an interface level between the lower edge of the turbine and drag disc both interface levels were very close. If the gamma densitometer indicates a liquid level below the DTT, the DTT liquid level is indicated at the bottom of the DTT which, of course, is consistent. Therefore these results show that there is consistency between the two density measurements and, therefore, good agreement when the results are interpreted correctly.

9.3 Velocity Comparison

From conservation of mass between the planes 0 and 2 it follows that

$$\alpha\rho_g V_g + (1-\alpha)\rho_l V_l \Big|_0 = \rho V \Big|_2 \qquad (9.5)$$

where V is the mass average velocity of the mixture at the turbine location. Fig. 9.3 shows the ratio of turbine velocity to mass average velocity for the 3" pipe tests (with $\alpha=\alpha_{DTT}, \rho=\rho_{DTT}$). This ratio is much closer to one than the ratio of turbine velocity to pipe section averaged homogeneous velocity (Figure 5.6).

An improvement is also reached for the 5" pipe tests:
Because the DTT was mostly surrounded by steam ($\rho_{DTT} \equiv \rho_g$), the velocity at the turbine location was V_g. Figure 5.3 showed that the turbine actually measured V_g.

9.4 Momentum Comparison

For the momentum flux at the drag disc position it was assumed that

$$(S V^2)_1 = \alpha_{DTT}\rho_g V_g^2 + (1-\alpha_{DTT})\rho_l V_l^2 \tag{9.6}$$

Figure 9.4 shows the ratio of drag disc momentum flux to the calculated momentum flux. Again this ratio is much closer to one than the ratio of drag disc reading to cross section averaged momentum flux shown in Figure 5.9. For the 5" pipe tests the momentum flux at drag disc position was $\sim\rho_g V_g^2$. Figure 5.8 showed that the drag disc reading was very close to this value.

In summary, it was shown that the DTT readings are consistent; the measured values correspond to the local values characteristic for the DTT location.

9.5 Calculation of Pipe Averaged Mass Flux

The drag disc measures the momentum flux of the fluid in the DTT. However, both the mass average velocity and the density exposed to the drag disc differ from the pipe average values. Although no information is available from the gamma densitometer DTT combination to correct the velocity, the gamma densitometer and ρ_{DTT} can be used to correct the density contribution to the drag disc.

The pipe average density can be estimated from ρ_{DTT} by calculating the water level in the DTT, adding the distance between the DTT and pipe bottom, and then calculating a pipe $\rho_{DTT,c}$ from the water level. This correction should be made if the drag disc signal is used.

The densitometer density in the pipe calculated as the length average value ρ_γ is also in error for the separated flow observed in these experiments. For the corrected value the same void fraction was taken as for the interface level $(y/d)_{\gamma,c}$ and converted to the density $\rho_{\gamma,c}$. This density $\rho_{\gamma,c}$ should be taken if the gamma densitometer reading is used.

The corrected mass fluxes are then given by

$$\dot{G}_{\gamma-T,c} = \frac{\rho_{\gamma,c}}{\rho_\gamma}\dot{G}_{\gamma-T} = \rho_{\gamma_c} \cdot V_T \tag{9.7}$$

$$\dot{G}_{\gamma\text{-DD},c} = \left(\frac{\rho_{\gamma c}}{\rho_\gamma} \frac{\rho_{DTT,c}}{\rho_{DTT}}\right)^{0.5} \dot{G}_{\gamma\text{-DD}} = \left(\rho_{\gamma,c}\,\rho_{DTT,c}\right)^{0.5} V_T \tag{9.8}$$

$$\dot{G}_{T\text{-DD},c} = \frac{\rho_{DTT,c}}{\rho_{DTT}} \dot{G}_{T\text{-DD}} = \rho_{DTT,c} V_T \tag{9.9}$$

These equations differ from (3.1)-(3.3) in the values of the corrected densities.

Figure 9. shows the results for all test points where the DTT measured an interface level between the upper and lower edges of the turbine. An improvement compared to Fig. 6.4 is clearly seen, especially for the combination of turbine and drag disc. Of the three mass flux calculations the combination of drag disc and gamma densitometer showed the least data scatter.

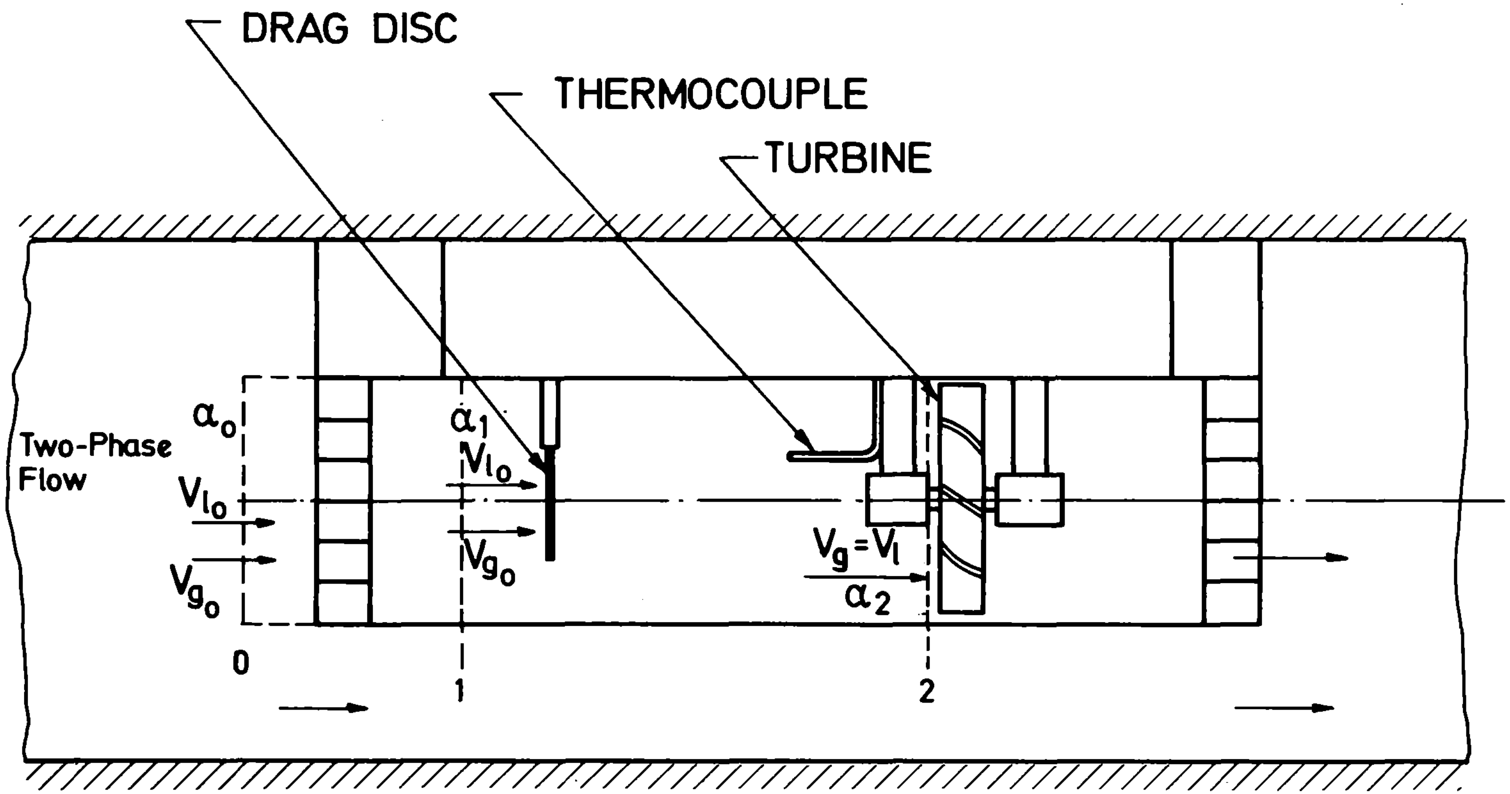

FIGURE 9.1 MODELING OF THE LOCAL BEHAVIOR OF THE DTT

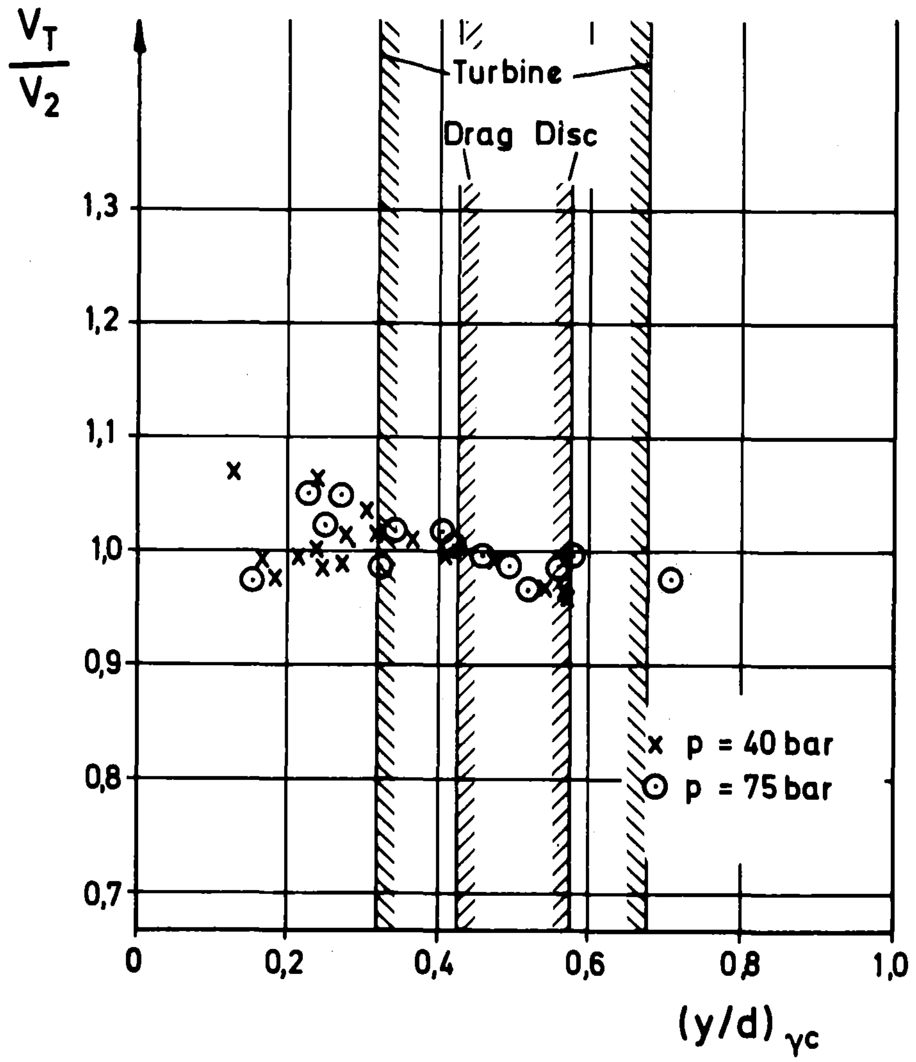

FIGURE 9.3 TURBINE VELOCITY COMPARISON (3" PIPE TESTS)

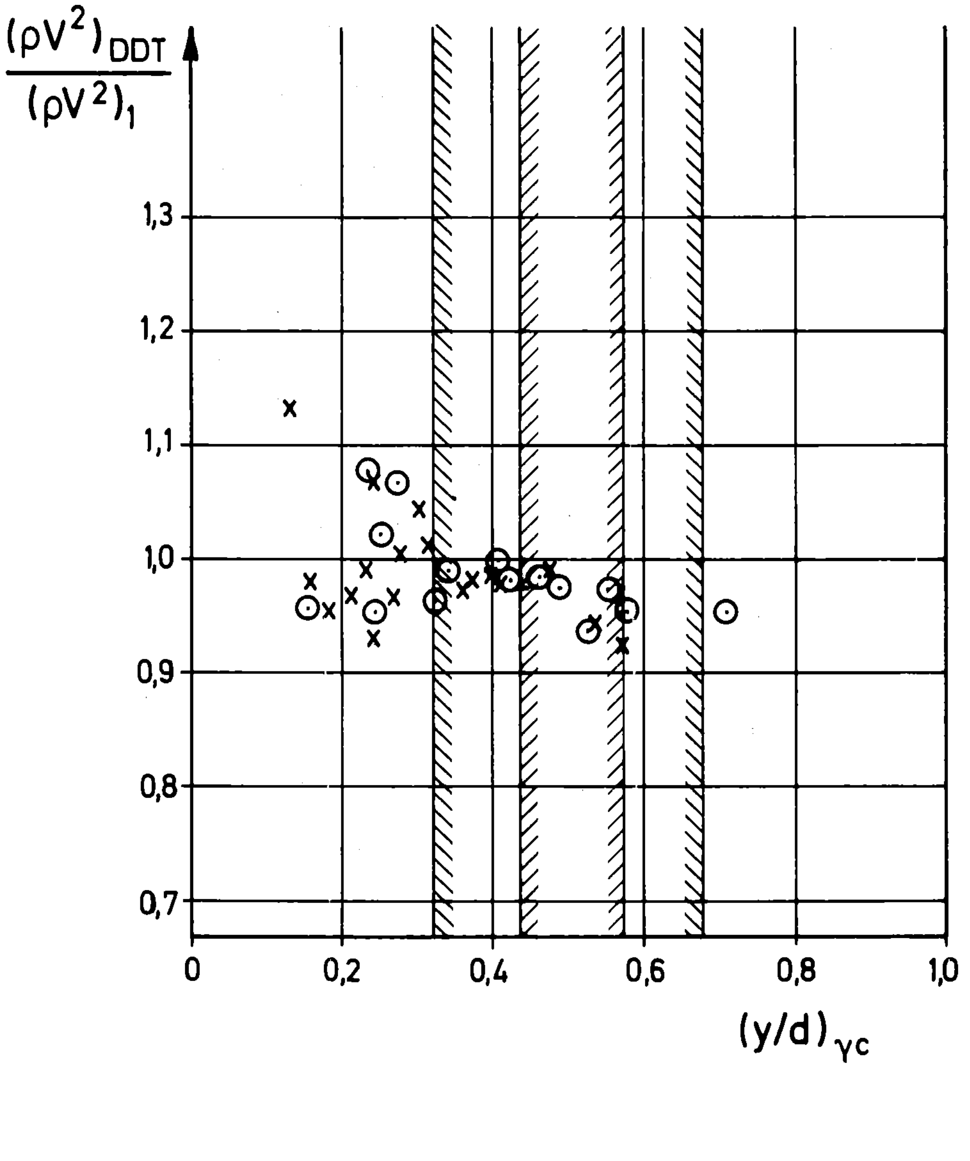

FIGURE 9.4 DRAG DISC MOMENTUM COMPARISON (3" PIPE TESTS)

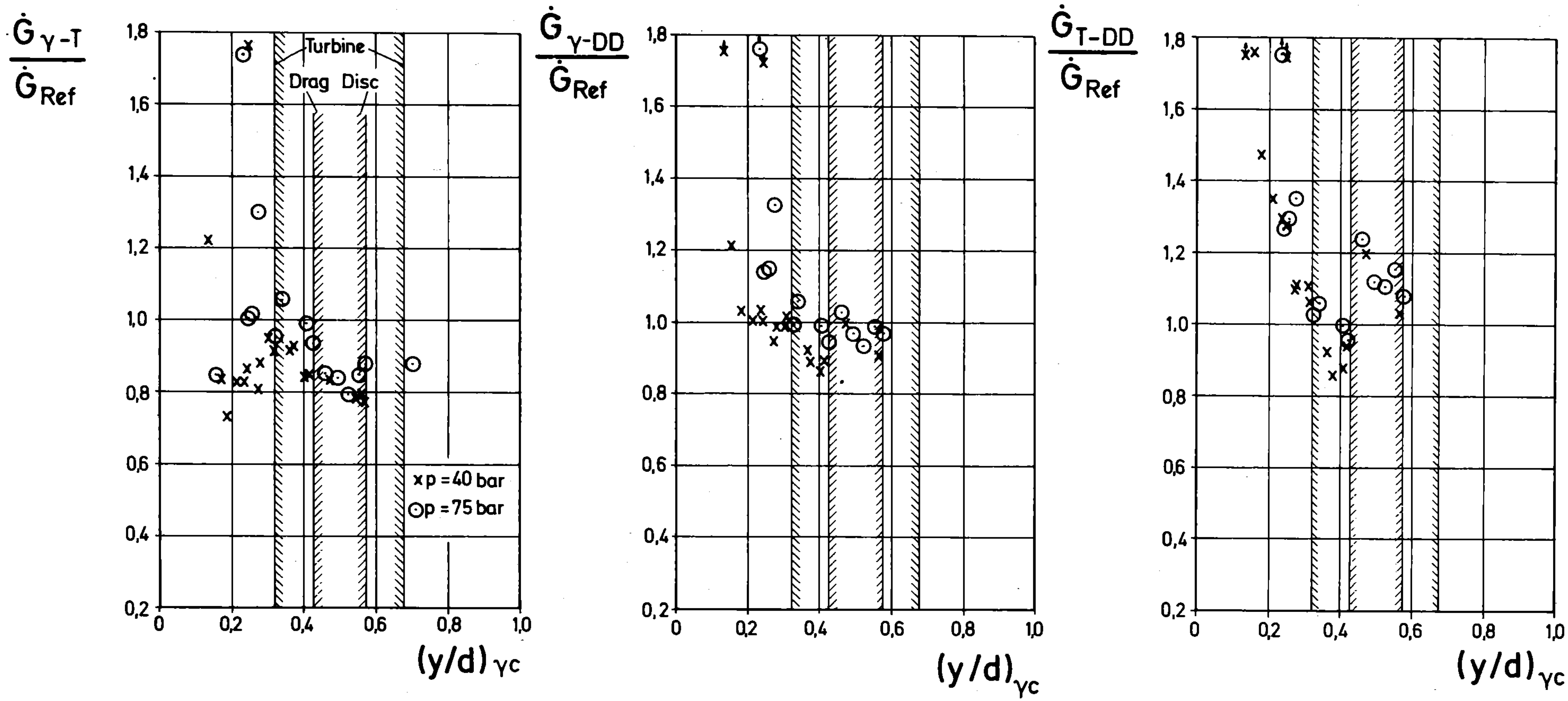

FIGURE 9.5 DENSITY CORRECTED MASS FLUXES (3" PIPE TESTS)

10. Mass Flow Rate from Radiotracer Velocities and Gamma Densitometer

For the 5" pipe tests the mass fluxes were evaluated with the radiotracer velocities taken at the position $\overline{D5\text{-}D7}$ (Figure 2.1) and the length weighted 3 beam densitometer void fraction (in the 5" pipe tests the corrections for stratification were neglectable, compare 5.1). Because of the upstream position $\overline{D5\text{-}D7}$ the phase velocity of water V_l is measured in general slightly too high. This explains the positiv mean error of about 4% in Table 3.1. The scattering of the data shown in Figure 3.4 can be explained by the relativ small number of injections per test point (Table 5.7).

For the 3" pipe tests the velocities were interpolated to the densitometer position by taking the arithmetic mean value between the measurements at $\overline{D3\text{-}D5}$ and $\overline{D5\text{-}D8}$ (Table 5.7). The mass fluxes in Figure 3.4 and Table 2.1 were evaluated with the phase velocities and the length weighted gamma densitometer void fraction. The mean error of the ratio $\dot{G}_{Rad-\gamma}/\dot{G}_{Ref}$ was +7% which could mainly be caused by the length weighted void fraction (if α_γ is too low, $\dot{G}_{Rad-\gamma}$ becomes too high because the term $(1-\alpha_\gamma)V_l\rho_l$ in eq (3.4) is dominant).

Table 10.1 shows the mass fluxes $\dot{G}_{Rad-\gamma}$ with the void fraction corrected for stratification. The mean error is slightly smaller but negative now, indicating that not for all test points the use of the void fraction correction is justified (compare Chapter 5.1).

Figure 8.1 shows the ratios $\dot{G}_{Rad-\gamma}/G_{Ref}$ as function of the flow regime for both the 5" and 3" pipe tests ($\dot{G}_{Rad-\gamma}$ evaluated with the length weighted α). The results do not show any clear dependency of flow regime and void fraction and slip, respectively. The measurement accuracy in the low velocity range where the DTT was below its measuring range is the same as that in the high velocity range.

In summary, it can be stated that this technique has a very high accuracy. Further improvement could be reached mainly by improving the evaluation of the cross section averaged void fraction.

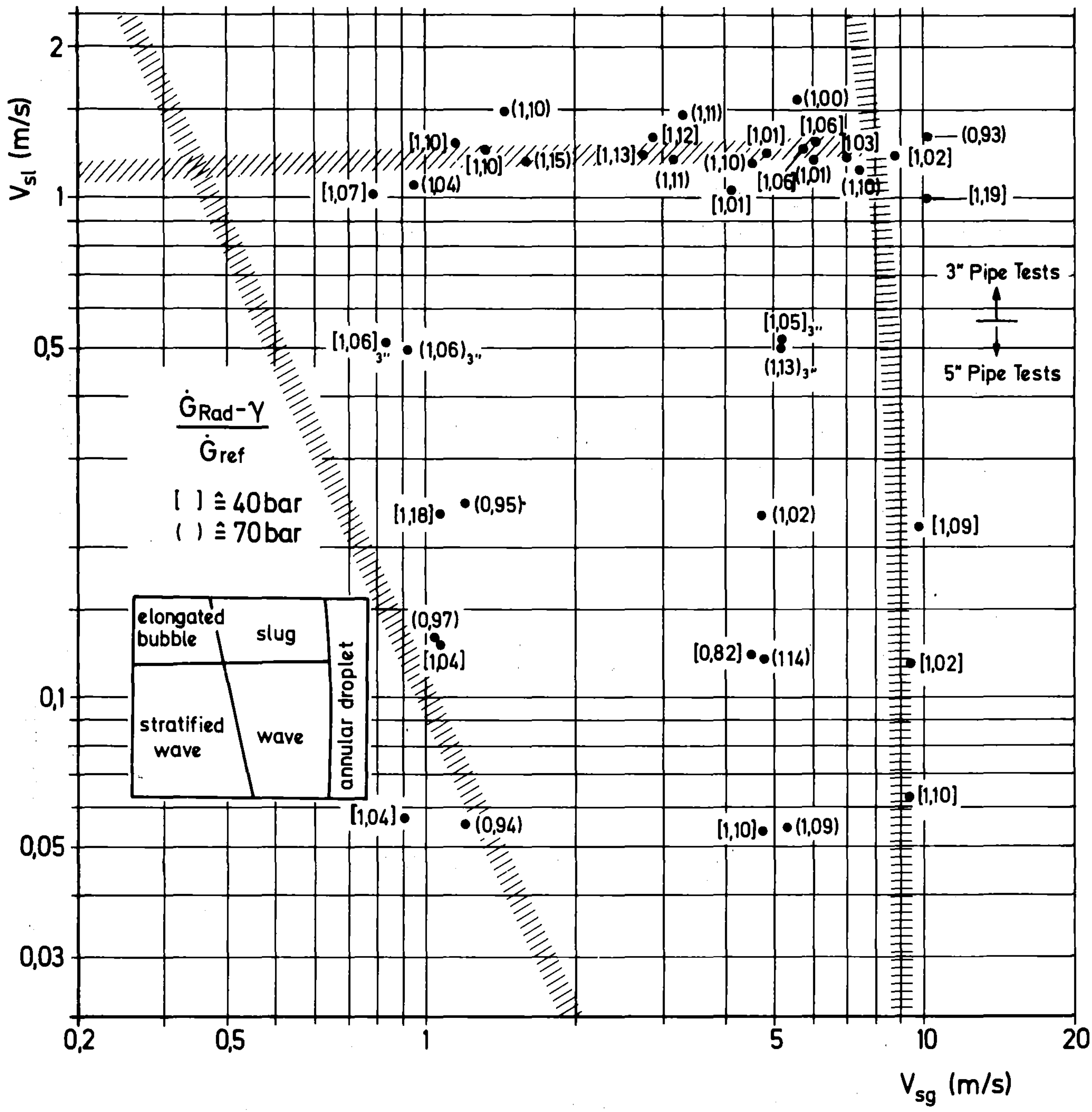

FIGURE 10.1 RADIOTRACER - GAMMA DENSITOMETER MASS FLOW RATES AS FUNCTION OF FLOW REGIME (5" AND 3" PIPE TESTS)

p ≈ 40 bar			p ≈ 75 bar		
Nr.	$\frac{G_{Rad-\gamma_{lw}}}{G_{Ref}}$	$\frac{G_{Rad-\gamma_c}}{G_{Ref}}$	Test Nr.	$\frac{G_{Rad-\gamma_{lw}}}{G_{Ref}}$	$\frac{G_{Rad-\gamma_c}}{G_{Ref}}$
6013	1,19	1,05	6052	1,10	0,99
6014	1,01	0,86	6053	1,15	1,07
6015	1,07	0,98	6054	1,06	0,93
6016	1,06	0,93	6055	1,04	0,99
6017	1,05	0,89	6056	1,13	1,01
6018	0,93	0,82	6057	1,11	1,00
6019	1,10	0,97	6058	1,10	0,98
6020	1,10	1,11	6059	1,01	0,88
6021	1,06	0,90	6060	1,11	1,00
6022	1,13	0,98	6061	1,10	1,03
6023	1,01	0,87	6062	1,00	0,93
6024	1,03	0,87	6063	0,93	0,86
6025	1,02	0,87			
6026	1,06	0,89			
6027	1,12	0,98			
x	1,07	0,93		1,07	0,97
σ	0,05	0,08		0,06	0,06

	p ≈ 40 + 75 bar	
x	1,07	0,95
σ	0,06	0,07

TABLE 10.1 RADIOTRACER MASS FLUXES WITH CORRECTED AND UNCORRECTED 3 BEAM GAMMA DENSITOMETER VOID FRACTIONS

Conclusions

The behavior of a LOFT DTT mounted in free field configuration and a LOFT type gamma densitometer installed in a 5" pipe and a 3" pipe test section in horizontal two-phase flow were investigated. The 5" pipe tests were carried out in wave, wave droplet and transition to annular droplet flow regimes associated with slip values up to 6 in the high-pressure experiments (steam-water flow at ≈40 and ≈75 bars) and up to 17 in the low pressure experiments (air-water flow at ≈2 bars, steam-water flows at ≈4 bars). The maximum mass flux was $\dot{G} \approx 600$ kg/m^{2}s, a typical value of void fraction was ≈ 0.9. The 3" pipe tests were made at higher mass fluxes ($G_{max} \approx 1500$ kg/m^{2}s) and lower void fractions ($\alpha_{typical} \approx 0.65$). The test points were mostly in wave droplet, slug or transition to annular droplet flow regimes, associated with slip values of <3 (steam-water flow at ≈40 and ≈75 bars). Although these test series included two different test geometries the conclusions can be generalized.

The deviations of the single instrument readings from the cross-section averaged values are different for different flow regimes. However, a closer examination shows that these deviations are for all flow regimes a definite function of the height of the water level (interface level) which is calculated from the gamma densitometer reading.

The error of the mass flow rate evaluated by using two of the three instruments is also dependent on flow regime and interface level. This is caused by the deviations of the single instruments and slip sensitivity of the equations used. The mass flow rate evaluated from the drag disc and densitometer readings showed the best overall accuracy.

The accuracy of the instrumentation is considerably higher in the high pressure tests than in the low pressure tests.

If the three instrument readings are used to calculated the mass flow rate with various turbine models the overall accuracy is not improved because the model assumptions are only poorly fulfilled in horizontal, nonhomogenized flow.

An DTT model was developed which showed that the local parameters were measured accurately. Of course, the DTT and the densitometer do not provide sufficient information for evaluating phase slip, thus, cannot be modeled to calculate the pipe averaged mass flux in a high slip condition such as in the 5-inch pipe tests. However, when the water phase is sufficiently in contact with the DTT, the approximate model provided reasonably good pipe averaged mass flux for this experiment. Using calibration factors as a function of the interface level, a simple calibration procedure is established, and provides a better fit of the data with respect to mass flow rate, slip, and phase velocities for these experiments. This procedure, which is restricted to a free field DTT, has to be checked with additional data.

The mass flow rates evaluated with the phase velocities measured by the radiotracer technique and the gamma densitometer void fraction have the highest accuracy and widest range. There is no distinct dependence on flow regime or water level, this technique shows the same accuracy in the stratified wave flow regime where the DTT was below its measurement range.

This report presents the analyses of test series made in Oct.-Nov. 1977. Analysis of tests performed in Feb.-March 1978 with the same type of instrumentation but a test matrix in the higher mass flow rate and lower void fraction range is under way; as well as the tests with the Semiscale instrumentation mounted in full flow configuration Nov.-Dez. 1977. The comparison of these tests should give an interesting insight on the behavior of the turbine meter at different d_T/d_{pipe} ratios (LOFT free field turbine in the 5" and 3" pipe, Semiscale full flow turbine in the 3" pipe).

APPENDIX : Primary Data

PIPE SIZE= 5 INCH DOUBLE EXTRA STRONG

INSIDE DIAMETER= 0.10320 M
TURB. DIA.= 0.0381 M
PIPE AREA= 0.0083647 M↑2

RUN ID TSN	PRESS. (BARS)	TEMP. (DEG C)	FLOW RATES STEAM SUP-VEL (M/S)	STEAM MASS (KG/S)	WATER SUP-VEL (M/S)	WATER MASS (KG/S)	TURB. VEL (M/S)	DRAG DISK (KG/ M*S↑2)	GAMMA DENSITOMETER A BEAM LOWER (KG/ M↑3)	B BEAM MIDDLE (KG/ M↑3)	C BEAM UPPER (KG/ M↑3)	Comments
Fluid: Air-Water												
4206	2.0	20.1	4.55	0.076	0.050	0.415	3.21	-	260	45	33	
4207	1.9	21.3	0.59	0.010	0.050	0.415	0.31	-	474	232	32	T below range
4208	6.2	20.8	1.32	0.069	0.225	1.868	0.39	582	361	134	45	T below range
4209	2.0	22.1	9.73	0.163	0.125	1.038	6.50	720	165	33	38	
4210	2.0	22.6	10.39	0.174	0.050	0.415	7.10	596	143	30	41	
4211	2.0	21.5	10.39	0.174	0.250	2.075	6.86	1315	134	39	39	
4212	6.0	21.7	6.25	0.312	0.230	1.9o9	5.10	587	143	45	40	
4213	2.0	20.9	10.29	0.172	0.500	4.151	7.54	2209	83	42	32	
4214	2.0	21.3	3.90	0.065	0.515	4.275	2.65	874	108	61	39	
4215	2.0	22.3	1.12	0.019	0.515	4.275	0.77	1016	352	179	30	
4216	2.0	23.3	0.62	0.010	0.515	4.275	0.89	1218	377	198	38	
FLUID: STEAM - WATER												
5031	4.4	121.8	5.84	0.115	0.478	3.681	1.13	494	172	56	42	
5032	5.6	121.0	10.42	0.257	0.238	1.822	3.74	603	59	19	39	
5033	5.6	155.7	0.83	0.020	0.227	1.736	0.16	69	285	132	25	T, DD below range
5034	4.2	142.9	0.82	0.015	0.484	3.734	0.45	283	-	-	-	T, DD below range
5035	4.4	146.0	4.49	0.089	0.090	0.693	0.15	133	150	32	38	T, DD below range
5050	4.6	144.7	9.90	0.202	0.119	0.915	4.65	784	104	30	47	
5051	4.3	145.8	4.53	0.088	0.246	1.899	0.29	206	175	43	39	T, DD below range
5052	4.9	154.2	0.76	0.017	0.109	0.837	0.14	288	527	351	54	T, DD below range

Table I: PRIMARY ENGINEERING UNIT DATA : 5" Pipe Low Pressure Tests

FLUID: STEAM - WATER
PIPE SIZE= 5 INCH DOUBLE EXTRA STRONG

INSIDE DIAMETER= 0.10320 M
TURB. DIA.= 0.0381 M
PIPE AREA= 0.0083647 M↑2

Preliminary Radiotracer Data Evaluation

(all 5" and 3" Pipe Tests)

↓

RUN ID TSN	PRESS. (BARS)	TEMP. (DEG C)	FLOW RATES STEAM SUP-VEL (M/S)	STEAM MASS (KG/S)	WATER SUP-VEL (M/S)	WATER MASS (KG/S)	TURB. VEL (M/S)	DRAG DISK (KG/M*S↑2)	GAMMA DENSITOMETER A BEAM LOWER (KG/M↑3)	B BEAM MIDDLE (KG/M↑3)	C BEAM UPPER (KG/M↑3)	RADIOTRACER VELOCITIES STEAM (M/S) (AT GAMMA DENS)	WATER (M/S)	Comments
5001	42.1	244.5	9.81	1.742	0.229	1.509	11.13	2533	146	46	33			T above range
5002	41.9	247.4	4.91	0.868	0.232	1.531	5.29	607	197	65	40			
5004	41.3	244.9	9.83	1.709	0.110	0.730	10.68	2348	96	45	42			T above range
5005	41.4	246.0	9.75	1.703	0.054	0.359	10.84	2384	54	37	44			T above range
5037	40.0	247.7	4.77	0.803	0.125	0.833	5.19	577	152	33	8			
5038	40.7	248.8	4.83	0.828	0.057	0.377	5.05	571	107	25	10			
5039	40.1	247.0	5.07	0.856	0.031	0.208	5.21	514	73	12	2			
5040	39.9	247.7	0.99	0.166	0.057	0.377	0.37	126	272	134	10			T, DD below range
5041	40.8	248.8	0.72	0.124	0.135	0.892	0.36	178	226	95	21			T, DD below range
5042	40.3	248.8	1.00	0.170	0.244	1.619	0.23	181	238	114	37			T, DD below range
5043	40.1	247.4	9.61	1.625	0.057	0.381	10.60	2065	72	31	41			T above range
5044	40.5	248.5	4.82	0.823	0.498	3.304	5.74	690	225	92	2			
5045	40.7	250.6	0.89	0.153	0.503	3.331	0.36	217	293	153	24			T, DD below range
5046	39.8	248.8	0.47	0.079	0.505	3.358	0.15	183	350	182	25			T, DD below range
5054	40.6	247.0	9.48	1.621	0.223	1.481	10.27	2121	124	36	15	10.27	3.27	T above range
5055	40.1	248.1	4.80	0.811	0.228	1.516	4.92	537	179	48	28			
5056	40.8	250.3	4.57	0.785	0.122	0.809	4.70	516	163	35	13	4.83	1.40	
5057	40.8	251.7	4.78	0.821	0.054	0.356	4.48	519	122	31	20	5.13	1.35	
5058	40.2	248.1	9.54	1.616	0.063	0.417	10.31	2169	91	32	24	10.00	2.30	T above range
5059	40.0	246.7	9.44	1.588	0.116	0.769	10.20	2106	112	32	27	10.00	2.53	T above range
5060	40.0	247.0	1.08	0.182	0.127	0.842	0.19	107	247	79	3	1.27	1.15	T, DD below range
5061	40.0	248.5	0.91	0.153	0.057	0.377	0.18	92	298	153	24	1.05	0.58	T, DD below range
5062	40.8	248.5	1.08	0.186	0.232	1.536	0.24	85	242	106	40	1.33	2.00	T, DD below range
5014	74.8	288.3	5.76	1.895	0.033	0.201	6.19	1334	76	27	29			
5015	75.0	288.0	5.12	1.689	0.063	0.389	5.61	1104	109	32	37			
5016	75.3	287.6	5.12	1.696	0.135	0.828	5.83	1183	136	41	37			
5017	75.2	288.7	0.97	0.323	0.127	0.780	0.68	61	223	101	37			T, DD below range
5019	75.7	288.3	0.83	0.277	0.243	1.490	0.52	99	247	118	39			T, DD below range
5021	74.8	287.6	7.60	2.499	0.233	1.435	8.73	2777	113	48	39			Rerun of 5020
5022	74.8	286.2	7.72	2.539	0.126	0.773	8.58	2689	90	44	46			
5023	74.6	288.0	7.69	2.524	0.054	0.332	8.36	2523	65	39	39			
5024	75.0	288.0	7.67	2.533	0.035	0.212	8.21	2475	50	37	44			
5025	75.3	288.0	4.82	1.596	0.243	1.490	5.59	1155	165	66	48			
5047	74.2	288.7	2.07	0.675	0.497	3.060	1.87	350	309	183	43			DD below range
5048	74.9	289.4	0.89	0.292	0.496	3.049	0.47	192	310	173	43			T, DD below range
5049	74.4	289.0	0.47	0.154	0.492	3.025	0.26	152	328	196	44			T, DD below range
5066	75.5	288.7	4.79	1.594	0.229	1.407	5.35	1106	181	76	51	5.22		
5067	76.0	289.4	4.76	1.595	0.124	0.762	5.23	1102	147	51	43	5.27		
5068	75.9	290.1	1.05	0.351	0.129	0.793	0.53	86	232	105	47	0.98	1.23	T, DD below range
5069	75.5	288.3	1.18	0.393	0.241	1.479	0.31	110	244	116	40	1.10	1.90	T, DD below range
5070	76.1	290.1	1.20	0.402	0.055	0.334	0.72	147	206	90	38	1.20	0.67	T, DD below range
5071	76.1	288.0	5.36	1.797	0.055	0.340	5.59	1291	109	51	55			

TABLE II: PRIMARY ENGINEERING UNIT DATA : HIGH PRESSURE TESTS (5" PIPE)

FLUID: STEAM - WATER
PIPE SIZE= 3 INCH SCHEDULE 160

INSIDE DIAMETER= 0.06665 M
TURB. DIA.= 0.0381 M
PIPE AREA= 0.0034889 M↑2

RUN ID TSN	PRESS. (BARS)	TEMP. (DEG C)	FLOW RATES STEAM SUP-VEL (M/S)	FLOW RATES STEAM MASS (KG/S)	FLOW RATES WATER SUP-VEL (M/S)	FLOW RATES WATER MASS (KG/S)	TURB. VEL (M/S)	DRAG DISK (KG/ M*S↑2)	GAMMA DENSITOMETER A BEAM UPPER (KG/ M↑3)	GAMMA DENSITOMETER B BEAM MIDDLE (KG/ M↑3)	GAMMA DENSITOMETER C BEAM LOWER (KG/ M↑3)	SCAN DENS (KG/ M↑3)	RADIOTRACER VELOCITIES STEAM (M/S) (AT GAMMA DENS)	RADIOTRACER VELOCITIES WATER (M/S) (AT GAMMA DENS)	Comments
6003	40.5	247.7	4.73	0.336	1.210	3.348	3.67	2125	208	310	499				
6004	40.7	247.0	9.15	0.654	1.212	3.350	6.55	3484	123	188	300				
6005	40.5	246.7	8.97	0.639	1.274	3.523	7.72	3716	122	166	265				
6013	40.2	248.5	10.15	0.717	1.017	2.815	9.61	3755	46	126	198	137	12.40	10.50	T above range
6014	41.0	248.8	4.11	0.296	1.048	2.896	4.18	1713	143	267	439	265	6.20	3.10	
6015	40.0	247.4	0.79	0.055	1.008	2.792	1.40	1459	369	507	746		1.80	1.60	
6016	40.2	248.5	0.83	0.058	0.508	1.407	0.93	565	295	421	648	370	1.65	0.95	
6017	40.4	248.5	5.23	0.371	0.516	1.427	6.33	1189	99	229	315	188	6.70	2.30	
6018	40.2	247.4	9.56	0.675	0.527	1.460	11.55	3281	18	117	163		11.00	4.14	T above range
6019	40.6	248.8	1.16	0.083	1.321	3.653	1.75	2524	386	515	752	476	2.10	2.10	
6020	40.0	248.1	1.32	0.093	1.251	3.465	1.83	2697	340	486	727	463	2.35	2.15	
6021	40.1	248.5	5.71	0.402	1.261	3.491	5.36	2618	91	257	400		8.50	4.60	
6022	40.2	248.5	2.72	0.192	1.235	3.419	2.82	2257	200	368	584		4.60	3.10	
6023	40.0	246.7	4.69	0.329	1.228	3.403	4.55	2250	119	279	448		6.90	3.70	
6024	40.4	248.5	6.96	0.494	1.223	3.383	6.38	3209	54	209	344		9.70	5.00	
6025	39.9	246.7	8.79	0.615	1.235	3.422	8.03	3721	34	165	261	173	11.40	7.20	
6026	40.1	247.7	6.05	0.426	1.331	3.687	5.40	2874	89	241	391		7.90	4.70	
6027	40.5	248.5	2.84	0.202	1.323	3.660	3.10	2360	201	356	571				
6048	39.2	246.3	5.09	0.350	1.649	4.579	4.79	2966	212	308	527				
6066	40.1	249.9	0.93	0.066	0.103	0.285	—	377	137	223	316				T failed; DD below range
6067	39.9	249.5	0.91	0.064	0.256	0.708	—	463	272	350	522				T failed;
6068	40.7	250.6	4.91	0.351	0.247	0.682	—	901	91	177	-				T failed; Densit., shifted
6069	40.1	249.5	10.29	0.725	0.262	0.726	—	4749	-	62	84	69	10.80	4.00	T failed; Densit., DD shifted
6070	40.1	249.5	5.31	0.375	0.268	0.741	—	1744	35	145	180	113	6.20	1.90	T failed; DD shifted
6071	40.1	249.5	4.95	0.348	0.131	0.363	—	1401	-	119	91		6.30	2.00	T failed; Densit., DD shifted
6035	78.1	291.2	0.21	0.030	1.779	4.530	1.86	2943	651	723	765	665			
6036	78.7	291.5	0.86	0.126	1.630	4.144	1.93	3150	485	550	740	537			
6037	78.4	292.3	1.48	0.215	1.589	4.042	2.36	3402	389	469	704	428			
6051	75.7	288.7	5.29	0.737	0.995	2.546	6.37	2866	139	223	334	178			
6052	75.5	289.0	7.36	1.021	1.188	3.042	7.04	3851	139	192	296		9.15	5.50	
6053	76.2	290.1	1.61	0.226	1.219	3.117	2.12	2507	318	407	608	357	3.00	2.50	
6054	75.6	287.6	0.91	0.126	0.507	1.299	0.99	536	290	379	556		1.75	-1.00	
6055	75.4	290.1	0.96	0.134	1.064	2.723	1.59	1649	358	428	634	437	2.10	1.90	
6056	75.8	290.5	5.10	0.711	0.510	1.305	6.55	2070	108	202	289		6.35	2.75	
6057	76.1	290.5	3.11	0.435	1.205	3.082	3.30	2222	236	329	508		4.90	3.15	
6058	75.8	290.1	4.51	0.628	1.216	3.111	4.60	2626	189	280	428	262	6.45	3.65	
6059	75.3	289.0	5.95	0.822	1.214	3.109	6.44	3762	146	205	315		7.85	4.90	
6060	75.7	289.4	3.31	0.460	1.491	3.815	3.62	2995	251	340	536		5.40	3.50	
6061	75.8	289.8	1.45	0.202	1.491	3.815	2.24	3434	362	455	682		3.20	2.50	
6062	75.3	288.3	5.52	0.763	1.613	4.132	5.74	3863	181	246	396		7.60	5.10	
6063	75.9	288.7	10.11	1.410	1.331	3.404	10.79	4162	89	125	167		7.30	5.70	T above range
6074	75.6	290.1	4.96	0.689	0.137	0.351	—	2772	28	104	63		5.30	1.90	T failed; Dens., DD shifted
6075	74.8	289.0	10.03	1.376	0.139	0.356	—	5360	3	60	2		9.80	4.20	T failed; Dens., DD shifted
6076	74.9	289.0	9.80	1.347	0.259	0.665	—	5456	9	70	41		9.80	5.80	T failed; Dens., DD shifted
6077	74.9	289.4	4.96	0.682	0.264	0.676	—	2544	39	143	153	111	5.20	2.20	T failed; DD shifted
6078	74.6	288.7	0.77	0.105	0.235	0.604	—	585	191	287	390	235			T failed; DD shifted
6079	75.8	290.1	0.85	0.119	0.156	0.398	—	559	145	252	333	242			T failed; DD shifted
6080	75.3	289.0	9.43	1.303	0.537	1.375	—	5465	41	107	108				T failed; DD shifted

TABLE III: PRIMARY ENGINEERING UNIT DATA : HIGH PRESSURE TESTS (3" PIPE)

References

/1/ Reimann, J; John, H.; Löffel, R.; Solbrig, C.W.; Stephens, A.G.; Goodrich, L.D.:
EG & G Mass Flow Rate Instrumentation Tests at Kernforschungszentrum Karlsruhe, Data Report Vol.1, KfK 2784, 1979

/2/ John, H.; Reimann, J.:
Gemeinsamer Versuchsstand zum Testen und Kalibrieren verschiedener Zweiphasen-Massenstrommeßverfahren, Anlagenbeschreibung
KfK 2731 B, Feb. 1979

/3/ J. Reimann, H. John, St. Müller,
Impedance Probe for Detecting Flow Regime and Measuring the Phase Distribution in Horizontal Air-Water- and Steam-Water-Flow; Two-Phase Flow Instrumentation Review Group Meeting, Troy, New York, March 13-14, 1978.

/4/ J. Reimann, H. John,
Measurements of the Phase Distribution in Horizontal Air-Water- and Steam-Water-Flow; Second CSNI Specialist Meeting on Transient Two-Phase Flow, Paris (France), 12th-14th June, 1978.

/5/ Govier, G.W.; Aziz, K.:
The Flow of Complex Mixtures in Pipes
von Nostrand Reinhold Co, New York, 1972, pp. 792

/6/ Taitel, Y.; Dukler, A.E.:
A Model for Predicting Flow Regime Transitions in Horizontal and Near Horizontal Gas-Liquid Flow
AIChE, Journal Vol 22, Nr. 1, 1976, p. 147

/7/ Lassahn, D.G.:
LOFT Three-Beam Densitometer Data Interpretation;
THREE-NUREG-1111; 1976.

/8/ Rouhani, Z.:
Application of the Turbine Type Flow Meters in the Measurements of Steam Quality and Void,
presented at the Symposium on In-Core Instrumentation,
Oslo, June 15, 1964.

/9/ Aya, I.:
Model to Calculate Mass Flow Rate and Other Quantities of Two-Phase Flow in a Pipe with a Densitometer, a Drag Disk and a Turbine Meter
ORNL/TM-475+ (1975).

/10/ Estrada, H., Sheppard, J.D.
Some Aspects of Interpreting Two-Phase Flow Measurements in Instrumented Piping Spool Pieces. NUREG-0280, 1977.

/11/ Reimann, J.; John, H.; Löffel, R.; Solbrig, C.W.; Stephens, A.G.; Goodrich, L.D.:
EG&G Mass Flow Rate Instrumentation Tests at Kernforschungszentrum Karlsruhe, Data Report Vol 2 in preparation

/12/ Reimann, J.:
Massenstrommeßverfahren für Zweiphasenströmungen (Dampf/Flüssigkeit); KTG-Fachtagung: Experimentiertechnik auf dem Gebiet der Reaktor-Fluiddynamik, Berlin, 10-12. März 1976.